Ultra-High Frequency Dynamics of Semiconductor Injection Lasers

Thesis by

Kam-Yin Lau

In Partial Fulfillment of the Requirements

for the degree of

Doctor of Philosophy

California Institute of Technology

Pasadena, California

1981

(Submitted May 18, 1981)

- ACKNOWLEDGEMENT -

It is a pleasure to express my appreciation to my advisor, Professor Amnon Yariv, for his constant encouragement and guidance throughout the course of this work. I particularly enjoyed his physical insight and keen intuition possessed only by scientists of unusual caliber.

Now that I am approaching the end of one phase of a long journey, I cannot help thinking of how it all started. To this end, I owe much to Professor John and Ellen Pierce, whose hospitality and guidance during my early and uncertain undergraduate years have been most unforgettable. Six years have not gone by without distressing moments, yet their concern has always been a source of comfort.

The part of this work on mode-locking of injection lasers was done in collaboration with Dr. Luis Figueroa and Dr. Charles Slayman of Hughes Research Laboratory. Apart from the fine setting of the laboratory atop the hills of Malibu Canyon, the collaboration was a particularly pleasant and fruitful one from which I learned much in high frequency opto-electronics. I also benefited from the expertise in microwave technology of George Lutes at Jet Propulsion Laboratory throughout the course of this work.

Dr. Michiharu Nakamura of the Central Research Laboratory of Hitachi assisted in the high-bit-rate experiment by providing some of the very best injection lasers available in the world today.

And, of course, the technical assistance of Desmond Armstrong and Lawrence Begay facilitated not only my experiments but the effort of the entire research group.

Dr. Hossein Izadpanah started the high-frequency laser effort in the Quantum Electronics group. Most of the laser and photodiode mounts used in this work were of his design. His untimely return to Iran was most unfortunate and regrettable.

To my past and present colleagues, whose company I have enjoyed, and from whom I learned much through many enlightening discussions, I extend my appreciation: Daniel Wilt, Dr. John Auyeung, Dr. Richard Moyer, Pei-Chuang Chen, Kit-Lai Yu, Liew-Chuang Chiu, Dr. Israel Ury, Thomas Koch, Christopher Harder, Jeffrey White, Henry Blauvelt and Joseph Katz. And I thank Daniel Wilt for proofreading this thesis.

I want to thank Linda Dozsa and Michelle Schroeder who gave me encouragement and help when they were most needed. Dominic and Teresa Orr have done likewise and have extended to me many times their hospitality. I am thankful to Professor Sunney Chan for his friendship and for his many attempts to teach me a trade more remunerable than science.

Finally, I thank Dr. Richard Sydnor of Jet Propulsion Laboratory for arranging my financial support in the last two years of my graduate studies. And, this research definitely could not have been undertaken without the generous supports from the Offices of Scientific Research of the U.S. Navy and Air Force.

- ABSTRACT -

Experimental and theoretical studies on the high frequency dynamics of (GaAl)As semiconductor lasers center on three main areas: 1) analog modulation response of laser diodes; 2) pulse (pulse code modulation) response of laser diodes and 3) generation and quenching of intensity pulsations in laser diodes coupled to external cavities.

The basic analog modulation and transient characteristics of injection lasers with various structures are studied and compared. The basic limitations on ultrahigh frequency (> 5GHz) modulation of lasers are considered. Self-pulsations in injection lasers are studied and their interaction with external cavities are clarified. These studies lead to the quenching of self-pulsation and ultra-short short pulse generation in laser diodes by coupling to an external cavity. A novel external fiber resonator is introduced for this purpose. Pattern effects in pulse code modulation of injection lasers are studied and a bipolar pulsing scheme devoid of the above effect is described. The transverse mode shift in a transverse junction laser under ultrashort electrical pulse excitation is investigated. Finally, the frequency response of superluminescent lasers (lasers without mirrors) is analysed.

- CONTENTS -

CHAPTER 1

INTRODUCTION

1.1 Fiber-optic communications and semiconductor lasers

Lightwave telecommunication systems using glass fiber guides seem destined for an important role in terrestrial communication[1]. The driving force for putting fibers into practical systems is their low transmission loss, light weight and attractive bandwidths. Installed cables have shown loss in the vicinity of 4dB/km at wavelengths of 0.82 - 0.85 μm, while laboratory samples have shown loss below 0.7 dB/km near 1.3 μm. This is to be compared with a loss of 20-30 dB/km for high quality ¾ inch thick coaxial cables. In the multimode fibers now being produced, dispersion would permit a bit rate of 50Mbit/sec for repeater spans of at least 10 km, and with a carefully designed refractive index profile larger bit-rate- distance products should become feasible. In single mode fibers, a bit-rate -distance product of 100Gbit/sec-km is feasible (from the standpoint of dispersion) for a laser system near 1.3 μm.

The key components needed for lightwave systems are the fibers, the carrier-wave sources and the light detectors. Semiconductor lasers and light emitting diodes (LED's) are the dominant candidates for fiber-guide transmission sources, but within that scope there are numerous options. Lasers[2] are near ideal sources of light for communication in fibers. This is due to the fact that lasers emit highly directional radiation which makes coupling into fibers very efficient. Furthermore their narrower spectral width reduces the effect of the intrinsic chromatic dispersion of the silica fibers, and they can be directly modulated at a very high speed (in the GHz range). They are thus used in high data rate systems, composed of short lengths of multimode fibers or long lengths of single mode fibers. On the other hand, LED's can be more attractive for low bit rate (< 100 Mbit/sec) short haul

connections, because of their lower sensitivity to temperature changes and because they do not require complex stablizing and driving circuitry.

Fig. 1.1 shows a diagram of a basic double heterojunction (GaAl)As semiconductor injection laser. The active region is the thin undoped layer of GaAs, where its lower bandgap retains the electrons and holes injected from the confining N and P doped GaAlAs layers, thereby facilitating radiative recombination. This heterostructure, in addition to electrical confinement, also provides optical confinement by dielectric waveguiding action perpendicular to the junction plane, which is crucial to the successful operation of a cw injection laser. The laser cavity is formed by the two parallel cleaved crystal facets. The narrow contact stripe confines the injection current to within a limited region in the tranverse direction along the junction plane.

The wide bandwidth available in fiber-optic lightguides cannot be fully utilized unless the transmission source can be modulated at very high speeds. Semiconductor injection lasers can be directly amplitude-modulated at frequencies up to 1-2 GHz, but numerous distortions and transient effects require special measures to be taken in analog and pulse-code modulation of the laser.

In addition to data and voice transmission, there is great interest in certain applications in directly modulating the laser with a microwave signal at very high frequencies : in the X-band (~ 10GHz) or even higher. As an example, because of its light weight, it is extremely attractive to use a laser- optical fiber system to synchronize airborn radar arrays[3], which is presently being done through bulky, heavy metallic waveguides. A similar application is to use optical fiber for transmitting precise frequency and timing signals between ground antenna stations many kilometers apart, so that the antenna network can be phase-arrayed to perform such experiments as the VLBI (Very Long Baseline Interferometry)[4]. It is therefore

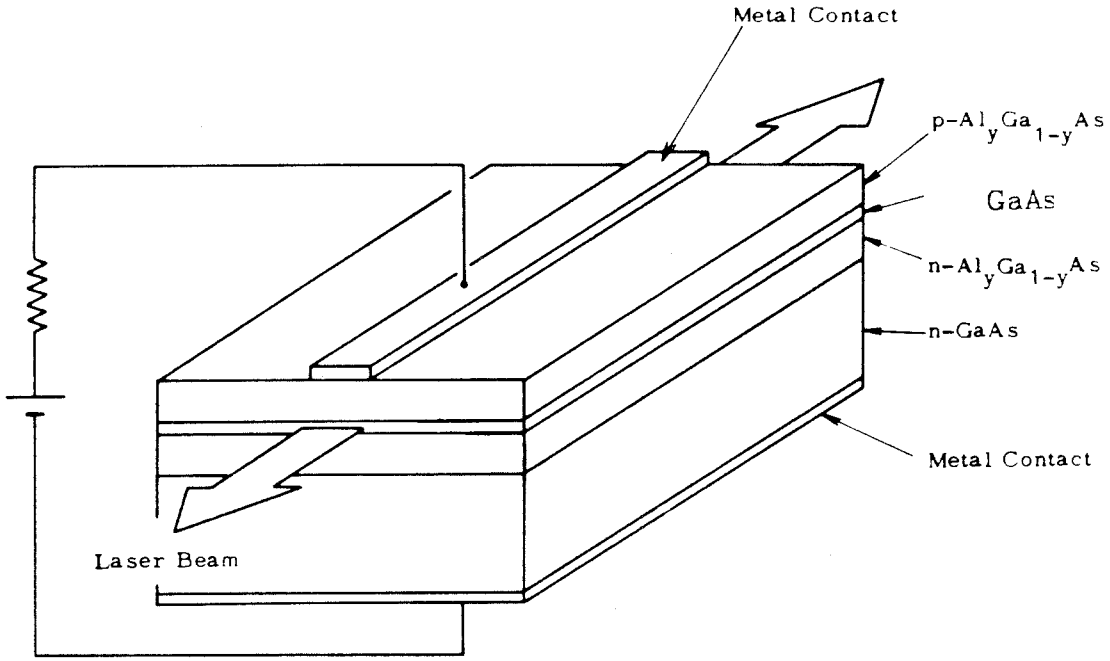

Figure 1.1. *Schematic diagram of a double heterostructure injection laser.*

necessary to seek the optimal laser design for high frequency modulation, and to ascertain whether modulation at such high frequencies is fundamentally attainable in injection lasers.

Another area concerning the high speed dynamics of injection lasers that recently has gained much attention is the generation of ultrashort pulses in semiconductor lasers[5,6]. A simple, light-weight semiconductor laser capable of generating optical pulses of widths in the picosecond range, repetitive at microwave frequencies, has considerable advantage over conventional bulky mode- locked laser systems, and can have such practical applications as airborn or space born range-finding lidar (laser radar)[14].

1.2 Summary of thesis

In the following, the content of this thesis is summarized.

Experimental and theoretical studies of the high frequency dynamics of semiconductor lasers center on three main areas:

1. analog modulation response of laser diodes;
2. pulse (pulse code modulation) response of laser diodes; and
3. generation of short pulses by mode-locking a laser diode inside an external cavity.

The dynamic chacteristics of lasers have been described successfully by a pair of spatially uniform rate equations[7] governing the photon and carrier densities inside the active region. These equations, though simple, are in fact approximate spatial averages of the more precise "local" rate equations[8], which take into account the fact that the photon and carrier densities vary along the laser. The range of validity of this approximation is summarized in chapter 2, using the line of approach of Moreno[8]. The approximation will be justified, and the chapters that follow will make heavy use of this pair of equations to explain many of the

modulation characteristics of injection lasers.

Some basic transient and analog modulation properties of injection laser will be discussed in chapter 3. The response of the laser diode to a microwave current drive is studied theoretically through the small signal analysis of the rate equations, and experimentally using various lasers and standard microwave equipments. The rate equations predict a relaxation oscillation resonance peak in the frequency response of the laser. Experimental measurements of the small signal amplitude and phase responses of the laser diode show characteristics very similar to that of a two-pole system, as the rate equations predict. The effect of lateral carrier diffusion in the modulation response is discussed briefly. The major effect of lateral carrier diffusion is a dampening of the relaxation oscillation resonance[11,12]. The maximum frequency response attainable in GaAs injection lasers under constraints of limited current density and optical power density is also examined in chapter 3. It is found that under a prescribed current and optical limit, an optimum cavity length exists at which the highest frequency response can be obtained. Fundamental frequency limitations under various operating conditions are depicted graphically.

Semiconductor lasers, when operated in cw mode, will sometimes emit a train of very short pulses at a microwave frequency repetition rate. This phenomenon is known as self-pulsation[9], and is believed to be caused by saturable absorbing defects inside the laser medium. In chapter 4, numerical studies are performed using the trap model for self pulsation. The results explicitly show how optical pulses are generated and quenched when the laser is coupled to an external cavity of various lengths. Experiments performed with various lasers yield results that agree closely with the calculated results.

Mode locked laser systems can generate optical pulses in the picosecond range. The laser diode-external cavity system is primarily a passively mode-locked system caused by saturable absorbing defects inside the laser medium. The presense of saturable absorbers causes self-pulsation of the laser diode itself. Thus the study of mode-locking of laser diode involves, to large extent, the study of self-pulsing lasers coupled to an external cavity. A laser diode with a sizable amount of saturable absorber, when coupled to an external cavity, does not always result in mode-locking. The external cavity length is a crucial factor in determining whether mode-locking occurs or not, among the other factors such as the absorber density, the bias current, and the coupling coefficient between the laser and the external cavity.

The presence of saturable absorbing defects in semiconductor injection lasers leads, on the one hand, to undesirable self-pulsation and on the other hand, to picosecond pulse generation by passive mode-locking. The latter would have been extremely useful if not for the fact that the absorbing defects in injection lasers cannot be reliably controlled, and that short pulses can be generated only with lasers aged to the point where catastrophic failure is imminent. To circumvent this difficulty, a laser with controllable amount of saturable absorption has been designed and fabricated. The absorber can be controlled by varying the pump current into part of the laser diode. This device can be made to exhibit all the dynamic characteristics of a self-pulsing laser but is otherwise extremely well behaved. It is expected that this device will form the basis of reliable picosecond pulse generation with compact laser diode sources.

Analytical calculations in chapter 5 shed light on the conditions of optical pulse generation. The analysis is based on a simplified saturable absorber model with a delayed photon feedback. The Nyquist diagram technique is used to determine the

stability of the system. It yields closed form solutions for the various conditions (external cavity length, absorber density, bias current, coupling coefficient) under which periodic optical pulse trains are generated spontaneously.

A primary concern for analog modulation is harmonic distortion, which is the subject of chapter 6. It is found analytically that such distortions (even at low modulation frequencies) are closely related to the relaxation oscillation itself, and this is supported by experimental evidence. Self-pulsation can be regarded as an extreme form of relaxation oscillation, and thus one would expect that the harmonic distortion in (even weakly) self-pulsing lasers is extremely severe. Experimental results confirm that this is indeed the case. In addition, intermodulation products between the modulaton signal and the self-pulsation produce anomalous distortion products at low frequencies.

The results of previous studies on the behavior of self-pulsing lasers in external cavities suggest a means of reducing such distortions. By coupling the laser to an external cavity of suitable length, the self pulsation was shown to be quenched. Since relaxation oscillation can be regarded as a milder form of self-pulsation, it follows that by coupling to an external cavity, relaxation oscillation can be suppressed too. Various distortions in analog modulation can consequently be minimized. This has been demonstrated experimentally using a multimode glass fiber as an external cavity. A lens formed on one end of the multimode fiber significantly increases the coupling between the laser and the fiber, which is a key factor in rendering the scheme successful.

For digital transmission, laser diodes are modulated by pseudorandom current

pulses at high rates. Small signal analysis is no longer applicable in this regime, and the rate equations have to be analyzed including the full non-linear terms. Extensive numerical analysis was performed to assess the role relaxation oscillation plays in pulse modulation. The strength of relaxation oscillation is an indication of the stability of the system. An unstable system responds swiftly, but is hard to control; whereas a stable system behaves smoothly but is slow. Relaxation oscillation can be suppressed by the same methods described in analog modulaton, only to sacrifice speed. This can be justified in an analog modulation scheme because it can improve the linearity of the response - which is not of special merit in pulse modulation. In chapter 7, the response of a laser to a long sequence of pseudorandom current pulses was simulated on a computer to study pattern effects and their dependence on bias current and excitation current pulse area. The numerical results and other published experimental data indicate that the highest data rate attainable in pulse modulation of a laser diode is limited primarily by the population relaxation time. This difficulty can be overcome by very precise control of drive current pulse parameters. A scheme free of these limitations is devised using very low threshold lasers and bipolar pulse modulation, and has experimentally achieved 3-4 Gbit/sec pattern-effect-free modulation. Numerical simulation indicates that with improved current pulse generators, even higher bit rates are possible. It is thus assessed that the limitation on the modulation bit rate of laser diodes is technical rather than fundamental.

In most analyses of pulse modulation of laser diode, the uniform rate equations are used which do not account for the transverse mode pattern. Indeed, when pulse modulated at high rates the transverse mode differs significantly from that of the cw profile. This effect is more prominent in gain-guided lasers, where the mode is supported by transient injection of the carriers. This is illustrated by experimental

and theoretical analysis of the transverse mode profile of a transverse junction stripe (TJS) laser under short pulse excitation, the subject of chapter 8.

The superluminescent diode[13] is a close relative of the injection laser : it is a laser without mirrors. Devoid of any optical feedbck, it is essentially a one-pass amplifier of spontaneous emission. The photon and electron distributions are highly non-uniform along the active region, and the common rate equations do not apply in the analyses of the transient response of such a device. In chapter 9, a systematic numerical study using the full "local" rate equations is made on the small signal modulation response of the superluminescent diode. The results indicate that under some conditions the superliminescent diode can excel usual laser diodes in modulation performance, though at the moment it is not obvious how these conditions can be practically realized.

References - Chapter 1

1. D.Gloge, **Optical Fiber Technology**, IEEE Press, 1976. For a most recent overview of this field, see the October issue of **Proceedings** of IEEE, 1980.

2. Almost every basic aspect of semiconductor lasers can be found in the following two books : H.C.Casey and M.B.Panish,**Heterostructure Lasers**, Parts **A** and B , Academic Press 1978; H.Kressel and J.K.Butler, **Semiconductor Lasers and Heterojunction LEDs**, Academic Press 1979.

3. H.W.Yen and L.Figueroa, Hughes Research Lab. quarterly report 1 for contract N00173-78-C-0192.

4. G.Lutes, Telecommunication and Data Acquisition Progress Report, **42-59** , Jet Propulsion Lab. (1980)

5. P.T.Ho, L.A.Glasser, E.P.Ippen and H.A.Haus, Appl. Phys. Lett., **33** ,241 (1978)

6. E.P.Ippen, D.J.Eilenberger and R.W.Dixon, Appl. Phys. Lett., **37**, 267 (1980)

7. D.A.Kleinman, Bell Sys. Tech. Jour., **43**, 1505 (1964)

8. J.B.Moreno, J. Appl. Phys., **48**, 4152 (1977)

9. N.G.Basov, IEEE J. Quant. Electron., **QE-4**, 855 (1968)

10. J.A.Copeland, Electron Lett., **14**, 809 (1979)

11. N.Chinone, K.Aiki, M.Nakamura and R.Ito, IEEE J. Quant. Electron., **QE-14**, 625 (1978)

12. D.P.Wilt and A.Yariv, unpublished.

13. T.P.Lee, C.A.Burrus and B.I.Miller, IEEE J. Quant. Electron., **QE-9**, 820 (1973)

14 J.AuYeung, private communication.

CHAPTER 2

LASER KINETICS, RATE EQUATIONS AND THEIR RANGE OF APPLICABILITY

Laser dynamics are commonly described by a pair of equations governing the photon and carrier densities inside the laser medium. This pair of equations, known as the laser rate equations, will be used extensively in the following chapters. It therefore seems appropriate, in this chapter, to summarize the results of Moreno[8] regarding the conditions under which the rate equations are applicable.

2.1 The "local" rate equations

The starting point for the analysis of laser kinetics involves the coupled rate equations which are basically local photon and injected carrier conservation equations[1] :

$$\frac{\partial X^+}{\partial t} + c\frac{\partial X^+}{\partial z} = c\kappa N X^+ + \beta\frac{N}{\tau_s} \qquad 2.1(a)$$

$$\frac{\partial X^-}{\partial t} - c\frac{\partial X^-}{\partial z} = c\kappa N X^- + \beta\frac{N}{\tau_s} \qquad 2.1(b)$$

$$\frac{dN}{dt} = \frac{J}{ed} - \frac{N}{\tau_s} - \kappa c N (X^+ + X^-) \qquad 2.1(c)$$

where X^+ and X^- are the forward and backward propagating photon densities (which are proportional to the light intensities), N is the carrier density, c is the group velocity of the waveguide mode, κ is the gain constant in cm^{-1}/(unit carrier density), β is the fraction of spontaneous emission entering the lasing mode, τ_s is the spontaneous recombination lifetime of the carriers, z is the distance along the active medium with z=0 at the center of the laser, J is the pump current density, e is the electronic charge and d the thickness of the active region in which the carriers

are confined. The following simplifying assumptions are made in writing down (2.1):

1. The quantities $X^{\pm}$ describe the photon number densities at a given position in the laser cavity, at time t, integrated over the lasing linewidth of the mode of oscillation, which is assumed to be much narrower than the homogeneously broadened laser transition line profile;

2. the gain coefficient (κN) is a linear function of the injected carrier density N;

3. variations of the carrier and photon densities in the lateral dimension are not significant, and

4. diffusion of carriers can be ignored.

(1) and (2) are very reasonable assumptions which can be deduced from detailed analysis[2-4]. The representation of the semiconductor laser as a homogeneously broadened system can also be derived from basic considerations [5]. Transverse modal and carrier diffusion effects, ignored in assumptions (3) and (4), can lead to modifications of the dynamic behavior of lasers[6,7]. This will be discussed in chapter 3.

Equation (2.1) is to be solved subject to the boundary conditions

$$X^{-}(\frac{L}{2}) = RX^{+}(\frac{L}{2}) \qquad 2.2(a)$$

$$X^{+}(\frac{-L}{2}) = RX^{-}(\frac{-L}{2}) \qquad 2.2(b)$$

where L is the length of the laser, and R is the reflectivity of the end mirrors. The steady state solution of (2.1) gives the static photon and electron distributions inside the laser medium, and has been solved by Casperson[2]. The solution is summarized as follows, where the zero subscript denotes steady state quantities :

$$X_0^+(z) = \frac{ae^{u(z)} - \beta}{\kappa c \tau_s} \qquad 2.3(a)$$

$$X_0^-(z) = \frac{ae^{-u(z)} - \beta}{\kappa c \tau_s} \qquad 2.3(b)$$

where a is a quantity given by the following transcendental equation:

$$(1-2\beta)\zeta + 2a\sinh\zeta = \frac{gL}{2} \qquad 2.4$$

$$\textit{where} \quad \zeta = \tfrac{1}{2}\sqrt{\frac{(R-1)^2\beta^2}{(Ra)^2} + \frac{4}{R}} + (R-1)\frac{\beta}{Ra} \qquad 2.5$$

and $g = \kappa J_0 \frac{\tau_s}{ed}$ is the unsaturated gain, and u(z) is given transcendentally by

$$(1-2\beta)u(z) + 2a\sinh u(z) = gz \qquad 2.6$$

The electron density $N_0(z)$ is given by

$$\kappa c N_0(z) = \frac{g}{1+2a\cosh u(z) - 2\beta} \qquad 2.7$$

Fig. 2.1 shows plots of $X_0^+(z), X_0^-(z)$ and $g_0(z) = \kappa c N_0(z)$ for a 300μm laser with three values of end mirror reflectivities, (a) 0.3, (b) 0.1 and (c) 0.9. The high non-uniformity in the distributions becomes apparent at low reflectivities.

2.2 Spatially averaged rate equations and their range of validity

Equations (2.1) constitute a set of three coupled non-linear differential equations in

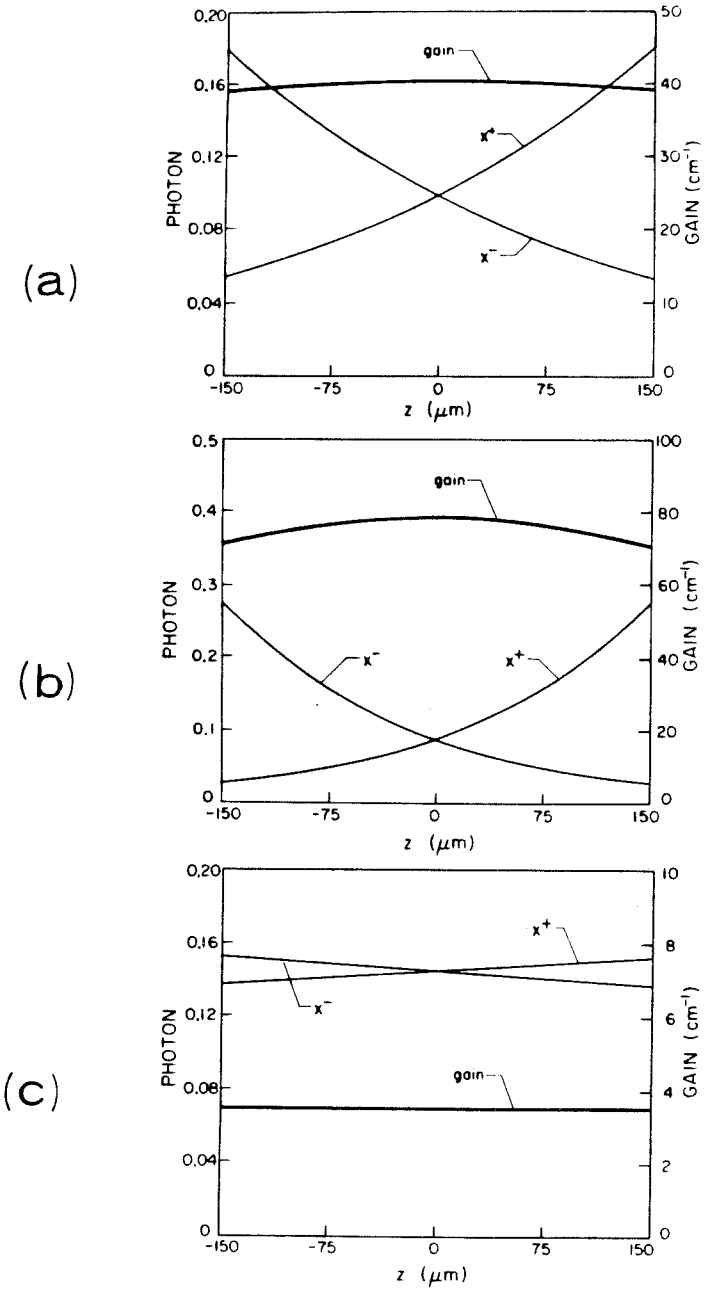

Figure 2.1. *Static photon and electron density distributions inside laser diodes with mirror reflectivities of (a) 0.3, (b) 0.1 and (c) 0.9.*

two variables and do not lend themselves to easy solution. Considerable simplification can be made if the spatial variable is integrated over the length of the laser. Such simplification is valid only when the end mirror reflectivity is "sufficiently large". A more precise definition of the range of validity is given in the following, using the approach of Moreno[8].

We start by integrating equations (2.1(a)) and (2.1(b)) in the z variable, resulting in

$$\frac{dX^{+*}}{dt} + c\left(X^{+}\left(\frac{L}{2}\right) - X^{+}\left(\frac{-L}{2}\right)\right) = c\kappa(NX^{+})^{*} + \beta\frac{N^{*}}{\tau_s} \qquad 2.8(a)$$

$$\frac{dX^{-*}}{dt} - c\left(X^{-}\left(\frac{L}{2}\right) - X^{-}\left(\frac{-L}{2}\right)\right) = c\kappa(NX^{-})^{*} + \beta\frac{N^{*}}{\tau_s} \qquad 2.8(b)$$

where * denotes the spatial average $\int_{\frac{-L}{2}}^{\frac{L}{2}} \frac{dz}{L}$. Adding equations (2.8(a)) and (2.8(b)),

$$\frac{dP^{*}}{dt} + \frac{2c(1-R)P(\frac{1}{2}L)}{L(1+R)} = c\kappa(NP)^{*} + 2\beta\frac{N^{*}}{\tau_s} \qquad 2.9$$

where $P = X^{+} + X^{-}$ is the total local photon density and the boundary conditions (2.2) have been used. Equation (2.1(c)) integrates straightforwardly to

$$\frac{dN^{*}}{dt} = \frac{J}{ed} - \frac{N^{*}}{\tau_s} - \kappa c\,(NP)^{*} \qquad 2.10$$

where we have assumed a uniform pump current density; J = constant in z.

Introducing factors f_1 and f_2 as follows:

$$f_1 = \frac{(NP)^*}{N^*P^*} \tag{2.11}$$

$$f_2 = \frac{P(\frac{1}{2}L)}{P^*(1+R)} \tag{2.12}$$

one can write the spatially averaged rate equations (2.9) and (2.10) in the following form:

$$\frac{dP^*}{dt} = c\kappa f_1 N^* P^* - 2c(1-R) f_2 \frac{P^*}{L} + 2\beta \frac{N^*}{\tau_s} \tag{2.13}$$

$$\frac{dN^*}{dt} = \frac{J}{ed} - \frac{N^*}{\tau_s} - \kappa c f_1 N^* P^* \tag{2.14}$$

which are recognized as the commonly used rate equations[9,10] if the conditions

$$f_1 = 1 \tag{2.15}$$

$$f_2 = -\frac{1}{2}\frac{\ln R}{1-R} \tag{2.16}$$

are satisfied. The first of these conditions requires, for the quantities N and P, that the spatial average of the product equals the product of the spatial averages. This condition is not satisfied in general, but it will be true if the electron density N is uniform, as in the case when R approachs unity, which is apparent from Fig. 2.1(c). The second condition requires the photon loss rate (eqn. (2.13)) to be inversely proportional to the conventional photon lifetime. It will also be satisfied if R is very close to unity, since both (2.12) and (2.16) converge to ½ in this limit.

A more precise delineation of the range of the applicability of conditions (2.15)

and (2.16) is obtained by calculating f_1 and f_2 from exact steady state solutions (2.3) through (2.7), and comparing them with (2.15) and (2.16). From (2.3) and (2.7),

$$f_1 = \frac{L \int \frac{P}{1+\kappa c \tau_s P} dz}{\int \frac{dz}{1+\kappa c \tau_s P} \int P \, dz} \qquad 2.17$$

$$f_2 = \frac{LX^+(\frac{1}{2}L)}{\int P \, dz} \qquad 2.18$$

where the integrals are evaluated over the length of the laser. These integrals can be numerically evaluated using eqns. (2.3) through (2.7), and the results are shown in Figs 2.2 and 2.3. Fig. 2.2 shows plots of f_1 and $\frac{1}{f_2}$ as a function of end mirror reflectivity R, the calculation was done with the laser biased above threshold. The dotted lines are the "ideal" values of f_1 and f_2 given by eqns. (2.15) and (2.16). The figure indicates that the usual rate equations will hold for R larger than approximately 0.2. Fig. 2.3 shows plots of $\frac{1}{f_2}$ as a function of the pumping level, expressed in terms of the total unsaturated gain gL. It shows that the usual rate equations are not valid below the lasing threshold as well as for low reflectivities or a low spontaneous emission factor, β.

The above results lead to the conclusion that the simple rate equations , expressed in the following form (where the N and P now denote averaged quantities):

$$\frac{dN}{dt} = \frac{J}{ed} - \frac{N}{\tau_s} - \alpha NP \qquad 2.19$$

$$\frac{dP}{dt} = \alpha NP - \frac{P}{\tau_p} + \beta \frac{N}{\tau_s}$$

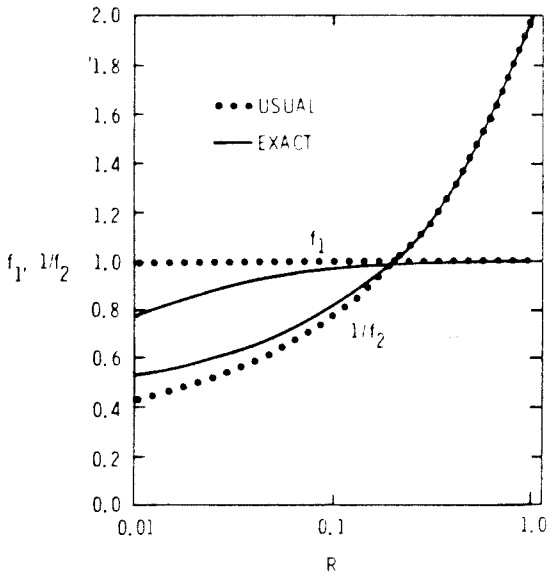

Figure 2.2. *Variations of* f_1 and $\frac{1}{f_2}$ with R, when $\beta \leqq 10^{-3}$ and gl > 10.

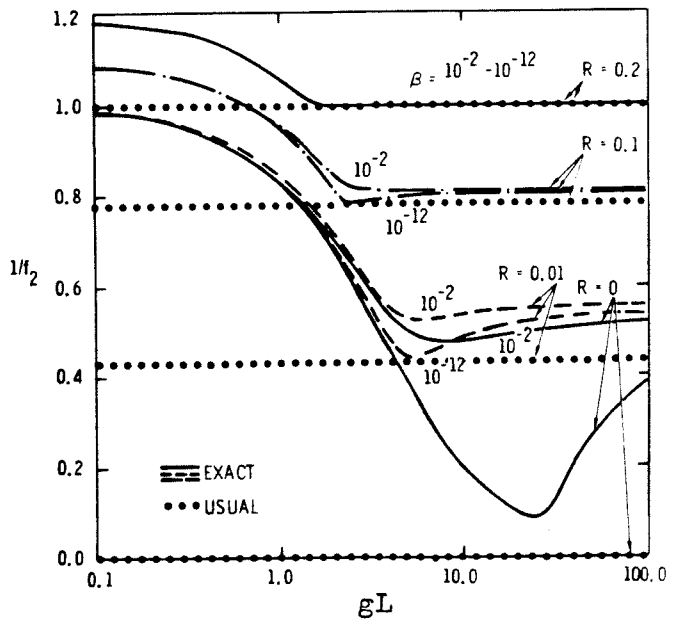

Figure 2.3. *Dependence of* $\frac{1}{f_2}$ *on the parameters* gL, β *and* R.

2.20

($\frac{1}{\tau_p} = \frac{c}{L}\ln\frac{1}{R}$ is the classical photon lifetime and $\alpha=\kappa c$) will hold if the end mirror reflectivity is above 0.2 and the laser is above threshold. The spontaneous emission factor β in (2.20) is a factor of two higher than that defined in (2.1) due to the inclusion of photons propagating in both directions. Common GaAs lasers, with the mirrors formed by the cleaved crystal facets, have a reflectivity of 0.31 and are thus well within the scope of equations (2.19) and (2.20). In a later chapter (chapter 9) describing the kinetics of superluminescent lasers, the exact small signal version of (2.1) will be solved and it will be found that (2.19) and (2.20) can very accurately describe the small signal frequency response of the laser for reflectivities as low as 10^{-3}. This is certainly not expected from any physical standpoint and serves as a surprise bonus for the simplification.

Another factor that can render the spatially-uniform assumption invalid is when "fast" phenomena, occurring on the time scale of a cavity transit time, are being considered. It is obvious that the "cavity lifetime" and the concept of cavity modes, appearing in eqn. (2.20), are no longer applicable on that time scale. In common semiconductor lasers where the cavity length is approximately 300 μm, the cavity transit time is about 3.5 ps. The usual rate equations are therefore not applicable in describing phenomena shorter than about 5 ps, or at modulation frequencies higher than 60 GHz.

In the following chapters, we shall make heavy use of equations (2.19) and (2.20) which will serve as the basis for most of the analysis of the modulation characteristic of lasers.

References - Chapter 2

1. W.E.Lamb, Phys Rev., **134A**, 1429 (1964); A.Icsevgi and W.E.Lamb, Phys Rev., **185A**, 519 (1969).
2. L.W.Casperson, J. Appl. Phys., **46**, 5194 (1975).
3. F.Stern, IEEE J. Quant. Electron., **QE-9**, 290 (1973).
4. H.Kressel and J.K.Butler, **Semiconductor Lasers and Heterojunction LEDs** ,pp 77, Academic Press 1977.
5. R.H.Pantell and H.E.Puthoff, **Fundamentals of Quantum Electronics** , pp294, Wiley 1969.
6. N.Chinone, K. Aiki, M.Nakamura and R.Ito, IEEE J. Quant. Electron., **QE-14**, 625 (1978).
7. D.P.Wilt and A.Yariv, to be published.
8. J.B.Moreno, J. Appl. Phys., **48**, 4152 (1977).
9. D.A.Kleinman, Bell Sys. Tech. Jour., **43**, 1505 (1964),
10. R. Salathe, C.Voumard and H.Weber, Opto-electron., **6**, 451 (1974).

CHAPTER 3

TRANSIENT RESPONSE AND SMALL SIGNAL MODULATION CHARACTERISTICS OF SEMICONDUCTOR INJECTION LASERS

Most type of lasers emit a series of sharp optical spikes in response to a step increase in the excitation level, and continue to "ring" for some time before the output settles to a steady state value[1]. This phenomenon, called relaxation oscillation, also occurs in some semiconductor lasers . The frequency of the ringing, due to the small size of the lasers and the short spontaneous lifetime (a few nanoseconds), is higher than those in most other types of lasers - in the GHz range. This presents a problem in high speed digital modulation of semiconductor lasers in optical communication, since the highly irregular spiking can interfere with the bit pattern. This temporal instability is manifested as a sharp resonance in the modulation frequency response of the laser, at the same frequency as that of the ringing. This puts an upper frequency limit on the analog modulation of the laser diode. However, injection lasers of different structures exhibit relaxation oscillations of different strengths, and some do not exhibit any. This can be accounted for by two features unique to injection lasers: that carriers can diffuse laterally within the active region, and that injection lasers have an unusually high amount of spontaneous emission entering the lasing mode due to the waveguiding structure. Both of these factors vary with laser structures, and can be controlled to some extent by pertinent laser design. In this chapter, we shall examine and compare some basic small signal modulation responses in lasers of different structures. In sections 3.1 and 3.2, the well known analytic results for the steady state and transient response of semiconductor lasers are summarized. In sections 3.3 through 3.5, previous experimental results on the transient characteristics and carrier diffusion effects are summarized and are compared with our experimental results on a number of laser structures. In section 3.6, results on ultimate limits in the modulation

response of GaAs lasers, drawn from basic considerations, are presented.

3.1 Steady state characteristics of injection lasers

Relaxation oscillation in semiconductor lasers and its frequency dependence on the pump current can be accurately predicted by the simple spatially-uniform rate equations, described in chapter 2, eqns. (2.19) and (2.20). In this section, we first examine the steady state solution of the rate equations which serves to illustrate the basic light versus pump current characteristics of an ideal injection laser. The rate equations are (eqn. (2.19) and (2.20)):

$$\frac{dN}{dt} = J - N - (N - N_{om})P \qquad 3.1(a)$$

$$\frac{dP}{dt} = \gamma((N - N_{om})P - P + \beta N) \qquad 3.1(b)$$

where, for convenience, the variables have been normalized as follows:

N, the electron density and N_{om}, the electron density for transparancy , have been normalized by $\frac{1}{\alpha\tau_p}$,

P, the photon density, has been normalized by $\frac{1}{\alpha\tau_s}$,

J, the pump current, has been normalized by $\frac{ed}{\alpha\tau_s\tau_p}$,

t, time, has been normalized by τ_s,

and $\gamma = \frac{\tau_s}{\tau_p}$, β = the fraction of spontaneous emission entering the lasing mode. An additional parameter, N_{om}, has been added in the stimulated emission terms in (3.1(a)) and (3.1(b)). This is a more accurate description of stimulated gain in GaAs, where the electron density must exceed a certain level for the medium to exhibit

positive gain. The inclusion of N_{om} in the rate equations would introduce an offset in the variable N, and otherwise would not affect the physics of the system in a significant way (except for an offset in the threshold current). Therefore in some later chapters when simplicity is desired, N_{om} will be set, without loss of generality, to zero.

Typical values of the parameters listed above are as follows[2]: τ_s = 4 ns, τ_p = 2 ps, d = 0.2 μm, $\alpha = 2.8\times10^{-6} cm^3 sec^{-1}$, $N_{om} = 7.5\times10^{17} cm^{-3}$, β varies between 10^{-5} to 10^{-3}, depending on the laser structure and guiding mechanism. With these numbers, γ = 2000 and N_{om} = 2.5. The steady state solution of (3.1), in the limit $\beta \rightarrow 0$, assumes the following simple form (where the zero subscript denotes steady state quantities):

$$P_0 = 0, \quad N_0 = J \qquad J < N_{om}+1 \tag{3.2(a)}$$

$$P_0 = J - (N_{om}+1), \quad N_0 = N_{om}+1 \qquad J > N_{om}+1 \tag{3.2(b)}$$

The optical output (proportional to the photon density) remains at zero up to the threshold pumping level, and increases linearly with further increase in the pump current. The electron density is clamped to the value $N_{om}+1$ when pumped above a current density equal to $N_{om}+1$, which is defined to be the threshold current density, J_{th}. When the laser is above threshold, all the electrons injected into the active region recombine to emit photons. The solutions are slightly different when one takes into account spontaneous emission, whose major effect is to "smooth out" the threshold point. The steady state solutions with $\beta \neq 0$ are, expressed to the lowest order in β:

above threshold, $J >> N_{om}+1$

$$N_0 = (N_{om}+1)-\beta(\frac{N_{om}+1}{J-N_{om}+1}) \qquad 3.3(a)$$

$$P_0 = J-(N_{om}+1)+\beta\frac{(N_{om}+1)(J-N_{om})}{J-N_{om}+1} \qquad 3.3(b)$$

at threshold, $J = N_{om}+1$

$$N_0 = N_{om}+1-\sqrt{(N_{om}+1)\beta} \qquad 3.3(c)$$

$$P_0 = \sqrt{(N_{om}+1)\beta} \qquad 3.3(d)$$

and below threshold, $J << N_{om}+1$

$$N_0 = J(1+\beta\frac{J-N_{om}}{J-N_{om}-1}) \qquad 3.3(e)$$

$$P_0 = \frac{\beta J}{N_{om}+1-J} \qquad 3.3(f)$$

Figure 3.1 shows plots of the electron density and photon density as a function of bias current, for the cases $\beta = 0$ and $\beta \neq 0$. The approximate formulas (3.3(a) - (f)) agree with the exact results extremely well except near threshold.

3.2 Relaxation oscillation and the influence of spontaneous emission on the transient behavior

Relaxation oscillation results from the interplay between the optical field and the population inversion, as governed by the rate equations (3.1). The relative temporal instability results from the following mechanism: an increase in the optical intensity

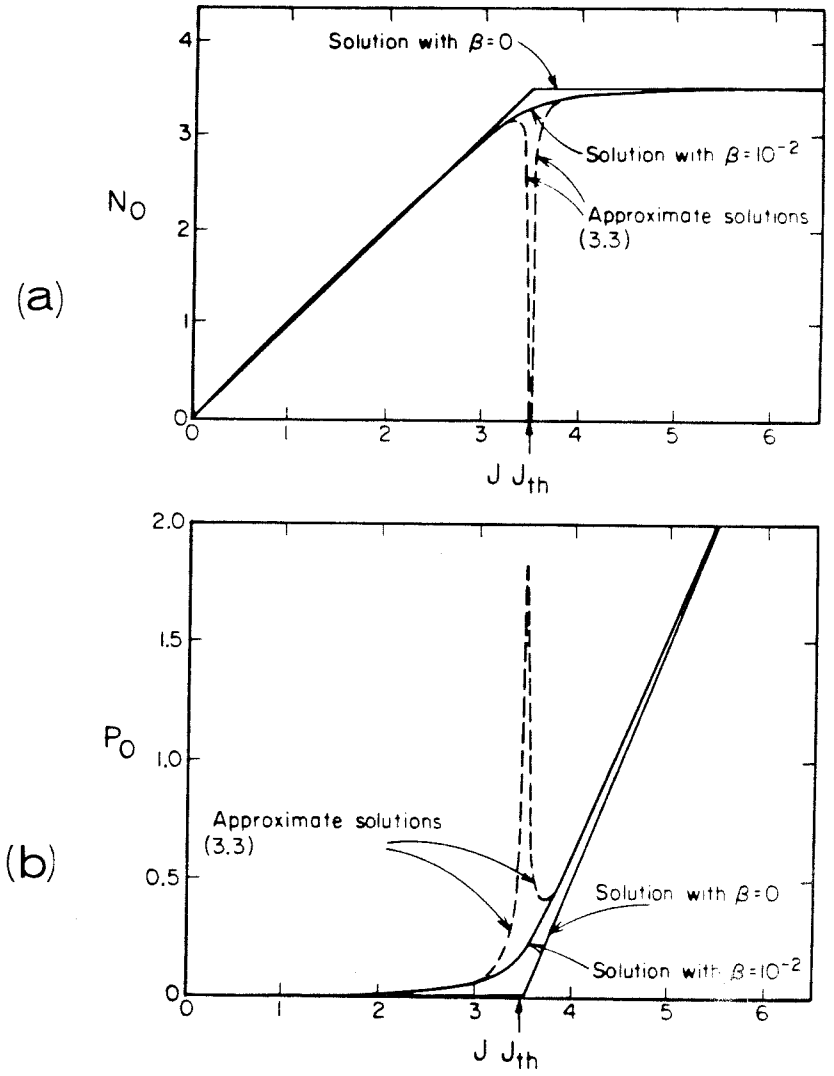

Figure 3.1. *Steady state solutions of the rate equations. Fig 3.1 (a) and (b) show the static carrier and photon densities respectively, versus the pump current J.*

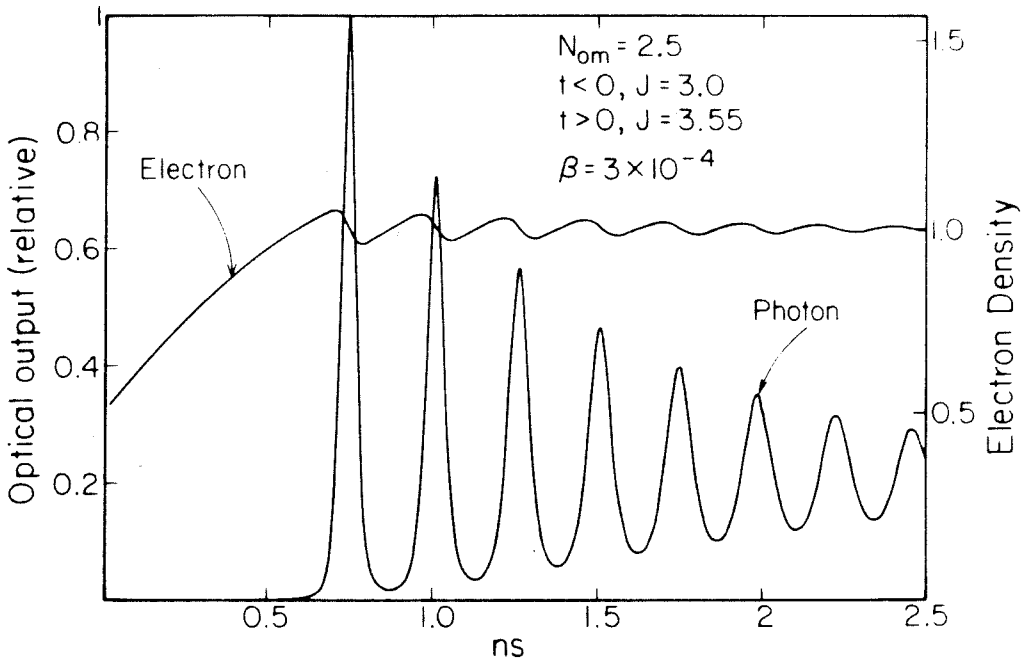

Figure 3.2. *Relaxation oscillation resulting from a step change in the excitation level.*

causes a reduction in the inversion due to the increased rate of stimulated transitions, which in turn causes a reduction in the gain that tends to decrease the field intensity. Fig. 3.2 shows the result of a numerical integration of eqn. (3.1), with $\beta = 10^{-4}$, $N_{om} = 2.5$, so that the threshold current is $J_{th} = 3.5$. The laser was biased at J = 3 before t = 0, and was excited to J = 3.55 after t > 0. One notices that there is a time delay between the onset of the current step and the emission of the first optical pulse. During this time delay the electron density builds itself up from the initial value to above the threshold inversion level.

Much information can be gained about the oscillation behavior by a small signal analysis of the rate equations - a procedure that linearizes (3.1). Writing

$$\begin{aligned} N &= N_0 + n e^{i\omega t} \\ P &= P_0 + p e^{i\omega t} \\ J &= J_0 + j e^{i\omega t} \end{aligned} \qquad 3.4$$

we separate the variables into the steady state part and a "small" sinusoidally varying part. Upon substitution into (3.1) and ignoring products of the "small" terms, one obtains:

$$i\omega n = j - n - nP_0 - (N_0 - N_{om})p \qquad 3.5(a)$$

$$i\omega p = \gamma(nP_0 + (N_0 - N_{om})p + \beta n) \qquad 3.5(b)$$

This represents a conjugate pole-pair type of frequency response, and the system is underdamped, critically damped or overdamped depending on whether F^2 is larger than, equal to or smaller than $4G$, where

$$F = \gamma(N_{om}+1-N_0)+P_0+1 \qquad 3.6(a)$$

$$G = \gamma(1+P_0-(1-\beta)(N_0-N_{om})) \qquad 3.6(b)$$

The underdamped case corresponds to the occurence of relaxation oscillation, and the critically damped case gives a flat frequency response with maximum bandwidth.

One can see easily, with the help of Fig. 3.1, that F increases and G decreases as β is increased. This suggests that with a sufficiently high spontaneous emission factor, the system will be critically damped and relaxation oscillation will eventually cease to occur. This was first pointed out by Boers and Vlaadingerbroek[3]. One can calculate, from eqns (3.5), (3.6) and (3.3), a condition for β to produce critical damping. Expressed to lowest order in $\frac{1}{\gamma}$:

$$\beta_{min} = 2\frac{(J-N_{om}-1)^{\frac{3}{2}}}{1+N_{om}}\gamma^{-\frac{1}{2}} \qquad 3.7$$

A plot of β_{min} vs the pump current J is shown in Fig. 3.3 with γ = 2000 and N_{om} = 2.5. Typical values of β_{min} range between 10^{-3} to 10^{-2}. Fig. 3.4 shows results of numerical calculation of the rate equations, with the same parameters for N_{om} and γ as in Fig 3.2. The system is biased at J = 3.6 at t < 0 and excited by a step current to J = 4.5 at t = 0. The successive increment in β from 2.9×10^{-4} to 1.4×10^{-2} clearly illustrates the damping effect in the response.

Lang and Kobayashi[14] first suggested and experimentally verified that injecting external coherent photons into the laser cavity can have the same effect as having a large spontaneous emission factor, thereby suppressing the relaxation oscillation.

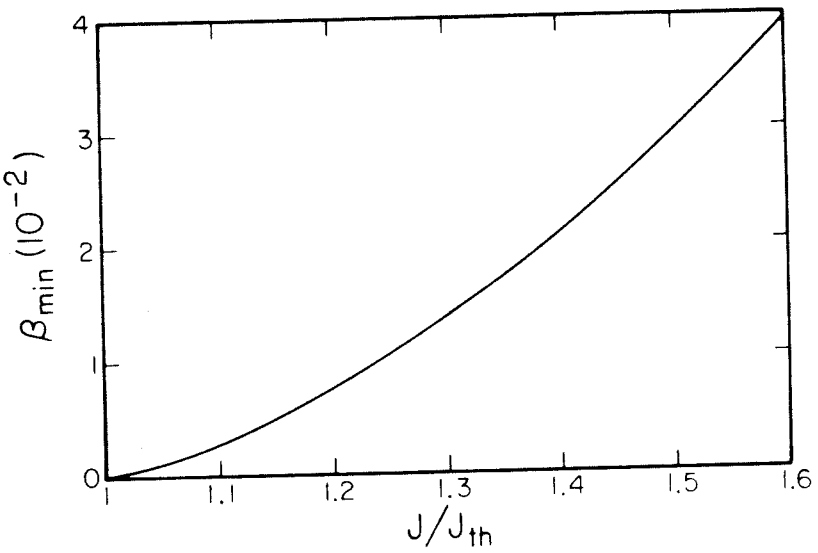

Figure 3.3. *The minimum amount of β for quenching relaxation oscillation.*

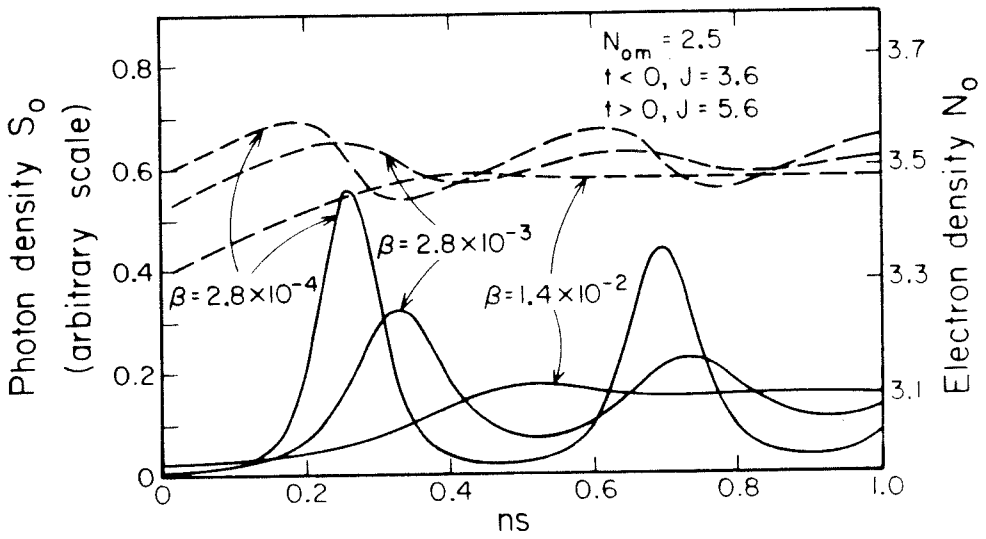

Figure 3.4. *Transient responses with various amounts of* β.

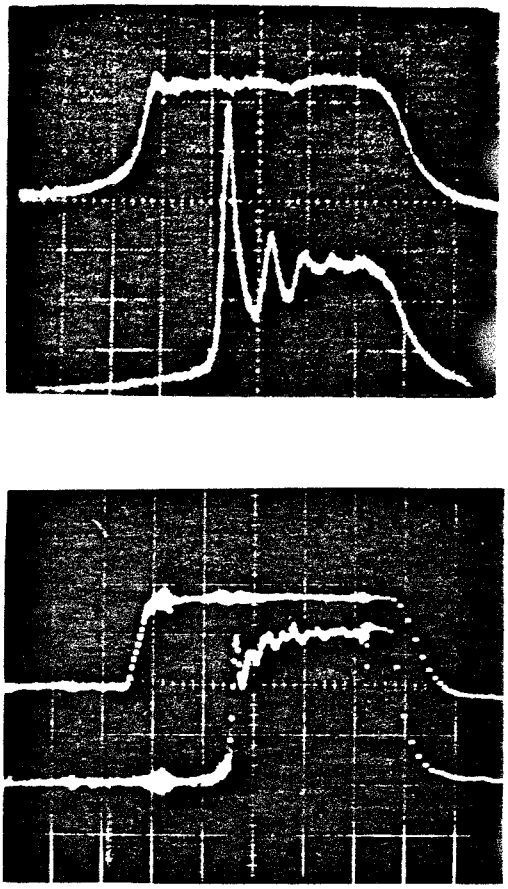

Figure 3.5. *Observed transient responses of (a) proton stripe and (b) CSP laser. Top traces : current, bottom traces : light. Hor. scale : 1ns/div. $I = 1.1I_{th}$ in each case.*

Otsuka[15] gave a detailed analysis of the effect and recently, an integrated version of the device was fabricated[16]. The analysis is done in a straightforward manner by adding an external injection term P_i into the right hand side of the photon rate equation (3.1(b)). Small signal analysis indicates that quenching of the relaxation oscillation occurs for $P_i < 10^{-2}$, ie., injecting 10^{-2} of the photons emitted from a similar laser is sufficient to harness the effect.

3.3 Comparision of transient responses of lasers with various structures

In this section, the transient responses of several types of lasers are compared. Fig. 3.5 shows the actual response of some lasers excited by a current step. Fig 3.5(a) shows the response of a proton bombarded stripe laser[4], which belongs to the general class of stripe geometry lasers[5]. This type of laser has neither carrier nor optical confinement in the transverse direction (along the junction plane), and has a typical stripe width of 10 μm. The transient response of this type of laser shows strong relaxation oscillation. Fig 3.5(b) shows the transient response of a CSP(Channelled Substrate Planar) laser[6], which belongs to a second class of lasers with transverse optical guiding but no transverse carrier confinement. The response shows little relaxation oscillations, and is suitable for medium bit rate (< 1Gbit/sec) optical transmitters. A third important class of lasers has transient responses lying somewhere between the first two classes - the spiking is more pronounced than the second type but less drastic than the first type. This class of lasers, exemplified by the BH(Buried Heterostructure)[7] and the embedded laser[8], have both carrier confinement and optical guiding in the transverse direction. Schematic diagrams of the cross sections of the above three classes of lasers are shown in Fig 3.6(a) - 3.6(e). Another laser structure that exhibits excellent characteristics (in terms of low threshold, single stable transverse and longitudinal mode) is the TJS(Transverse Junction Stripe) laser[9,10], which is different from most lasers in that the carriers

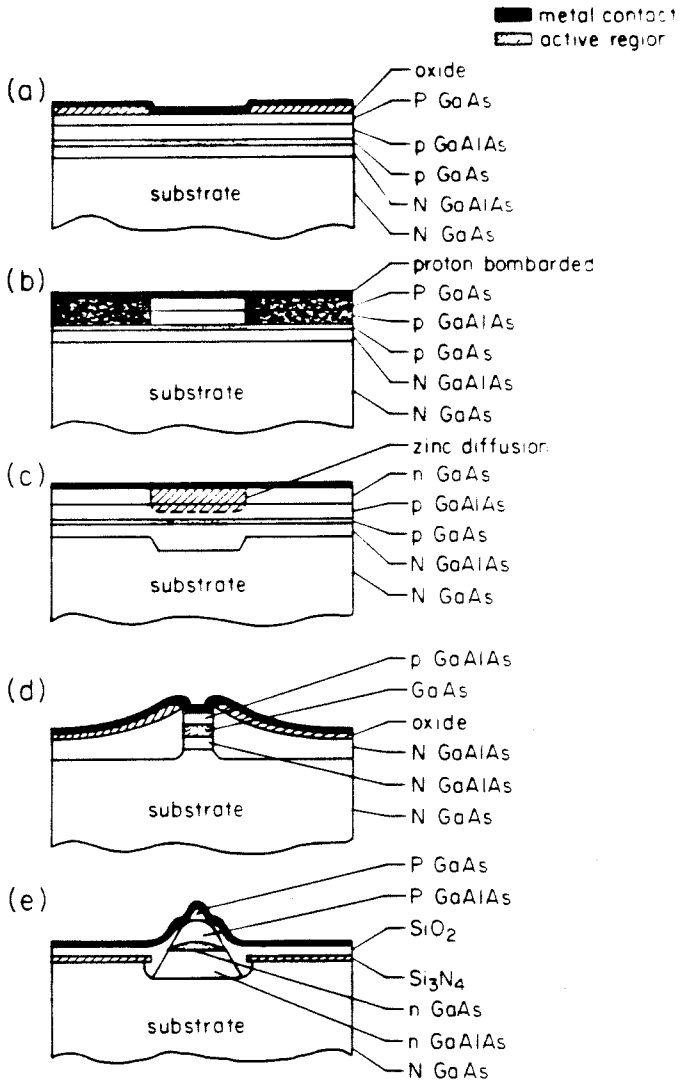

Figure 3.6. *Cross sections of various GaAs injection lasers : (a) simple oxide stripe, (b) proton bombarded stripe, (c) channeled substrate planar (CSP), (d) buried heterostructure (BH) and (e) embedded stripe lasers.*

are injected transversely across a pn homojunction instead of across the GaAs/GaAlAs heterojunctions. This will be discussed in more detail in chapter 8. The transient response of the TJS laser resembles that of the CSP laser and is thus ideal for transmitters.

The different transient behaviors of various lasers can be partly explained by the calculations in section 3.2. The spontaneous emission factor β varies among structures and directly influences the strength of the relaxation oscillation. The calculation of β is done by first evaluating the radiation efficiency of an infinitesimal dipole radiator into the specific optical mode, which is assumed to be known for the laser structure. The total spontaneous emission factor is obtained by integrating the dipole radiation efficiency over the entire carrier distribution[11,12]. This quantity is found to be inversely proportional to the optical mode volume. Therefore, lasers with a tight optical confinement in the transverse direction, such as the BH and the embedded laser, have a high value of β and hence show relatively weak relaxation oscillation. It does not, however, explain why the CSP or the TJS lasers show even weaker relaxation oscillation. This is due to transverse carrier diffusion effects, which have been neglected in the simple rate equation approach. The separate roles played by spontaneous emission and lateral carrier diffusion in the transient response were first clarified by Chinone et.al.[13], by numerically solving the full rate equations including the diffusion term, and comparing them to real lasers. The results will be summarized in the next section.

3.4 Effect of lateral carrier diffusion on the transient characteristics of various types of lasers

Except for those lasers which have built-in structures for confining carriers in the lateral direction such as the BH and the embedded lasers, lateral carrier diffusion

within the active layer plays a role, sometimes very significant and sometimes less so, in dampening the transient spiking. The mechanism can be visualized through the following heuristic consideration, suggested by Wilt and Yariv[17]: assuming that, for simplicity, the injection current and the optical mode are in the form of a δ-function in the transverse direction along the junction plane - ie., in the limit of zero stripe width and infinite optical confinement. The diffusion of carriers in the transverse direction, neglecting the optical field, is described by the following:

$$\frac{\partial N}{\partial t} = D\frac{\partial^2 N}{\partial x^2} + J(x,t) - \frac{N}{\tau} \qquad 3.8$$

where N is the carrier density, J is the injection current : J(x,t) = J(t) δ(x), x is the transverse coordinate, D is the diffusion constant, and τ is the recombination lifetime. The optical mode, having a transverse distribution of δ(x), sees a gain proportional to N(x=0,t). Separating the variables into a steady state and a sinusoidally varying part,

$$N = N_0(x) + n(x)e^{i\omega t} \qquad 3.9(a)$$

$$J = J_0(x) + j(x)e^{i\omega t} \qquad 3.9(b)$$

the small signal diffusion equation reads:

$$D\frac{\partial^2 n}{\partial x^2} - n\left(\frac{1}{\tau} + i\omega\right) = j\,\delta(x) \qquad 3.10$$

which has the solution

$$n(x) = \frac{jL}{2D}e^{\frac{-|x|}{L}} \qquad 3.11$$

where $L=\sqrt{D\tau}$ is the small signal diffusion length, and $\frac{1}{\tau'} = \frac{1}{\tau} + i\omega$. The amplitude of the sinusoidal modulation in the optical mode gain is proportional to n(0), given by

$$n(0) = \frac{j}{2D}\sqrt{D\frac{\tau}{1+i\omega\tau}} \qquad 3.12$$

Hence, diffusion effectively introduces a "one-half pole" in the modulation response and acts to damp the resonance. A self-consistent analysis, including the optical field, has been worked out by Wilt and Yariv[17] in this limit of zero stripewidth.

Chinone el.al.[13] classified injection lasers into three main categories, in the same way as that described in section 3.3: type I, those with neither carrier nor optical confinement in the lateral direction; type II, those with lateral optical confinement but with no lateral carrier confinement; and type III, those with both lateral carrier and optical confinement. The analysis was based on the following local rate equations which include spatial dependence in the lateral direction:

$$\frac{\partial N}{\partial t} = D\frac{\partial^2 N}{\partial x^2} + \frac{J(x,t)}{ed} - \frac{N}{\tau} - g_t P(x) \qquad 3.12(a)$$

$$\frac{d}{dt}\int_{-\infty}^{\infty} P(x)dx = \int_{-\infty}^{\infty}(\Gamma g_t - \frac{1}{\tau_p})P(x)dx + \beta\int_{-\infty}^{\infty}\frac{N}{\tau}dx \qquad 3.12(b)$$

where P(x) is the optical mode profile, Γ is the confinement factor, g_t is the local gain coefficient, and β is the spontaneous emission factor as defined before. The optical mode profile P(x) is solved independently in the case when a built-in waveguide exists, and must be solved self-consistently with the carrier distribution N(x) when guiding is provided by the gain profile. The system (3.12) is excited with a step increase in the pump current, and the strengths of the resulting relaxation oscillations, defined by the peak to valley ratio of the first spike of the relaxation

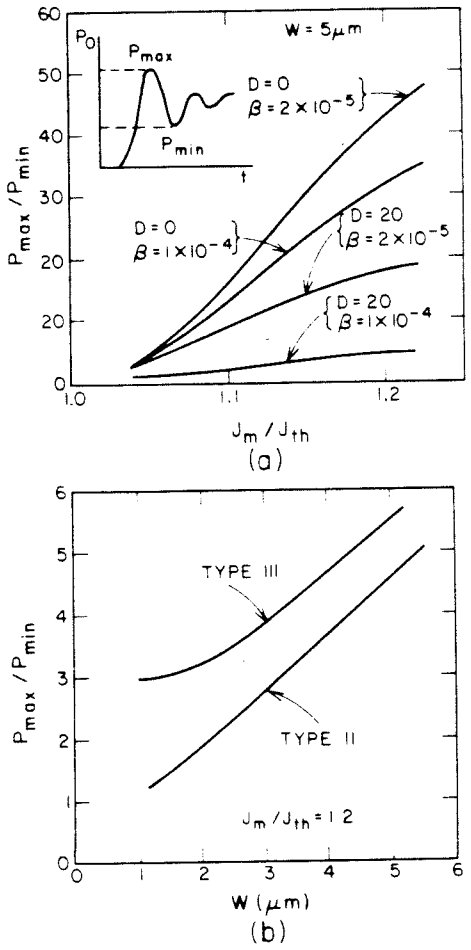

(a)

(b)

Figure 3.7. *Comparison of the strengths of relaxation oscillations with (a) various β and diffusion coefficients D, for type II lasers, and (b) between type II and type III lasers.*

oscillation, $\frac{P_{max}}{P_{min}}$, are shown in Fig 3.7(a) and (b) for various type of lasers. Fig 3.7(a) shows the relaxation oscillation strength vs pump current for type II lasers (e.g. CSP) of 5 μm stripe width. It can be seen that both carrier diffusion and spontaneous emission have substantial effects on the strength of the relaxation oscillation. However, it is also observed that carrier diffusion is more effective in this respect. In type III lasers (BH, embedded) no carrier diffusion occurs and spontaneous emission is the primary factor for reducing the spiking. Fig 3.7(b) shows a comparision between type II and type III lasers of various stripe widths. Narrow stripe lasers always show larger damping because, for type III lasers, the spontaneous emission factor is larger and for type II lasers, the effect of diffusion is more substantial. For type I lasers with stripe widths larger than a diffusion length of the carriers, neither carrier diffusion nor spontaneous emission are significant enough to reduce spiking, and $\frac{P_{max}}{P_{min}}$ of over 100 can be observed.

Summarizing the above findings: in lasers whose stripe width is narower than ~10 μm, carrier diffusion plays a heavier role than spontaneous emission in suppressing the relaxation oscillation, especially for lasers without a lateral carrier confinement structure. On the other hand, the fraction of spontaneous emission going into the lasing mode is primarily responsible for suppressing the spiking in lasers with a lateral carrier confinement structure.

3.5 Small signal analog modulation response of injection lasers

The small signal analysis of section 3.2 leads to a conjugate-pole-pair type of frequency response. Equation (3.5) leads to the following transfer function for the small signal photon density:

$$p = \frac{j\gamma(P_0+\beta)}{(i\omega+1+P_0)(i\omega+\gamma(1+N_{om}-N_0))+\gamma(N_0-N_{om})(P_0+\beta)} \qquad 3.13$$

The corner frequency of this response function occurs at

$$f_r = \frac{1}{2\pi}\sqrt{\gamma(J_0-1)} + \textit{higher order terms in } \beta \qquad 3.14$$

where J_0 is the d.c. bias current (normalized by J_{th}, the threshold current), $\gamma = \frac{\tau_s}{\tau_p}$, and f_r is normalized by $\frac{1}{\tau_s}$ as mentioned before. The spontaneous emission factor β determines the Q of the resonance but has no significant effect on the corner frequency itself. The phase of the modulated output, in the case of a high Q, undertakes an abrupt transition from 0° to −180° at the corner frequency, but exhibits a soft transition in the case of a low Q. At low bias currents, a prominent resonance peak seldom exists, because a very low β is sufficient to produce a very low Q. All these features follow directly from the typical characteristics of a second order transfer function.

The kinds of amplitude and phase response described above are actually observed in various types of injection lasers, and the corner frequency is found to follow the square-root dependence of (3.14) extremely well. Fig 3.8(a) and (b) shows results of measurements on a proton stripe laser. The relationship between the phase and the Q of the amplitude response is evident. Fig 3.9 shows the amplitude and phase response of a TJS laser. The frequency response is relatively flat, as would be expected from the absence of the relaxation oscillation as described in section 3.3. Fig 3.10 shows plots of the corner frequency vs $\sqrt{\frac{J}{J_{th}}-1}$ for the two lasers. The modulation bandwidth of the two lasers are very similar, but the flat response of the

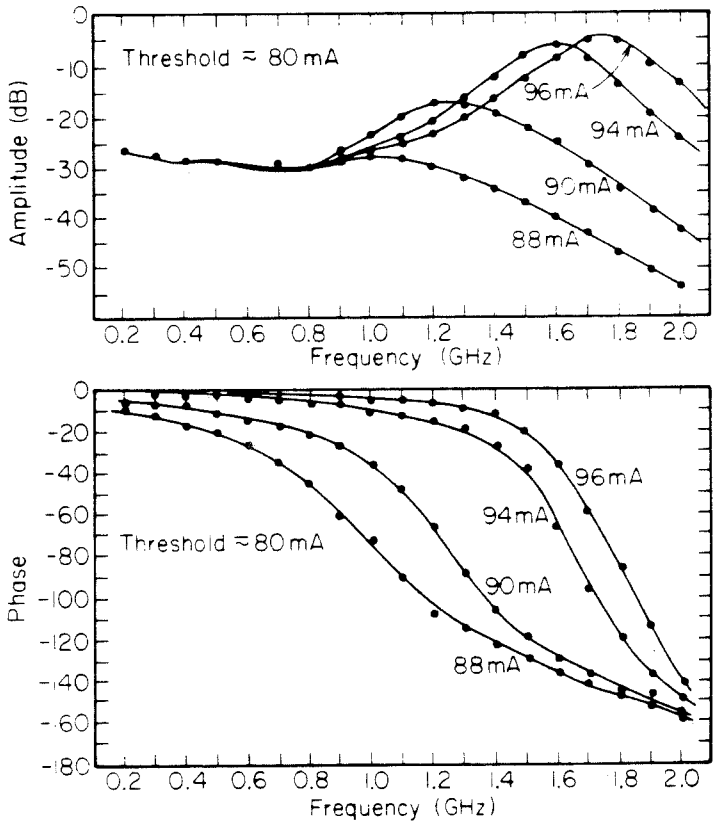

Figure 3.8. *Measured (a) amplitude and (b) phase responses of a proton stripe laser.*

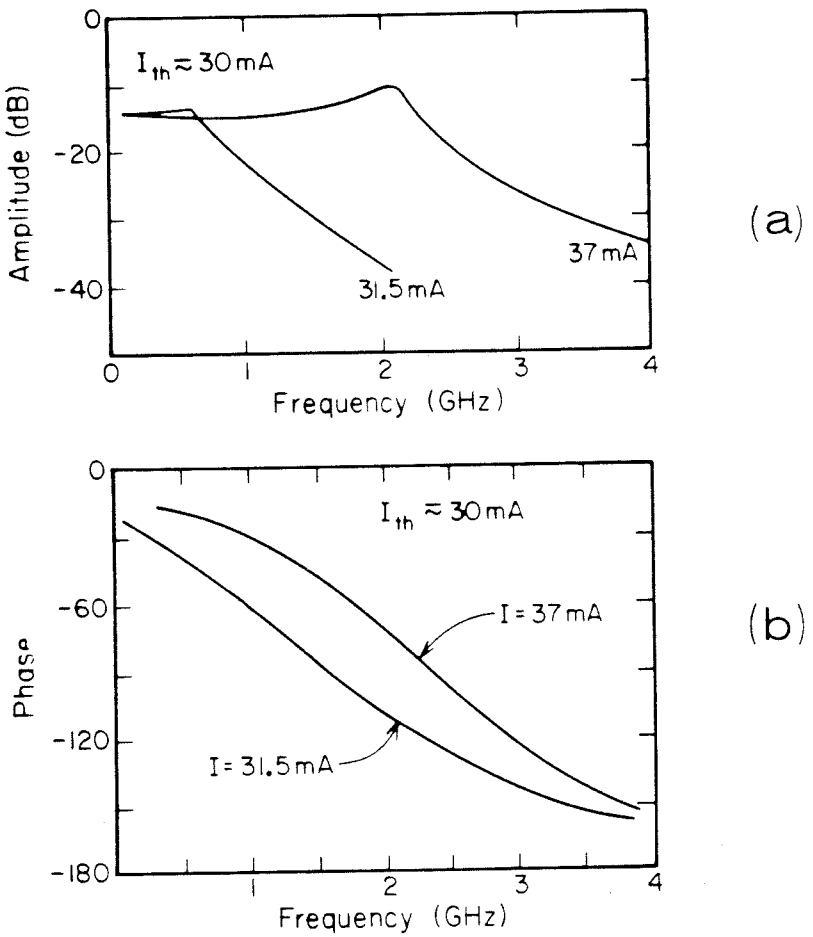

Figure 3.9. *Measured (a) amplitude and (b) phase responses of a TJS laser.*

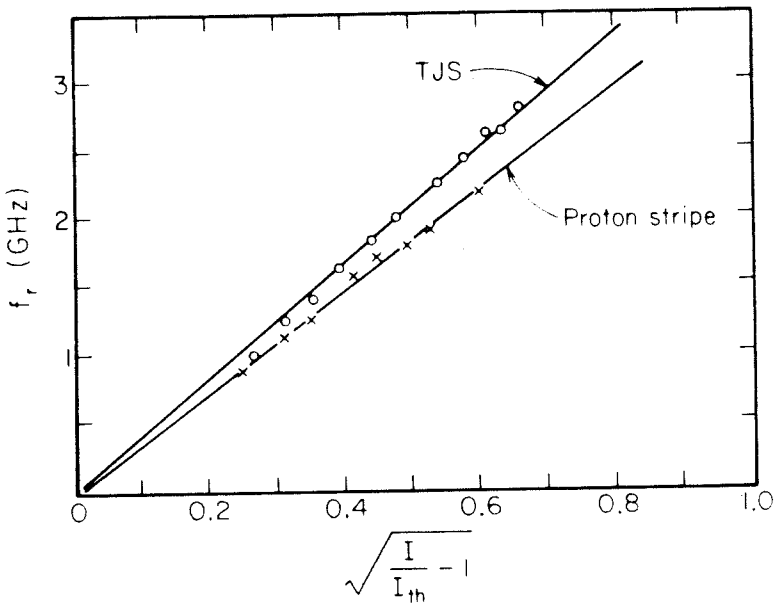

Figure 3.10. *Measured corner frequencies of a proton stripe and a TJS laser vs pump current.*

TJS laser is certainly a more desirable feature, not to mention its much lower threshold current(≈ 30mA, versus 70mA for stripe lasers).

3.6 Ultimate frequency response of GaAs injection lasers

The ability of GaAs semiconductor lasers to be modulated at the GHz frequency range opens up some interesting applications concerning transmission of microwave signals through optical fibers[18]. From the analysis of previous sections, it is clear that the useful modulation frequency range is limited to that below the relaxation oscillation resonance, which occurs at around 2-3 GHz, depending on the structure and the internal parameters of the laser. Questions are being raised as to whether it is fundamentally possible to push the modulation frequency into X-band (~10GHz) or even higher : how should one design such a laser, and what price one has to pay in obtaining such a wide bandwidth.

The laser relaxation resonance frequency is given by eqn. (3.14). In the unnormalized form it reads:

$$f_r = \frac{1}{2\pi}\sqrt{\frac{1}{\tau_s \tau_p}\left(\frac{J}{J_{th}}-1\right)} \qquad 3.15$$

where the variables are as defined before in section 3.1. This frequency increases with increasing bias current, so that one can obtain a wider bandwidth simply by raising the pump current. Operating at a high current density is not compatible with reliability, and the corresponding increase in optical power may even cause catastrophic facet damage. If one tries to shorten the internal laser parameters such as τ_s and τ_p to obtain a higher f_r, one simultaneously increases the threshold current density J_{th} and one might not gain at all. The pertinent question is thus : given certain limits in the operating current density* and optical power density, what is the

highest achievable f_r? And, how can it be achieved?

To analyze this problem in a systematic manner, we first express J_{th} in terms of the internal laser parameters (section 3.1)

$$J_{th} = \frac{ed}{\tau_s}\left(\frac{1}{\Gamma\alpha\tau_p} + N_{om}\right) \qquad 3.16$$

where e,d,α,Γ and N_{om} are the electronic charge, active layer thickness, gain constant, confinement factor and electronic density for transparency as defined before. Substituting (3.16) into (3.15)

$$f_r = \frac{1}{2\pi}\sqrt{\frac{J}{ed(1/\Gamma\alpha + N_{om}\tau_p)} - \frac{1}{\tau_s\tau_p}} \qquad 3.17$$

One immediately sees that for a fixed current density J, a *longer* spontaneous lifetime τ_s would increase f_r, and there exists an optimum photon lifetime τ_p for which f_r attains its maximum. The photon lifetime is related to the length of the laser by

$$\tau_p = \frac{L}{v(\rho L - ln(R))} \qquad 3.18$$

where ρ is the free carrier absorption coefficient, v is the group velocity of the mode, and R is the end facet reflectivity. Fig 3.11(a) - (c) shows equi-f_r contour plots on the L-J plane, represented by solid lines, for three different temperatures T = 300K, 250K and 80K. The values of the parameters are listed in Table 3.1. The dependence of the spontaneous lifetime on the carrier density is neglected for convenience; its inclusion would not lead to significantly different results. The heavily shaded areas are regions below threshold. At T = 300K, for example, fig 3.11(a) shows that if one

* Actually, the limit to be imposed should be the injected carrier per unit volume, but we shall assume a uniform active layer thickness of 0.2 μm and express the limiting quantity in terms of the more familiar current density.

Table 3.1*

$\tau_s = 3ns$

d = 0.2 μm

R = 0.3

$\alpha = 15\ cm^{-1}$

$\Gamma = 0.6$

$N_{om} = 7.5\times10^{17}\ cm^{-3}$ at T= 300K

$N_{om} = 5.9\times10^{17}\ cm^{-3}$ at T= 250K

$N_{om} = 1.0\times10^{17}\ cm^{-3}$ at T= 80K

$\alpha = 2.8\times10^{-6}\ cm^3sec^{-1}$ at T = 300K

$\alpha = 3.5\times10^{-6}\ cm^3sec^{-1}$ at T = 250K

$\alpha = 1.0\times10^{-5}\ cm^3sec^{-1}$ at T = 80K

---

* These numbers are taken from Ref. 20.

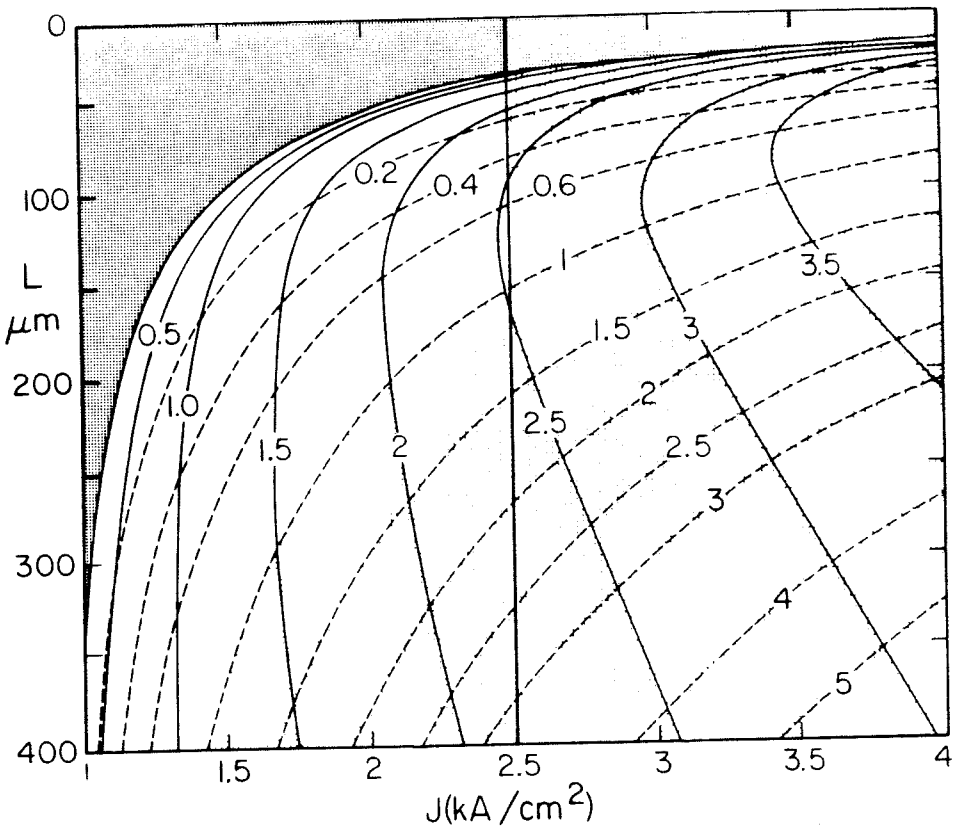

Figure 3.11(a). *Equi* - f_r (solid lines) and equi - Φ (dashed lines) contour plots on the L - J plane, at T = 300 K.

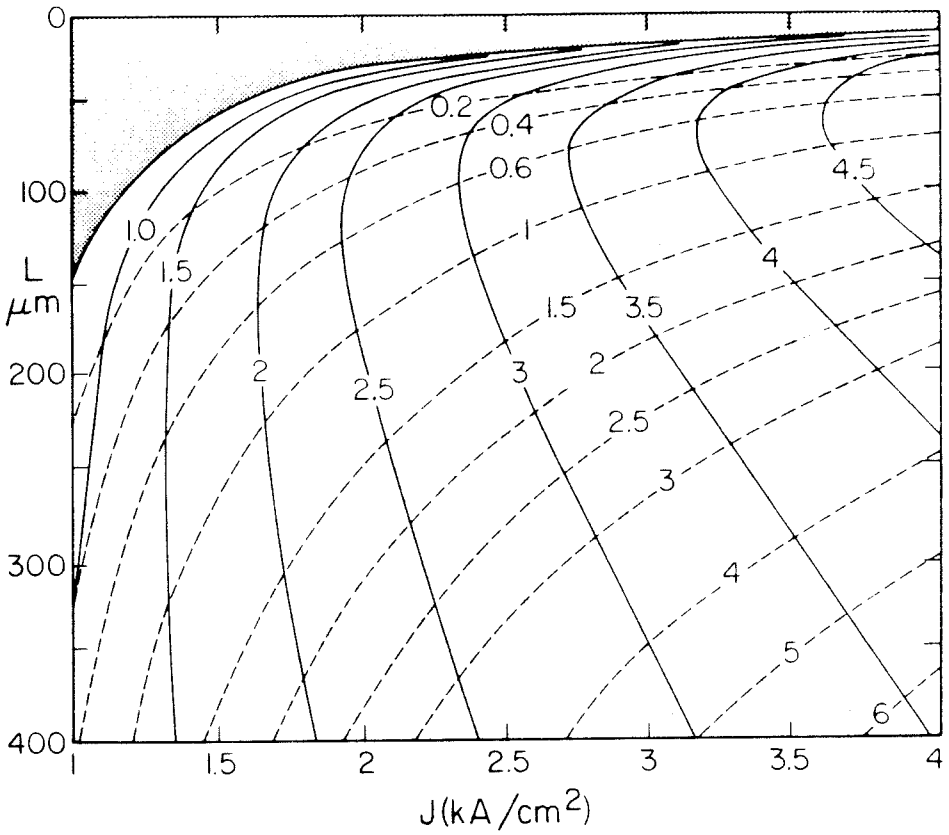

Figure 3.11(b). *Same as fig. 3.11(a) but at T = 250 K.*

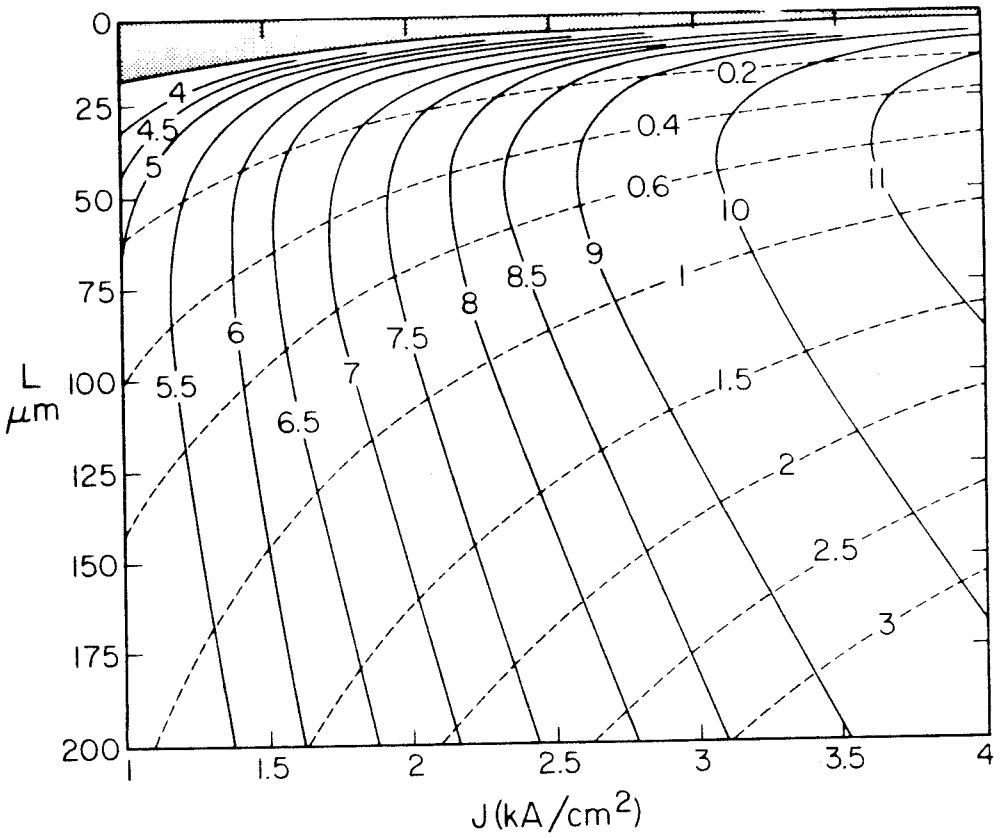

Figure 3.11(c). *Same as fig. 3.11(a) but at T = 80 K.*

limits the current density to 2.5 kA/cm^2, then the highest f_r achievable is about 2.5 GHz, and the laser should be about 150 μm long to achieve that maximum. For the same current constraint, the maximum f_r would be about 8.5 GHz when one cools the laser down to 80K (fig 3.11(c)) and the optimum length of the laser should be about 50 μm. The main factor associated with this increase in f_r is the increase in the optical gain α and the decrease in N_{om} at lower temperatures.

In addition to the current constraint, one should also consider the optical constraint. The optical power density inside a mirror facet is given by

$$\Phi = \hbar\omega P_0 \frac{(mode\ volume)}{2\tau_p'(1-R)(cross\ section\ area)} \qquad 3.19$$

where P_0 is the static photon density, τ_p' is the photon lifetime associated with mirror loss only = $\frac{L}{v} ln(\frac{1}{R})$, and ω is the optical frequency. Substitute into (3.19) the expression for P_0 one has:

$$\Phi = \frac{ln(R)}{ln(R)-\alpha L} \frac{\hbar\omega}{(1-R)} (\frac{J}{ed} - \frac{1}{\tau_s}(\frac{1}{\Gamma\alpha\tau_p} + N_{om}))L \qquad 3.20$$

Equi-Φ contours are represented by dashed lines on the L-J plane in figs 3.11(a) - (c). At 300K, for example, if one limits the pump current to no more than 2.5 kA/cm^2 and an optical power density to no more than 1 MW/cm^2, the only operational region is the unshaded region as shown in Fig 3.11(a). One should then search for the point in this region where f_r is maximum. For conventional 300 μm lasers, one usually first runs into the optical power limit as one increases the pump current. This can be avoided by shortening the cavity to the optimum value, in which case the response is current limited. The current levels shown in fig 3.11 may be somewhat optimistic, for we have assumed zero leakage current in the calculations.

It appears that the specific structure of the laser itself does not play a direct role in the frequency response. As mentioned above, a laser with high gain would have a higher frequency response simply because it can be biased to a higher ratio of $\frac{J}{J_{th}}$ before running into a prescribed current limit, while the optical limit can always be overcome by keeping the laser length short or by antireflection coating. Specific structural designs can push these limits to a high level - for instance, a higher optical power limit can be tolerated in lasers with a crank structure [21]. All of the structural designs aiming towards a low threshold laser, such as reduced current leakage, increased optical confinement factor, etc., would also be helpful in the quest for higher frequency response. The basic properties of the material system of GaAs, however, impose a fundamental limit on the frequency response as depicted in figures 3.11. Still, the problem of exactly how high a current density a laser diode can sustain without reducing its lifetime and the reliability of the device at low temperature have not been clearly settled, and probably should be the direction of further research.

Appendix - Chapter 3

Experimental notes concerning high frequency measurements of injection lasers

Components and experimental arrangements for high frequency measurements of injection lasers are briefly described in this appendix. For high frequency measurements, the laser chip is mounted at the end of a 50Ω microstrip line, as shown in fig A3.1(a), for lasers fabricated in our liquid phase epitaxy laboratory. Commercial lasers come in special packages, which usually provide a fly-lead for bonding onto the stripline (Fig A3.1(b)). For impedance matching, a 40Ω microwave resistor should be placed in series with and close to the laser chip. The optical output is focussed with a microscope objective onto a photodetector, usually a high speed sili-

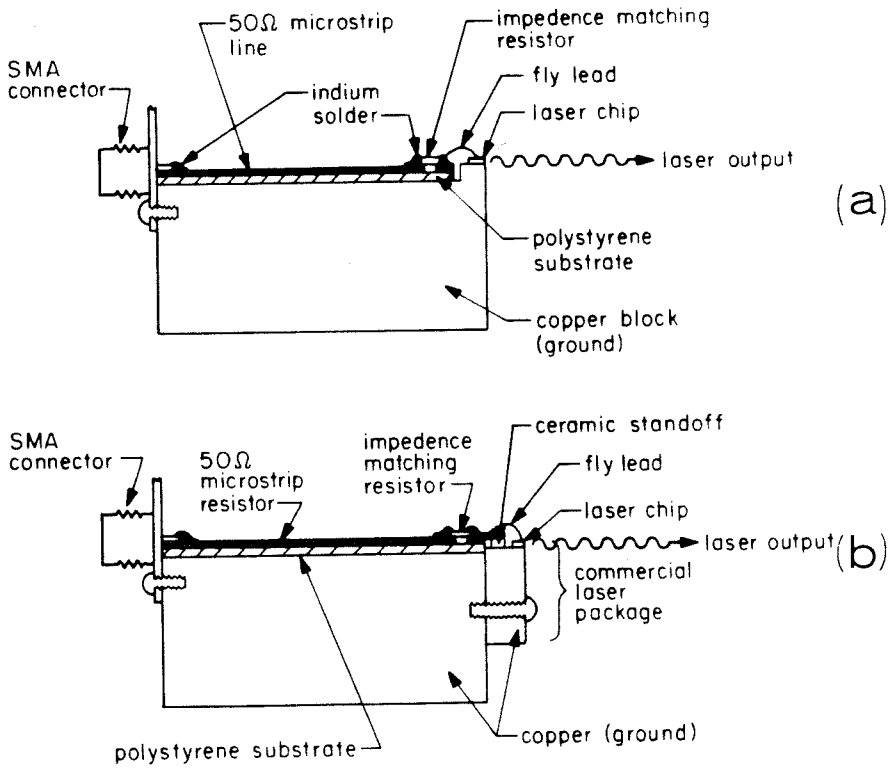

Figure A3.1. *Injection laser mounting for high frequency measurements. (a) laser chip mount, (b) mounting for commercial lasers.*

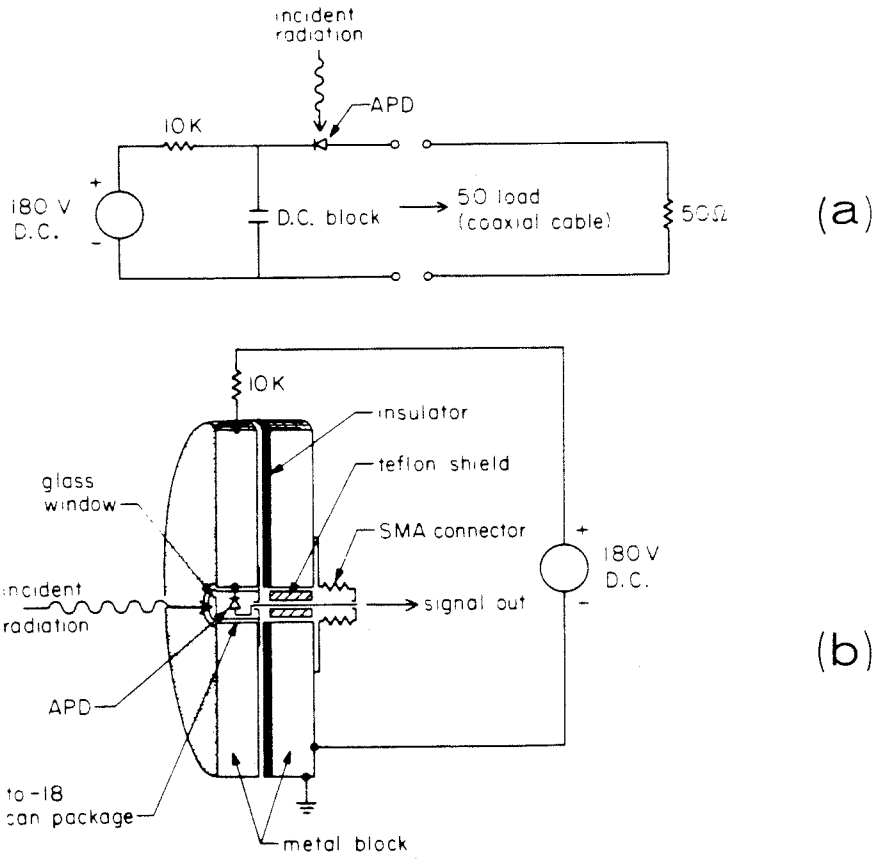

Figure A3.2. *Avalanche diode mount, (a) bias circuit and (b) cross section of the actual mount.*

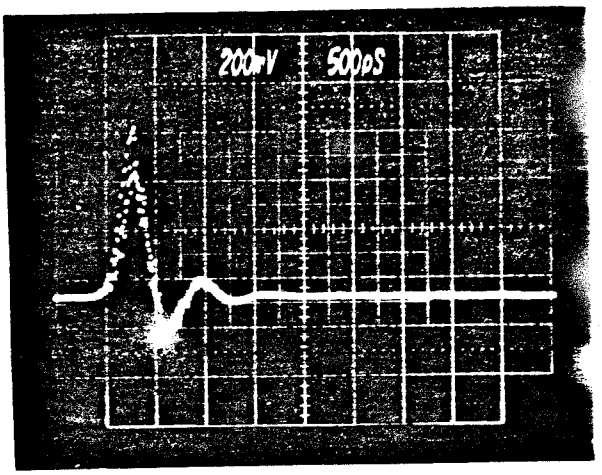

(a)

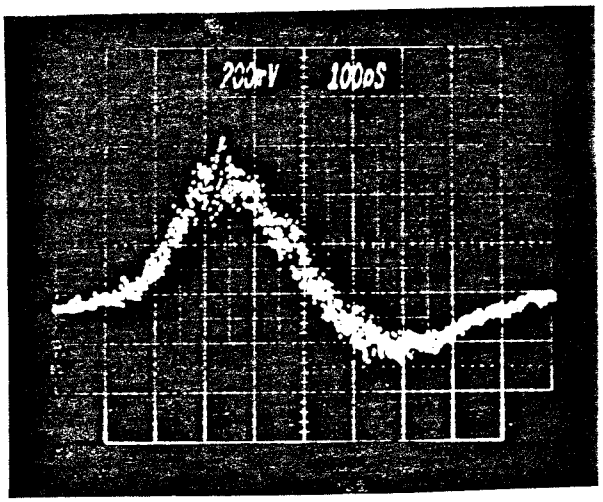

(b)

Figure A3.3(a). *Impulse response of the APD. Upper trace : 500 ps/div, lower trace : 100 ps/div.*

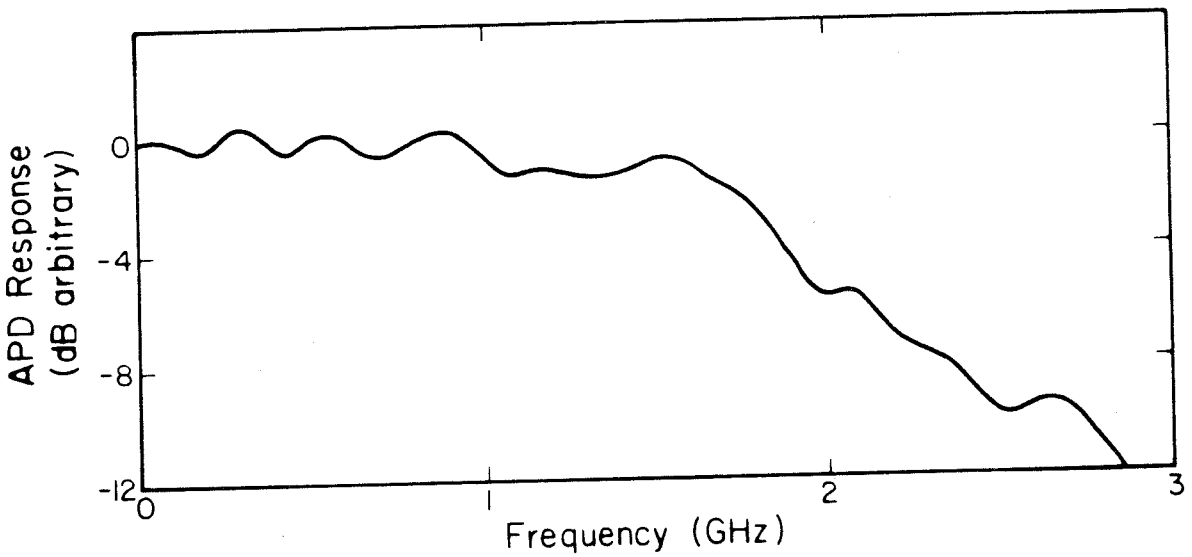

Figure A3.3(b). *Fourier transform of fig. A3.3(a).*

con avalanche photodiode (APD). The APD is reverse biased to near avalanche breakdown (fig A3.2(a)). At this bias voltage, the ratio of the signal current (due to the incident light) to the background reverse current reaches a maximum [22], leading to the highest signal to noise ratio. In some cases where the signal power is abundant, it can be advantageous to bias at a lower reverse voltage, which reduces the avalanche gain but increases the detector speed. To ensure good frequency response, the commercial APD in a TO-18 package is mounted as shown in fig A3.2(b). The impulse response of the APD package is checked with a cw mode-locked dye laser, which produces a train of pulses of width ~1ps at ~6100 Å. Fig A3.3(a) shows a typical impulse response of an APD, showing a risetime of about 130 ps and very weak ringing. The fourier transform of fig A3.3(a) produces the frequency response characteristics of the APD, shown in fig A3.3(b). The -3dB point is observed to be around 2 GHz. Thus for measurements above 2GHz, it is necessary to normalize the measured frequency response with the APD response curve.

A typical setup for the frequency response measurement of the injection laser is shown in fig A3.4. The laser can be excited with a fast current step (½ ns risetime), or by a sharp current impulse (70 ps) generated by a step recovery diode generator (Hp33002), or by cw microwave sources from 25 MHz to 4 GHz (Hp 8690, 8640). The signal is fed into the laser via a microwave bias tee (Hp33150) through which a dc bias current is applied. In earlier experiments when commercial bias tees were not available, a chip capacitor was mounted on the 50Ω stripline, and the dc was directly applied to the laser through an rf choke.

The laser output was usually focused onto the APD by a microscope objective. Alignment was done with the help of an infrared viewer. The signal output from the APD, in the case of a weak signal, was fed into a variable gain wideband microwave amplifier (B&H3002, bandwidth 0 - 2 GHz), and then through a sampling head

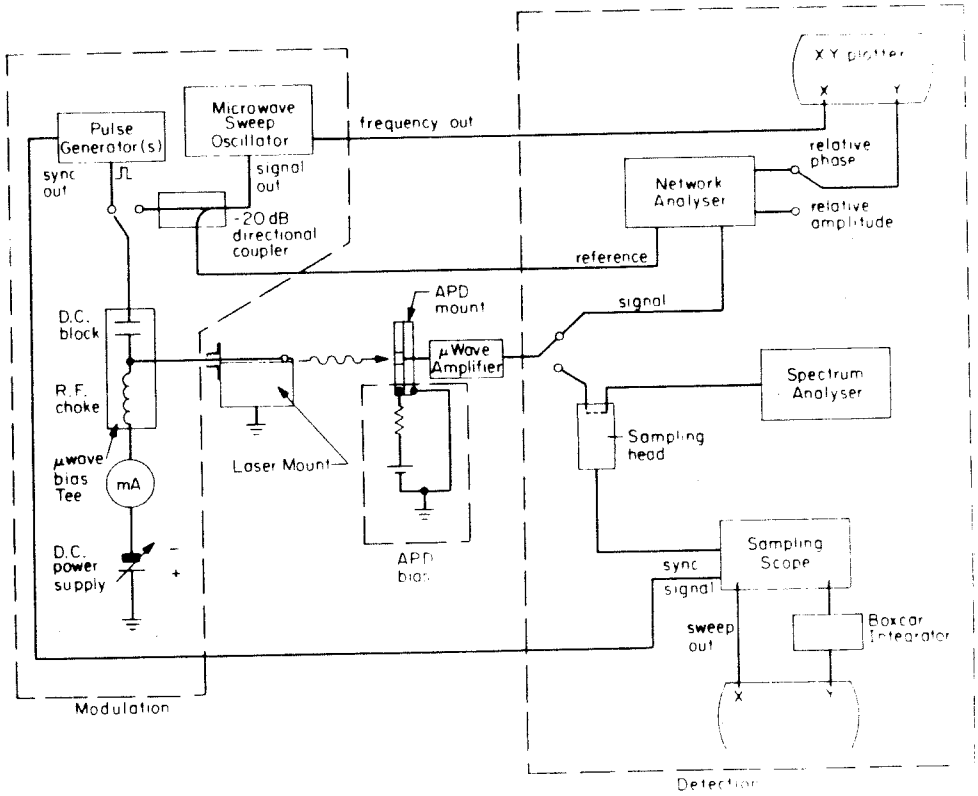

Figure A3.4. *High frequency laser response measurement system.*

(Tektronics S-4, 25 ps risetime)and into a microwave spectrum analyzer (Hp8565) which is capable of detecting frequency components as high as 18 GHz. The detected signal can also be fed into a microwave network analyser (Hp8410), which compares the phase and amplitude of the microwave signal with a reference signal split off from the sweep oscillator by microwave directional couplers (Hp778 series). In the automatic frequency- sweep mode, this arrangement provides a very convenient way of measuring the amplitude and phase response of the laser at various bias currents. The step and pulse responses of the laser were displayed in the time domain on a sampling oscilloscope. The spectrum analyser was used to measure the harmonic distortions and noise characteristics, and was extremely useful in self-pulsation and mode-locking experiments, which will be described in chapters 4 and 5.

References - Chapter 3

1. A.Yariv, **Quantum Electronics** , pg 273, Wiley 1973.
2. H.Kressel and J.K.Butler, **Semiconductor Lasers and Heterojunction LEDs** , pg 77, Academic Press 1977.
3. P.M.Boers and M.T.Vlaadingerbroek, Electron. Lett., **11**, 206 (1975).
4. J.C.Dyment, L.A.D'Asaro, J.C.North, B.I.Miller and J.E.Ripper, Proc. IEEE, **60**, 726 (1972).
5. R.A.Furranage and D.K.Wilson, U.S. Patent # 3363195, (Jan. 1968)
6. K.Aiki, M.Nakamura, T.Kuroda and J.Umeda, Appl. Phys. Lett., **30**, 649 (1977).
7. T.Tsukada, J. Appl.Phys., **45**, 4899 (1974).
8. J.Katz, D.P.Wilt, N.Bar-chaim and A. Yariv, to be published.
9. H.Namizaki, H.Kan, M.Ishii and A.Ito, J. Appl. Phys., **45**, 2785 (1974).
10. C.P.Lee, S.Margalit, I.Ury and A.Yariv, Appl. Phys. Lett., **32**, 410 (1978).
11. Y.Suematsu, k. Furuya, Trans. IECE Japan, **E-60**, 467 (1977).
12. K.Petermann, IEEE J. Quant. Electron., **QE-15**, 566 (1979).
13. N.Chinone, K.Aiki, M.Nakamura and R.Ito, IEEE J. Quant. Electron., **QE-14**, 625 (1978).
14. R.Lang and K.Kobayashi, IEEE J. Quant. Electron., **QE-12**, 194 (1976).
15. K. Otsuka, IEEE J. Quant. Electron., **QE-13**, 520 (1977).
16. D.Fekete, W.Streifer, D.R.Scrifres and R.D.Burnham, to be published.
17. D.P.Wilt and A.Yariv, unpublished.
18. H.W.Yen and M.Barnoski, Appl. Phys. Lett., **32**, 182 (1978).

19. H.Kressel and J.k.Butler, **Semiconductor Lasers and Heterojunction LEDs** , pg 159, Academic Press 1977.

20. F.Stern., IEEE J. Quant. Electron., **QE-9**, 290 (1973).

21. S.Takamiya, Y.Seiwa, T.Tanaka, T.Sogo, H.Namizaki, W.Susaki and K.Shirahata, 7th IEEE International Semiconductor Laser Conference, Paper 8, London 1980.

22. H. Melchior, J. Luminescence, **7**, 390 (1973).

CHAPTER 4

INTENSITY SELF-PULSATIONS IN SEMICONDUCTOR LASERS AND THEIR INTERACTIONS WITH AN EXTERNAL CAVITY

4.1 Self-pulsation in semiconductor injection lasers

It has been observed that some injection lasers, when driven by a dc current, emit a continuous train of sharp optical pulses, at a microwave repetition rate somewhere between 200 MHz and 2 GHz. This phenomenon, called self-pulsation, apparently occurs in all types of III-IV semiconductor lasers that have ever been fabricated; the pulsation is more pronounced in some types and less in others. Basov[1] first attempted an explanation of this peculiar phenomenon by assuming a non-uniformity in the pump current over the length of the laser diode, so that the regions depleted in pumping will form saturable absorption centers. The coexistence of both saturable absorption and saturable gain within a cavity mimics a passively mode-locked laser[2,3]. However, the pulsations observed in injection lasers cannot be caused by mode-locking, since the pulsation frequency is much lower than the cavity mode separation of 40-50 GHz. The pulsation is actually a form of undamped relaxation oscillation. Lee et.al.[4] fabricated laser diodes with a purposely built-in non-uniform pump current, and produced pulsations as predicted by Basov. However, another theory was advanced by Paoli and Ripper[5] who speculated that the pulsations, though not produced by the locking of the cavity modes, can be produced instead by the locking of the combination-tones [6] of the modes, called second-order mode-locking. They supported their theory by the experimental observation that when light is selectively fed back into the laser by a diffraction grating to produce single mode oscillation, the pulsations are quenched. However, later experiments by Chinone et.al.[7] and Figueroa et.al[8] showed that the pulsation can be quenched even with optical feedback from a non-frequency-selective element like a plane mirror. There was no further experimental evidence to support the theory of

second order mode-locking. As the quality of injection lasers improved and their commercialization required serious life-tests to be undertaken, it became apparent that pulsations are related to the aging and degradation of lasers. Massive amount of relevant data was gathered. The test results of Paoli[9] and Hartman et.al.[10] unmistakeably relate self-pulsation to absorbing defects in the active region of the lasers. The exact nature of the defects is still a matter of controversy; some believe them to be deep level traps[11,12] and micro-degradations distributed throughout the active region[13], but there is also evidence that pulsations are due to mirror facet degradation[14] or proton induced damaged [15,16]. There exist little experimental data that can verify any one of the above proposed mechanisms conclusively. The correlation between theory and experiment is further complicated by the different laser geometries and the mathematical similarities between the different models. Self-pulsation is the only remaining outstanding problem in semiconductor lasers that has not been solved completely, and is still an area of active research in industrial laboratories. Here, we list the major properties of self-pulsation:

1. a large percentage of lasers that do not self-pulsate when they are "fresh" will eventually do so after several thousands (or hundreds, or even tens) of hours of continuous operation;

2. when self-pulsations first develop in a laser, they are in the form of a weak sinusoidal undulation at relatively high frequencies (> 1 GHz). However, as the laser continues to age and degrade, the undulation develops into sharp spiking in the output at ever decreasing frequencies; some lasers pulsate at as low as 200 MHz which would severely interfere with the modulation signal if they were used as a signal transmitters;

3. the self-pulsation frequency increases as the dc bias current is increased; however it does not follow the simple square-root dependence of the relaxation oscilla-

tions described in section 3.5.

4.2 General behavior of self-pulsing lasers coupled to an external cavity

Interests in studying the behavior of self-pulsing lasers coupled to an external cavity arises, on the one hand, from intentions to quench the pulsations by optical feedback, and on the other hand, from attempts to enhance the pulsations to produce extremely short and stable picosecond optical pulses. It has been reported that pulsations can be quenched by coupling a self-pulsing laser to a short external cavity[7]. However, other experiments by Paoli[17] showed no quenching effect in coupling the laser to an external cavity; instead the pulses were even sharpened and the pulsation frequency was locked to an external cavity harmonic (ie., harmonics of the external cavity mode separation). These observations were not successfully explained.

Recent interest in ultra-short pulse generation in injection lasers was revived by the mode-locking experiments of Ho and Glasser et.al.[18-20], who reported generating 18 ps optical pulses from actively mode-locked injection lasers coupled to an external cavity. Studies by Figueroa et.al.[21] and Lau et.al[22] suggested that the mechanism for short pulse generation can be passive mode-locking, due to the very same degradation-induced defects that cause self-pulsation. Later mode-locking experiments by Ippen et.al.[23] using badly degraded lasers generated the shortest pulse yet, 5 ps wide, confirming the predictions by Figueroa and Lau. The length of the external cavity was also found to be very important for effective mode-locking [21,22], and the theory also predicts that non-self-pulsing lasers can be induced to self-pulse when coupled to an external cavity of appropriate length. When this happens, the pulsation frequency locks to the beat frequency between the external-cavity modes or its harmonics. In essence, this is passive mode-locking, or self-

locking as it is commonly called. This in fact has been previously observed by Broom et.al.[24], but has never been satisfactorily explained. The model used to analyze passive mode-locking can also predict the quenching and frequency locking effects described in the beginning of this section. Thus, the numerous and apparently unrelated major experimental observations in the dynamic interaction of injection lasers with external cavities can be explained with a single theory in a coherent fashion. In the following sections of this chapter, the experimental observations and the theoretical model will be described. Results on the use of a section of multimode optical fiber as the external cavity will also be reported. This novel arrangement can render the laser external-cavity system highly compact and thus practical. An analytic small signal theory of the laser-external cavity interaction, to be presented in the next chapter, will give insights into how the pulsation behavior depends on the external cavity length, coupling coefficient, trap density and other parameters.

4.3 Quenching and frequency locking of self-pulsations in (GaAl)As injection lasers operating in an external cavity

As mentioned in the last section, Chinone et.al.[7] reported on a method for the suppression of intensity pulsations by using a short external cavity (0.3 - 2cm), while experimental results by Paoli et.al.[17] showed that the external cavity locks the self-pulsation frequency to a cavity harmonic, with no significant quenching effect. These results are not adequately explained by the conventional rate equations, which do not predict sustained pulsations. In this section we present a study of a self-pulsing (GaAl)As injection laser operating in an external cavity. The conventional set of rate equations widely used to analyze relaxation oscillation in lasers (Chp. 2 and 3) are used as the starting point. These are modified by the addition, in the manner of Copeland[12], of absorbing electron traps, and also by a term

accounting for the feedback due to the external resonator. Using these equations, we show that the aforementioned observations are not independent, and fit well within the scope of a single model. The analysis is confirmed by our experimental results on a self-pulsing laser. Although Copeland's equations are used in our calculation, we believe that other well known models for self pulsations, when modified to include the external cavity, will produce similar results. Secondly, we describe a novel method for suppressing self-pulsations using an optical fiber resonator. The compactness of the laser-fiber system makes it a very attractive method for stabilizing self-pulsing lasers in practice.

According to Copeland, self-pulsations are produced by electron traps distributed throughout the active region which can modulate the gain of the laser. The model is described by the following set of equations:

$$\frac{dN(t)}{dt} = \frac{J}{ed} - \frac{N(t)}{\tau_s} - \alpha P(t)(N-N_0) + \frac{dT(t)}{dt} \qquad 4.1$$

$$\frac{dP(t)}{dt} = \frac{-P(t)}{\tau_{ph}} + \alpha P(N-N_0) + \beta\frac{N}{\tau_s} - \sigma_0 c_0 P(t)(T_0-T) + \varepsilon\frac{P(t-\tau)}{\tau_{ph}'} \qquad 4.2$$

$$\frac{dT(t)}{dt} = \sigma_0 c_0 P(t)(T_0-T) - \sigma_0 v N(t) T(t) \qquad 4.3$$

The first two equations with the exception of the last terms (those involving T and ε) are the conventional rate equations, with N being the electron density, and P the photon density. The term $\varepsilon\frac{P(t-\tau)}{\tau_{ph}'}$ represents the delayed feedback from the external mirror where τ represents the roundtrip time in the external cavity, ε is the fraction of light fed back into the laser, which we define to be the *coupling coefficient* , and τ_{ph}' only includes the mirror loss. The use of the delayed photon

feedback term, which neglects the optical phase, to describe the external cavity can be justified as follows: for sharply pulsing solutions, the situation is that of one or more discrete photon packets bouncing back and forth between the laser diode and the external mirror. It is clear that in this case the inclusion of the phase term is not necessary. In the case of nonpulsing (steady) or slowly varying solutions (slow compared to the external cavity roundtrip time), the result could be affected by coherent effects [25,26]. However, if one neglects small variations (on the order of an optical wavelength) in the external cavity length, the overall picture can be well described by the above approach.

The last equation (4.1(c)) represents the equation of motion for the traps, the parameters are as follows: c_0 is the speed of light in the medium, T is the density of empty traps, T_0 is the total density of traps, σ_e is the electron capture cross section, v is the thermal velocity, and σ_0 is the photon capture cross section by a trap occupied by an electron (whose density is (T_0-T)). In the calculations we use typical values for the laser parameters: $\alpha=1.5\times10^{-6}cm^3sec^{-1}$, τ_s=3ns, τ_{ph}=2.9ps, d=0.2μm, $N_{om}=5\times10^{17}cm^{-3}$, $\beta=10^{-4}$, $c_0=8\times10^9 cmsec^{-1}$, $\sigma_e=1.5\times10^{-17}cm^2$, v = $4.42\times10^7 cmsec^{-1}$, and $\sigma_0=3\times10^{-16}cm^2$. The calculations were performed by integrating eqns. (4.1) - (4.3) using the Runge-Kutta fourth-order algorithm. The system is excited with a step change in the current and run until steady-state oscillation or its absence is confirmed.

Calculations were first performed without the external cavity (ε=0). A plot of the frequency and the amplitude of the pulsation versus injection current is shown in Fig 4.1(a) and (b). Depending on the bias level, the trap density must exceed a certain value for pulsation to occur. One can also observe the increase of the pulsation frequency with the bias current, and the decrease of the pulsation frequency with

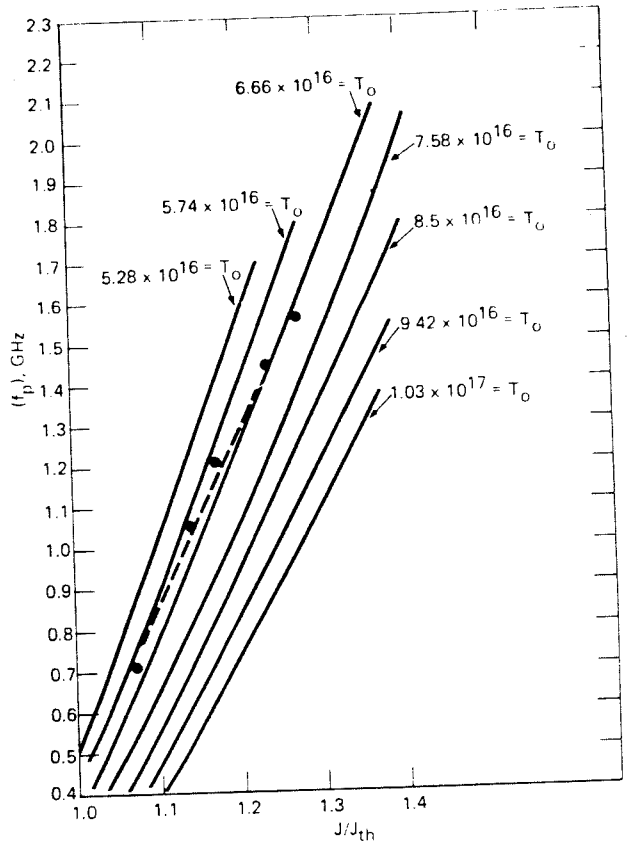

(a)

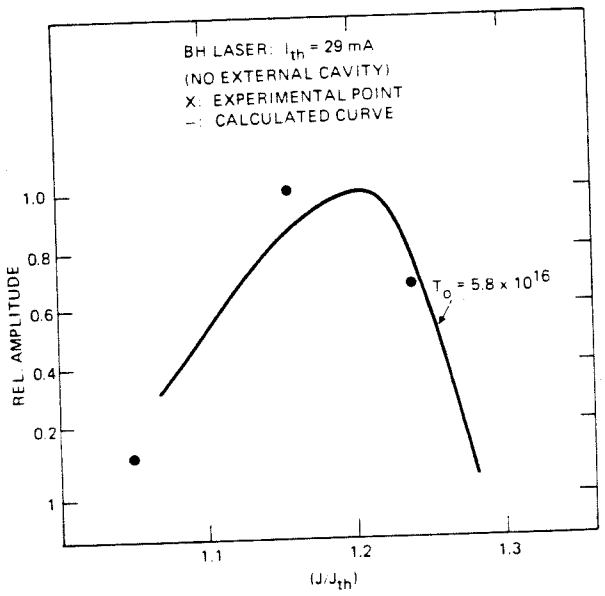

(b)

Figure 4.1. *(a) Calculations displaying frequency of self pulsation vs injection current. The dots represent experimental results. (b) Calculation of the amplitude of self pulsations vs injection current.*

increasing trap density. As lasers age, the defect density inside the active region increases, and the calculated results above can explain the corresponding drop in the pulsation frequency. The results also show the rapid increase in the pulsation amplitude when the bias current is raised above threshold, which is also observed experimentally.

The experiment (fig 4.2) consists of collimating the light from one facet of a Hitachi buried heterostructure (BH) laser, operating cw, using a 40X objective. A portion of this light is returned to the laser by using a mirror mounted on a micrometer stage. The light from the other laser laser facet is focused onto a TI XL55 Avalanche diode (risetime ≈ 130ps). The signal from the APD is amplified and displayed on a spectrum analyzer. In the absence of an external cavity, the BH laser self-pulses for currents slightly above threshold ($I > 1.02I_{th}$). The observed pulsation amplitude and frequency are also plotted on fig 4.1, and it can be seen that a good fit can be obtained with an assumed trap density of $T_0 = 5.8\times10^{16}cm^{-3}$.

Figure 4.3 shows an experimental plot of the amplitude and frequency of self-pulsation versus the external cavity length L, for $I=1.15I_{th}$. We note that there is a broad minimum in the amplitude of the self-pulsation for $6< L< 10$ cm. Similar results are obtained for currents varying from $1.04I_{th}$ to $1.25I_{th}$. An estimate of the coupling coefficient ε can be made from the measured reduction in threshold curent when the external reflector is aligned (section 4.4). Our results indicate a coupling coefficient in the range 0.01 - 0.05. We find no significant variation in ε as the mirror is moved, indicating that the output laser beam is well collimated. In Fig 4.4, we show the suppression of the self-pulsation using an external fiber resonator (EFR). The resonator consists of a piece of multimode graded index fiber with one end formed into a lens using the thermal melting technique[27], while the other end is cleaved, polished and is evaporated with gold to form a reflector. The operation

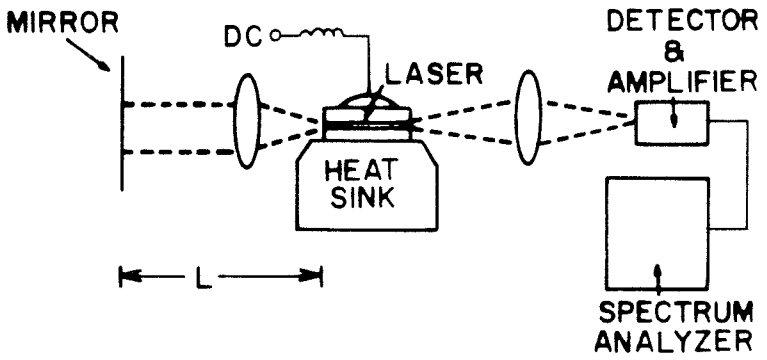

Figure 4.2. *Experimental setup for coupling of laser diodes to an external cavity.*

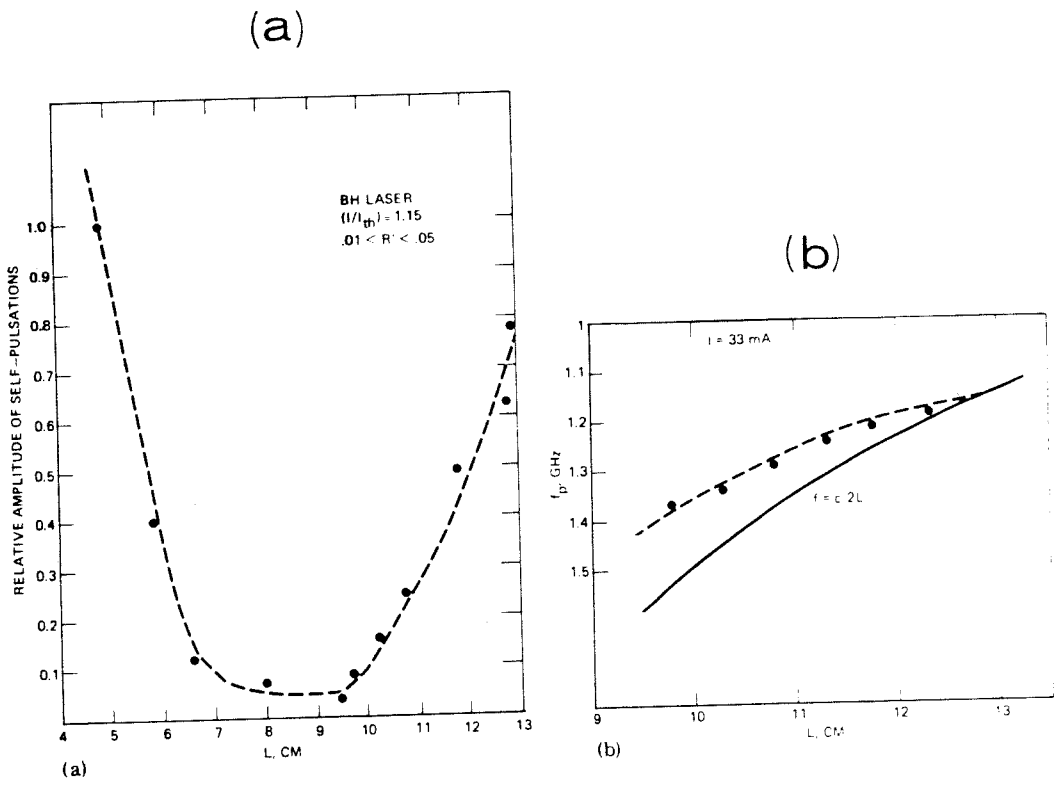

Figure 4.3. *(a) Amplitude of self-pulsations vs external cavity length, (b) frequency of self-pulsation vs cavity length.*

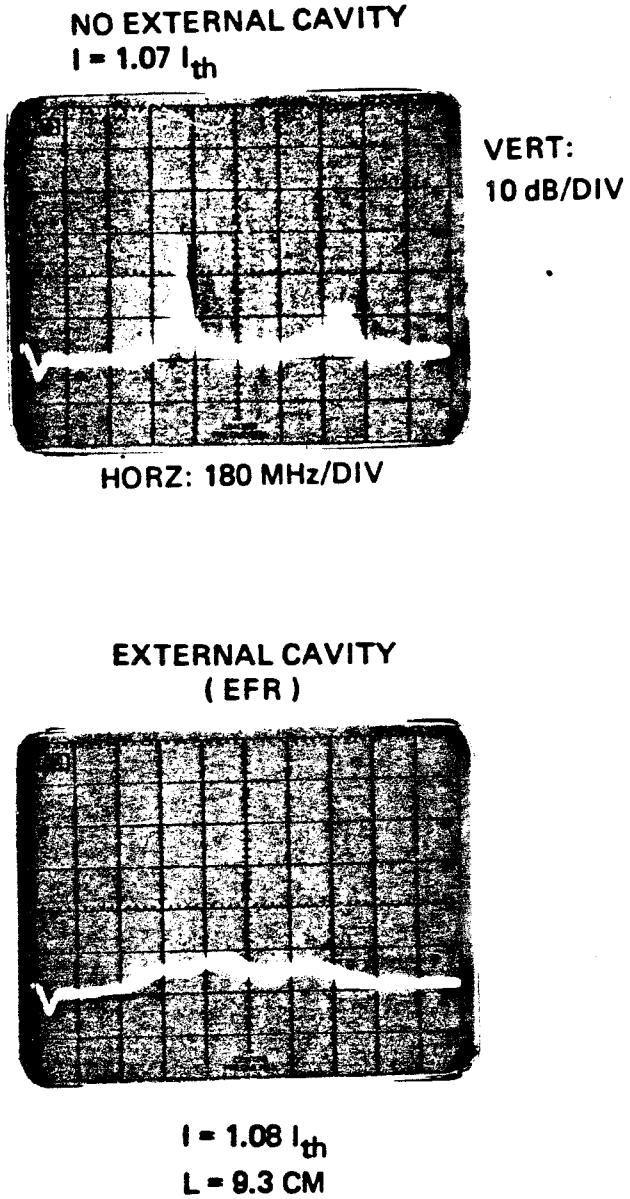

Figure 4.4. *(a) Photograph display of self-pulsation without and (b) with a fiber resonator. Hori : 180MHz/div.*

characteristics of injection lasers in an EFR will be discussed in more detail in the next section.

When the fiber resonator is aligned with the injection laser and the length of the fiber is properly chosen, we are able to suppress self-pulsation with very little coupling into the EFR (ie., the change in I_{th} is not measurable). The suppression of the self-pulsation is maintained for currents up to $1.1I_{th}$.

The calculated amplitude and frequency of the self-pulsations are plotted versus external cavity length in fig. 4.5. The bias was at 1.1 × threshold, and $\varepsilon = 0.01$; however, the results do not change significantly for $0.01 < \varepsilon < 0.2$. Several important observations can be pointed out. First, we find regions of L where the self-pulsations are suppressed. The first band occurs for $3 < L < 12$cm. This region corresponds roughly to our experimental results. In practice, the self-pulsation is not quenched completely in the suppressed region, leaving a resonance significantly broadened and greatly reduced in amplitude. In all the regions where the pulsations are not suppressed (except for L< 3cm), their frequency corresponds to $f_p = mc/2nL$ where m is an integer, and n is the refractive index. Starting with the first cavity harmonic, the pulsation locks to successively higher harmonics as L is increased. Near the region where frequency jumping occcurs, the oscillation is relatively unstable and takes place in both harmonics.

The results presented in fig. 4.5 conform qualitatively to the experimental results of Paoli et.al.[17] who used an external cavity approximately 75cm in length. Our calculations show that the self-pulsation cannot be suppressed for all L > 50cm, and the pulsation frequency is locked to successive cavity harmonics as the cavity length is increased, as observed by Paoli et.al. Chinone [7] observed the quenching effect in a CSP laser, but for cavity lengths much shorter ($0.3 < L < 2$cm) than that

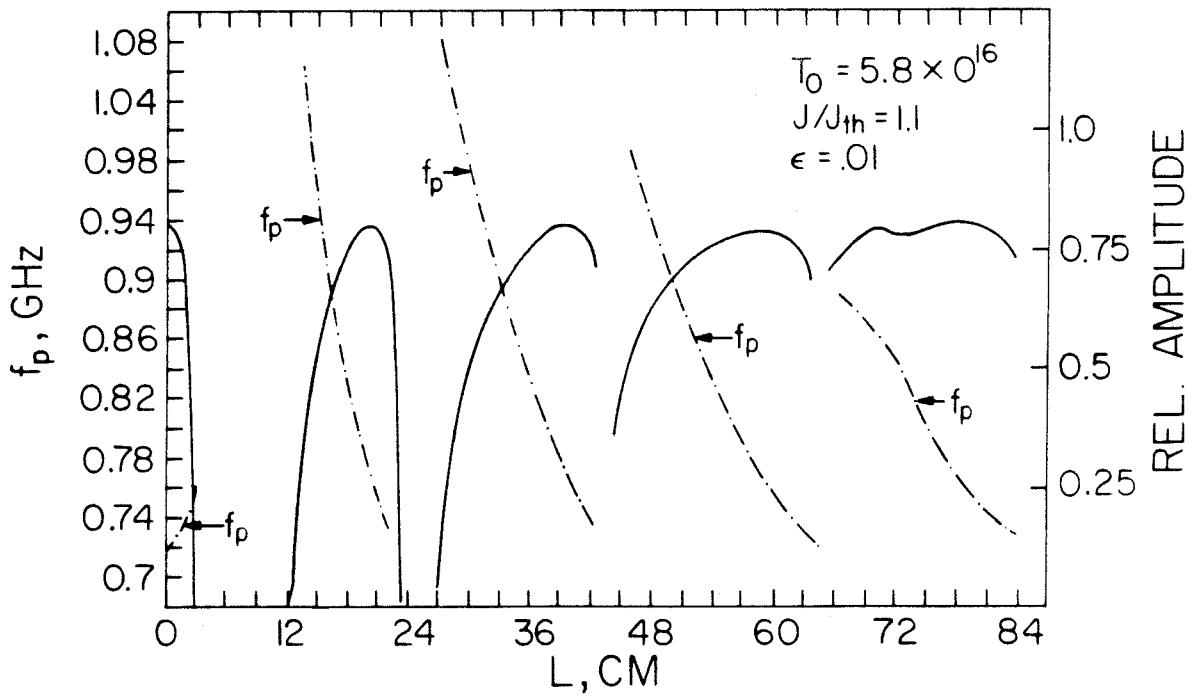

Figure 4.5. *Calculated plots of the self-pulsation amplitude and frequency vs external cavity length.*

predicted by our calculations. We believe the results obtained by Chinone could be explained by using a shorter photon lifetime in the calculations.

The mechanism involved in the suppression of the self-pulsations is the locking action produced by the external cavity feedback. By introducing external feedback, the injection laser is forced to pulsate at a frequency f_p equal to $mc/2nL$. As L is decreased, the laser is forced to pulsate at higher frequencies. If τ, (i.e., $1/f_p$) is shorter than the time required to replenish the electrons consumed in generating an optical pulse, then the pulsation cannot be sustained. As expected, higher pump currents can sustain pulsations at a higher frequency, and thus a shorter cavity is necessary for quenching. For very short cavity lengths (L < 3cm) the pulse width is comparable to the transit time of the light in the external cavity and no frequency locking occurs. Thus the pulsation is primarily determined by the parameters of the injection laser. On the other hand, if L is too long, the self-pulsation frequency will lock to a higher cavity harmonic, with a frequency above the natural pulsation frequency and below the quenching frequency.

In conclusion, it has been demonstrated that self-pulsation in a cw injection laser can be suppressed by an external cavity. A useful external cavity for this purpose can be made using an optical fiber. Lastly, the numerical calculations using the electron trap model of Copeland confirm our experimental results and predict that suppression of self-pulsation in lasers occurs over a small range in external cavity lengths.

4.4 Operation characteristics of an external fiber resonator

In the last section, the quenching of intensity self-pulsations by a novel external resonator using a multimode graded index fiber was described. The laser-fiber combination can be relatively compact, rugged, light weight, mechanically stable, and

therefore useful. The theoretical coupling coefficient expected from this arrangement is examined in this section, which would be a useful piece of information during the actual alignment procedure.

Figure 4.6 shows the experimental arrangement. The laser used in the experiment should operate in the fundamental lateral and transverse mode, otherwise coupling would be extremely difficult. A piece of multimode graded index fiber with a numerical aperture of 1.4 was used in the experiment. One end was cleaved, polished and coated with about 2500 Å of Au to form a reflector. A spherical lens (shown in fig 4.7) was formed on the other end of the fiber using the thermal melting technique, resulting in a typical radius of curvature of 80 - 120 μm. The laser was mounted in the same way described in chapter 3, but so arranged that both laser facets were accessible. The fiber was placed inside a capillary tube which was mounted on an x-y-z translation stage with provision for rotation about two of the axes. The alignment was performed using PZT(lead zirconate) piezoelectrically controlled micrometers. The light from the second facet of the laser focused onto an APD and displayed on a spectrum analyzer or sampling oscilloscope.

Fig 4.8 shows typical light output versus current characteristics for an external fiber resonator. Also shown are the characteristics with no external fiber resonator present. An important figure of merit for the external fiber resonator is the threshold reduction factor, K, given by

$$K = \frac{J_{th\ EFR}}{J_{th}} \qquad 4.4$$

where $J_{th\ EFR}$ and J_{th} are the threshold current densities with and without the external fiber resonator, respectively. This reduction in threshold is related to the coupling coefficient ε, defined before as the fraction of light returned from the external

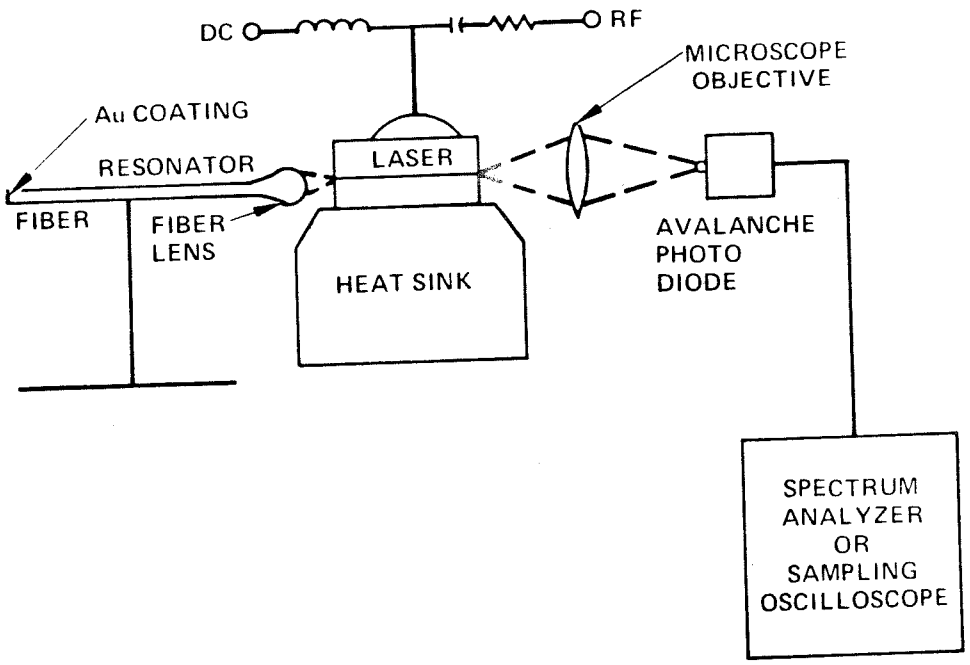

Figure 4.6. *Experimental setup.*

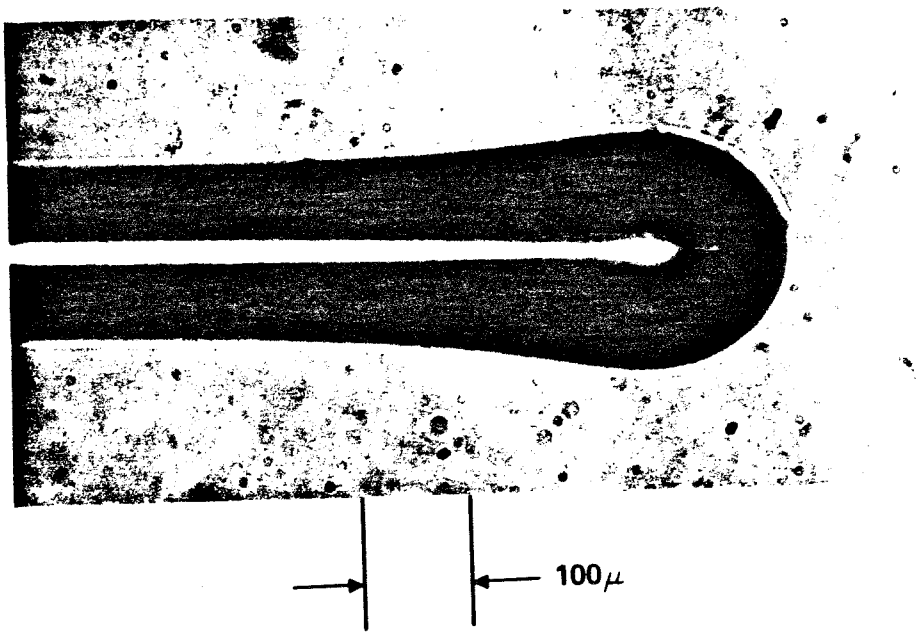

Figure 4.7. *Top view of optical fiber showing a lens tip.*

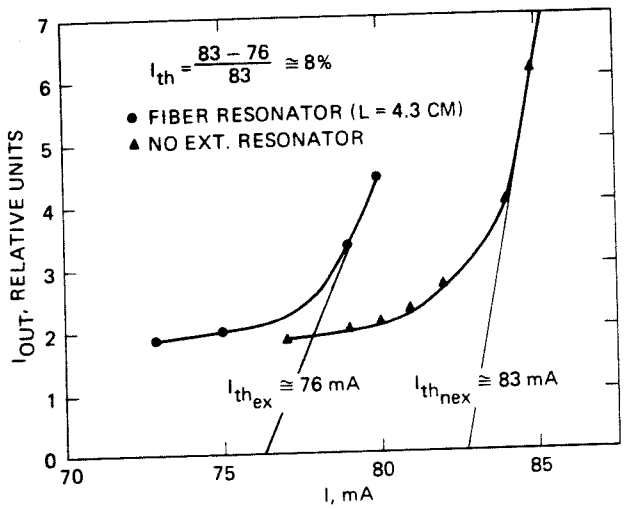

Figure 4.8. *Light output vs current for the optical fiber external resonator configuration.*

resonator *into the lasing mode*, by the following:

$$K = \frac{\alpha N_{om} + \frac{1}{\Gamma}(\rho+(1/2L)ln(1/R)(1/\varepsilon))}{\alpha N_{om} + \frac{1}{\Gamma}(\rho+(1/L)ln(1/R)} \qquad 4.5$$

where the definitions of α, N_{om}, Γ, ρ, L and R are the same as that in chapters 2 and 3. As a reminder, α is the gain coefficient, N_{om} is the carrier density for transparency, Γ is the confinement factor, ρ is the internal absorption loss, L is the length of the laser and R is the mirror reflectivity. The coupling coefficient can be expressed as[30]

$$\varepsilon = \frac{R + 2\sqrt{R}\sqrt{R_f}\cos 2\delta + R_f}{1 + 2\sqrt{R}\sqrt{R_f}\cos 2\delta + R_f R} \qquad 4.6$$

where 2δ is the round trip optical phase delay between the laser cleaved facet and the end reflector of the fiber, and R_f is the effective reflectivity of the entire external fiber resonator, including various loss mechanisms. Since the laser is a free oscillator, the phase factor 2δ will adjust itself such that ε is maximized, ie.,the laser oscillates at a frequency closest to the maximum on the gain curve[38]. Then ε becomes

$$\varepsilon = (\sqrt{R} + \sqrt{R_f})^2 / (1+(R_f R)^{\frac{1}{2}})^2 \qquad 4.7$$

In fig 4.9 we plot K as a function of R_f with $\alpha_0 = \alpha N_{om}$ as a parameter. For the calculation the following numbers were used: L=150 μm, d=0.3μm, Γ=0.8, R=0.3, and ρ = 20 cm^{-1}. These numbers were either measured or assumed to be typical for injection lasers. A reasonable value for α_0 is 100 - 200 cm^{-1}, and its variation among different laser structures can help explain the different laser sensitivity to external

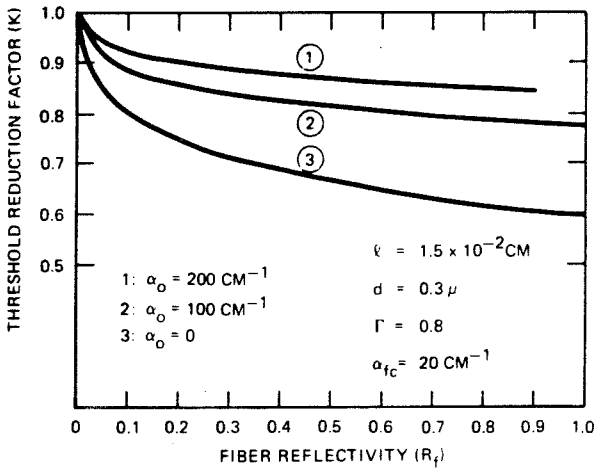

Figure 4.9. *Calculation of* $J_{th\ EFR}/J_{th}$ vs external reflectivity R_f.

feedback.

To estimate the coupling coefficient ε we first make an estimate of the effective reflectivity of the fiber resonator, R_f as follows:

$$R_f = R_{Au}\eta_c\eta_p\eta_R \tag{4.8}$$

where R_{Au} is the reflectivity of gold, η_c is the input coupling coefficient at the fiber lens, η_p is the coupling due to polarization effects, and η_R is the air/glass transmission = 0.96. The factors η_c and η_p are estimated as follow:

1. η_c is calculated by first calculating the half acceptance angle, ψ for a spherical lens on a multimode step index fiber, given by[31]

$$\psi = \sin^{-1}[n_c \sin(\sin^{-1}(d/2r) + \cos^{-1}(n_{cl}/n_c))] - \sin^{-1}(d/2r) \tag{4.9}$$

where n_c and n_{cl} are the core and cladding index, respectively, d is the diameter of the core, and r is the radius of the fiber lens. Assuming n_c = 1.5, n_{cl} = 1.4935, d = 65μm, and r = 100μm we have ψ = 0.312 rad. The coupling coefficient η_c is estimated [32] by integrating the farfield distribution I(ϑ) of the laser over the acceptance angle of the fiber and normalizing by the total power emitted:

$$\eta_c = \frac{\int_0^{\psi} I(\vartheta)\sin\vartheta\, d\vartheta}{\int_0^{\frac{\pi}{2}} I(\vartheta)\sin\vartheta\, d\vartheta} \tag{4.10}$$

where we have assumed the beam divergence in the lateral direction to be negligible and the distance between the laser and the fiber lens is sufficiently small such that the beam pattern falls within the fiber core cross section. The far field distribution of the laser in the transverse plane can be approximated by[39]:

$$I(\vartheta) = I_0 \cos(2.4\vartheta), \qquad \vartheta \leq 0.65 rad, \tag{4.11(a)}$$

$$I(\vartheta) = 0 \qquad\qquad \vartheta \geq 0.65 rad, \tag{4.11(b)}$$

Using eqns.(4.9) and (4.10) we find $\eta_c = 0.43$ One effect of the lens is to significantly increase the coupling efficiency of the external fiber resonator compared with a flat fiber end. For example, when d/2r = 0 (ie. a flat end) $\eta_c \approx 0.1$ and increases to above 0.9 when d/2r $\approx$ 0.5. Another effect of the lens is to provide beam *refocusing* into the active layer of the laser, which is extremely important. Since the lens is an integral part of the external fiber resonator, the tolerances in alignment can be relaxed compared to a discrete fiber and lens combination.

2. The depolarization coupling coefficient η_p is related to the rotation of the input polarization. Since the laser output is polarized along the junction plane (TE), polarization conversion in the fiber effectively reduces the efficiency of the coupling. It has been observed that a length of 50 cm in a step index multimode fiber randomizes the polarization of the incident wave[33]. For a single mode fiber, the fiber length required for depolarization is much larger (> 300m). However, the results are a strong function of fiber stress and inhomogeneities. Thus the effect of depolarization is difficult to estimate. At worst, the polarization is completely mixed and we assume $\eta_p = 0.5$.

Using the above numbers, the threshold factor K, eqn.(4.4), is estimated to be $0.86 < K < 0.91$, while the experimental value of K is 0.9(from fig. 4.8). The coupling obtained in the experiment can thus be as good as could be expected. Further improvements can be made by using a fiber lens with a smaller radius of curvature.

4.5 Passive mode-locking of injection lasers in an external cavity

As mentioned in the general review section 4.2, very short optical pulses can be generated by active mode-locking a laser diode operating in an external cavity. Another simple method to generate pulses of moderate width (30-40 ps)is by directly driving the isolated laser diode with a very strong sinusoidal signal near the relaxation oscillation frequency, or by driving the laser with very sharp and intense electrical pulses [35,36]. But by far the shortest pulses were generated by passive mode-locking of badly degraded lasers coupled to an external cavity. (Incidentally, passively mode-locking produces shorter pulses than active mode locking in general - the passively mode-locked dye laser produces subpicosecond pulses unmatched by other actively mode-locked systems.) Passive mode-locking can also be produced with some undegraded lasers that do not self-pulse, but the optical pulses generated were generally sinusoidal and are far from being sharp. Generation of pulsations in a non-pulsing laser by coupling to an external cavity is sometimes called *self-locking*. It was also observed that the pulse repetition rate is not always at the inverse round trip time but at multiples of it. The above observations can be explained by the same trap model used in section 4.3. This model, although originally introduced for self-pulsing lasers, can also be applied to non-self-pulsing lasers. We assert that a sizable amount of traps or other absorption centers, whose density is below the critical density for self-pulsation, exists in non-self-pulsng lasers. When the laser is coupled to an external cavity, the coexistence of the saturable absorption and the laser gain medium mimic a weak passive mode-locking system.

The theoretical treatment is based on the same equations of the trap model, eqns. (4.1) - (4.3). The trap density T_0 is set at values below the critical value required for self-pulsation. When the laser is coupled to an external cavity with a sufficiently large coupling coefficient, the system becomes unstable and self-pulses.

The strength of this induced pulsation depends on the actual trap density. Fig 4.10 shows the calculated results of induced pulsations with different trap densities. The output in 4.10(a) resembles a sinusoid, while in 4.10(b) the pulses are considerably sharper. The diffference in trap density is about $9\times10^{15}cm^{-3}$, indicating that only a small difference in the density of absorbers can affect the pulse shape. These results can help explain the sharp contrast between the results of Broom et.al.[24] and other workers[23,37]. Fig 4.11 shows plots of the amplitude and frequency of the induced pulsations versus the external cavity length. The plots are taken for the same parameters as previously described in section 4.3, but for a much larger coupling coefficient ε of 0.2. The results are very similar to the observations by Broom et.al.[24]. One should also note the frequency jumping phenomenon as has been previously observed [11], but never fully explained.

In the following, we present some experimental results on the self-locking and passive mode-locking of injection lasers. In our studies we have observed in some cases results similar to those reported by Broom et.al[24]. However in other cases we observed a spiking of the light output at the cavity transit time or a harmonic of it. Using the model developed above we are able to qualitatively explain our results.

The microwave spectrum of several lasers coupled to an exteral cavity are shown in Fig 4.12(a) → (c). These lasers display a flat microwave spectrum when the external cavity is blocked, indicating that they are not self-pulsing. Spikes are induced in the spectrum at the cavity round trip frequencies(except in (b), where the resonance occurs at twice the round trip frequency) indicating self-locking. The difference in the strength of the pulsations in these three lasers can be attributed, according to the above theoretical model, to the difference in absorber densities present in the lasers. As a matter of fact, the laser in fig 4.12(c) has been operated for a considerable longer period of time than those in fig 4.12(a) and (b). The

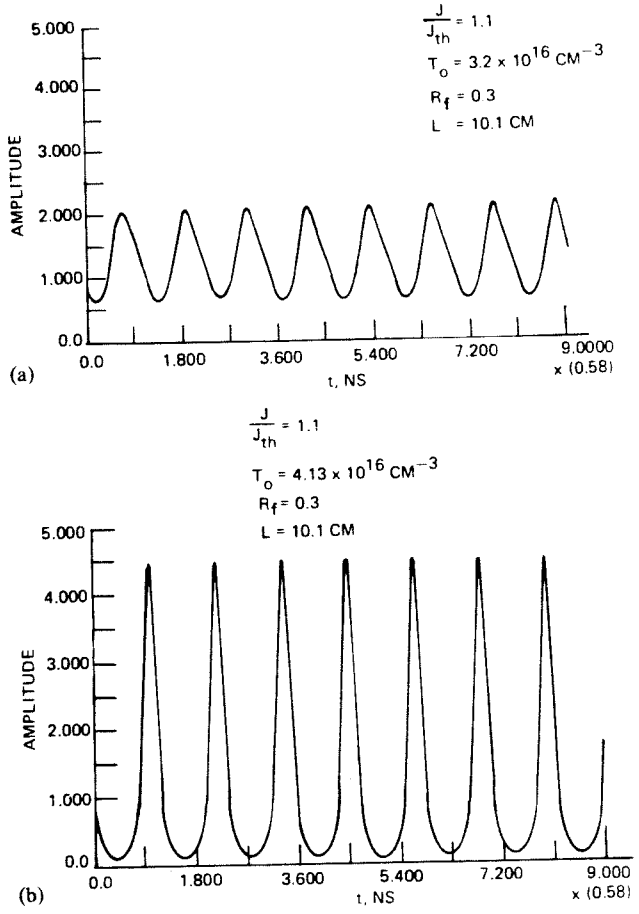

Figure 4.10. *Calculated pulsation outputs of injection lasers coupled to external cavities. (a)* $T_0=3.2\times10^{16}/cm^3$, *(b)* $T_0=4.13\times10^{16}/cm^3$. *In both cases the laser does not pulse without the external cavity.*

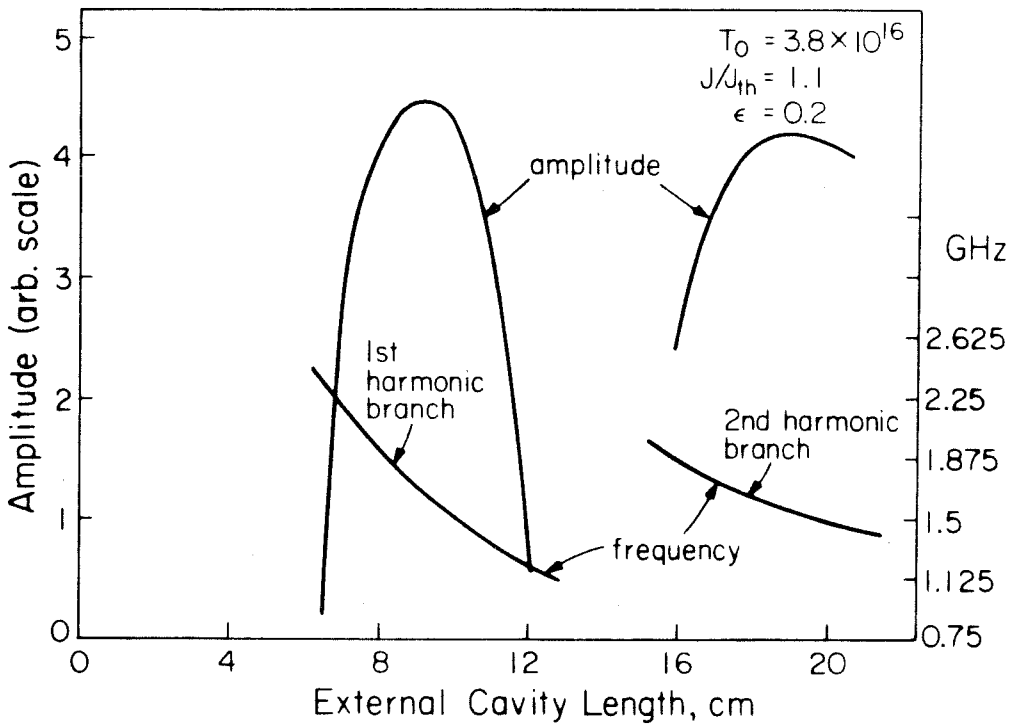

Figure 4.11. *Calculations showing the amplitude and frequency of the induced pulsations vs external cavity length.*

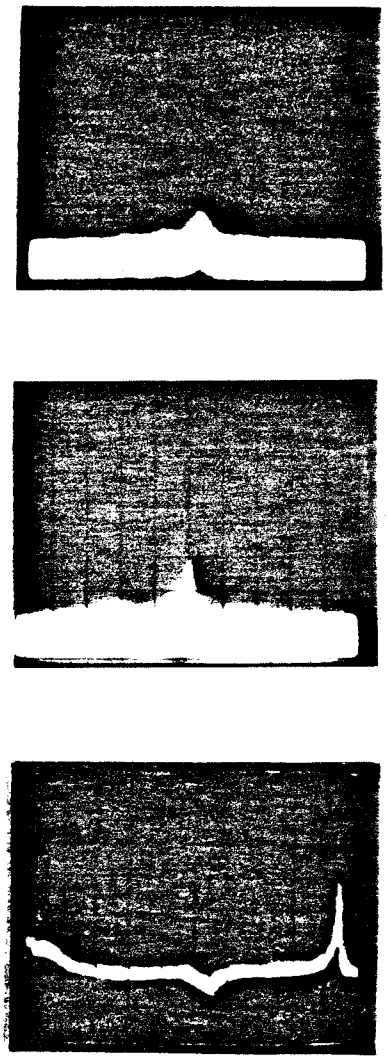

Figure 4.12. *Microwave spectrum of output of three different lasers coupled to external cavities. Vert.: 10dB/div, Hori.: 50MHz/div, center at 2.3 and 2.1GHz respectively for (a) and (b), 0 - 1.8GHz full scale for (c).*

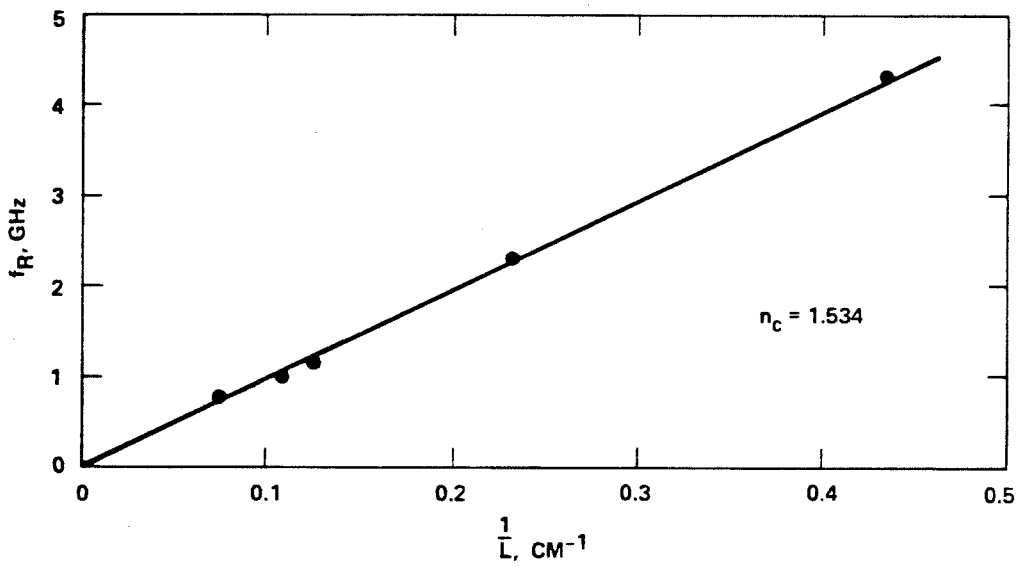

Figure 4.13. *Round trip resonance frequency vs inverse of external cavity length.*

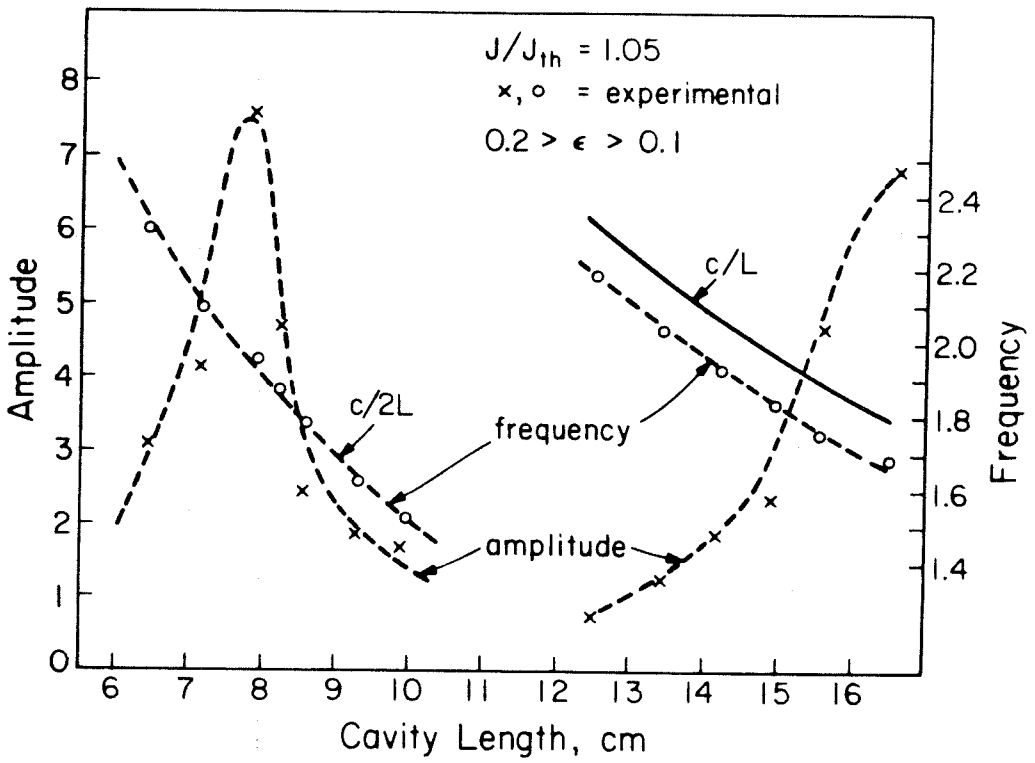

Figure 4.14. *Experimental amplitude and frequency of induced resonance vs external cavity length.*

pulsation frequency locks to the external cavity round trip frequency as it length is varied, as shown in fig 4.13. The amplitude and frequency of the induced pulsation of the laser in fig 4.12(c) are shown in fig 4.14 ; these results are very similar to the results as plotted in Fig 4.11.

The temporal display of the light output of the laser shown in fig. 4.12(a) is shown in fig. 4.15, with a small microwave drive applied at the spiking frequency to stablize the pulses. The output is modulated, but the pulses do not appear sharp. This is similar to the computed low-trap-density case in fig. 4.10(a). Fig 4.16 shows the temporal pulsing output of the laser in fig 4.12(c); the pulses are about 150ps in width and is detector limited. The results are very similar to the calculated result in fig 4.10(b) corresponding to the high-trap-density case.

With a self-pulsing laser, the trap density T_0 is sufficiently high that the isolated laser pulses without an external cavity. The effect of the external cavity is either to enhance or suppress it, depending on the cavity length, as illustrated in section 4.3. Fig. 4.17 shows the pulse output of a self-pulsing laser coupled to a cavity of such a length that the spiking is enhanced. The pulses in this case is detector limited to 50 ps. Nonlinear second harmonic generation (SHG) autocorrelation measurements have shown that this kind of passively mode-locked system can give pulses as short as 5 ps [23].

In closing, we would like to mention that the results presented above provide a method for diagnosing self-pulsing before it develops. Using equations (4.1) - (4.3) presented in section 4.3, we can correlate the amplitude and bandwidth of the induced resonance versus external cavity length and absorber density T_0. The experimental curves can be fitted to the calculations to give T_0. The test can be performed in a laser which does not self-pulse initially, but still contains a high density

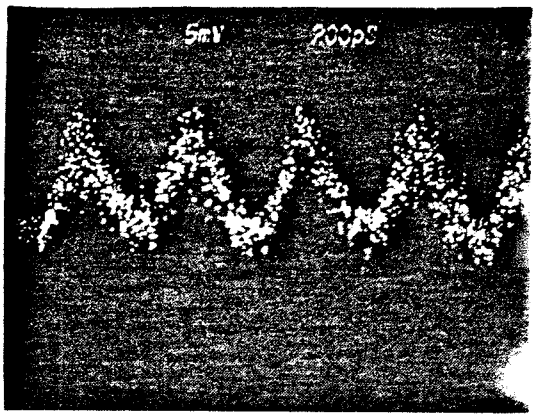

Figure 4.15. *Output pulse shape (positive going) of an incompletely mode-locked laser. Hori. : 200ps/div.*

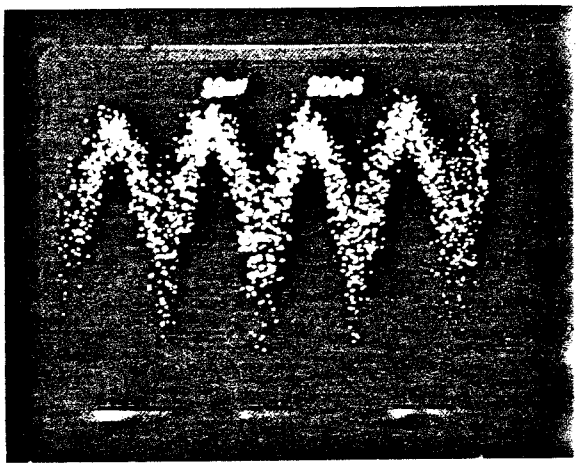

Figure 4.16. *Detector limited output pulse (negative going) of a passively mode-locked laser which initially does not self-pulse. Hori. : 200ps/div.*

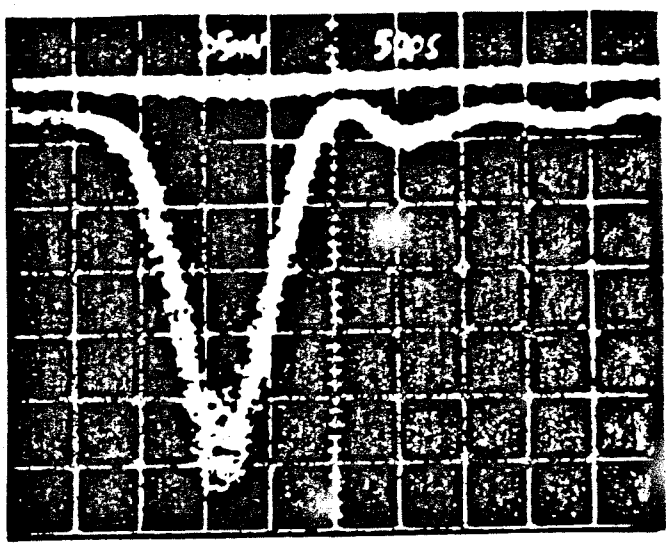

Figure 4.17. *Detector limited output of a passively mode-locked laser which self-pulses without an external cavity. Hori. : 50ps/div.*

of absorbers. When this laser is placed in an external cavity, an induced resonance can be obtained. By monitoring the amplitude and bandwidth of the induced resonance versus time one can determine the time rate of change of the absorbers dT_0/dt. It should then be possible to correlate laser structure and fabrication process to dT_0/dt. These measurements can be made before the isolated laser starts to self-pulse. This technique should provide a convenient and non-destructive test.

4.6 Operation characteristics of a buried heterostructure laser with controllable amount of saturable absorption.

As we have seen in the above sections, the presence of saturable absorbing defects leads, on the one hand, to undesirable self-pulsation, and on the other hand, to picosecond pulse generation by passive mode-locking. The latter would have been extremely useful if not for the fact that the absorbing defects in injection lasers cannot be reliably controlled, and that short pulses can be generated only with lasers aged to the point where catastrophic failure is imminent. Controlled saturable absorption has been introduced in semiconductor lasers by Lee et al [4] more than a decade ago with a two-section contact conficuration, and indeed verified that self-pulsation can be generated with this structure. Recently, this double-section scheme was applied on a more advanced laser structure (the transverse junction stripe laser)[40] and subsequent streak-camera measurements showed that the pulsations so generated have pulse widths of about 16ps. Due to the fact that contacts had to be made to both of the tandem sections, the lasers could not be bonded junction-down and cw operation was difficult, which made the device not suitable for practical applications. Recently, Carney and Fonstad [41] fabricated an eight-section contact on a proton-stripe laser, and, despite relatively high thresholds (> 150 mA) managed cw operation of the device. They observed some nonlinearities

in the light-current characteristics. In this section, independent results of a segmented contact laser using very low threshold state-of-the-art laser devices will be described. The following characteristics of a "classical" self-pulsing laser have been observed: non-linearities in the light-current characteristics, light-jumps, hysteresis, self-pulsation above the light-jump, and strong coupling with the external electrical circuit near the light-jump region [42]. The device is a buried heterostructure (BH) laser with a two-segment contact as shown in fig 4.18. The use of the sophisticated BH structure eliminates other extraneous effects such as lateral carrier diffusion, unstable lateral optical modes or damage defects as in a proton-stripe laser. These are effects that mask the artificially introduced nonlinearity and can lead to self-pulsations and light-jumps by themselves[16]. These BH lasers have cw thresholds in the 30-40 mA range with junction-up and diode lengths of 250 μm. The results described below show that this device should prove useful in reliable picosecond pulse generation by passive mode-locking.

The currents through the two sections are provided by independently controlled current sources. The measured cw light-current characteristics of the device are shown in fig. 4.19. The curves are the light vs the current (I_1) passing through one of the contact segments (the segment with length 125 μm) with the current through the other segment (I_2) held at a fixed value. The measured characteristics with I_2 = 0 shows a lasing threshold of about 27 mA and a linear light-current relation up to an output power of 3 - 4 mW/facet. This is not expected since, with a zero pump current, the second section should act as a saturable absorber and non-linearities should result. The possibility that the pump current from one section can leak to the other cannot be justified since the resistance between the two contacts was measured to be about 1 $k\Omega$. A possible explanation is due to the difference in the band-gap of the two sections under different pumping conditions and the saturation

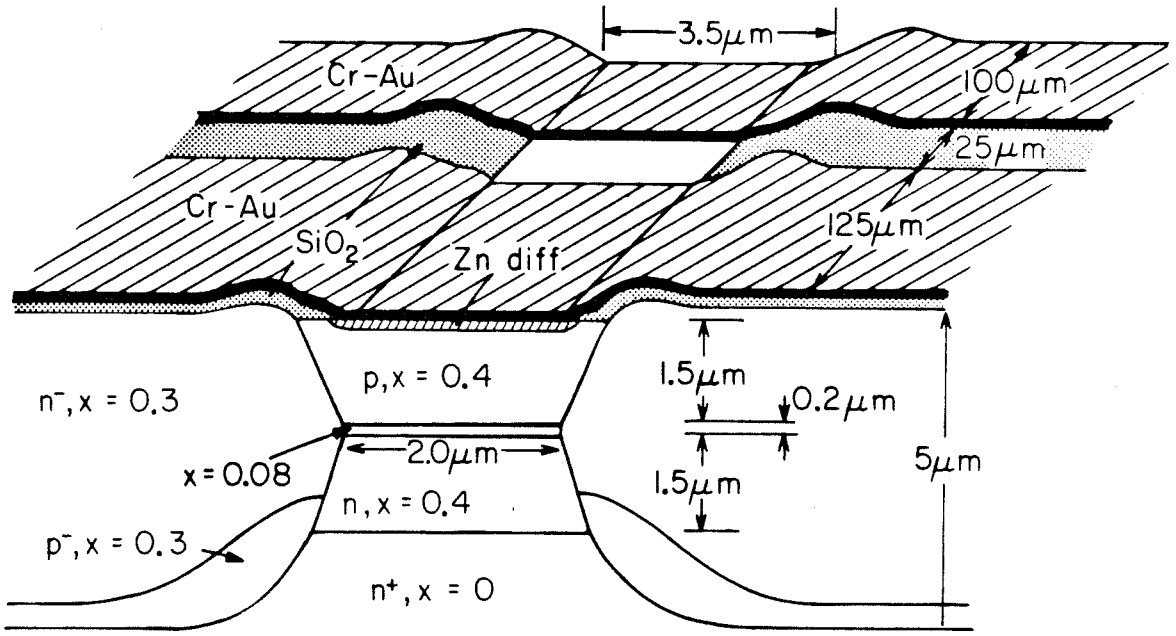

Figure 4.18. *Buried heterostructure laser with segmented contact.*

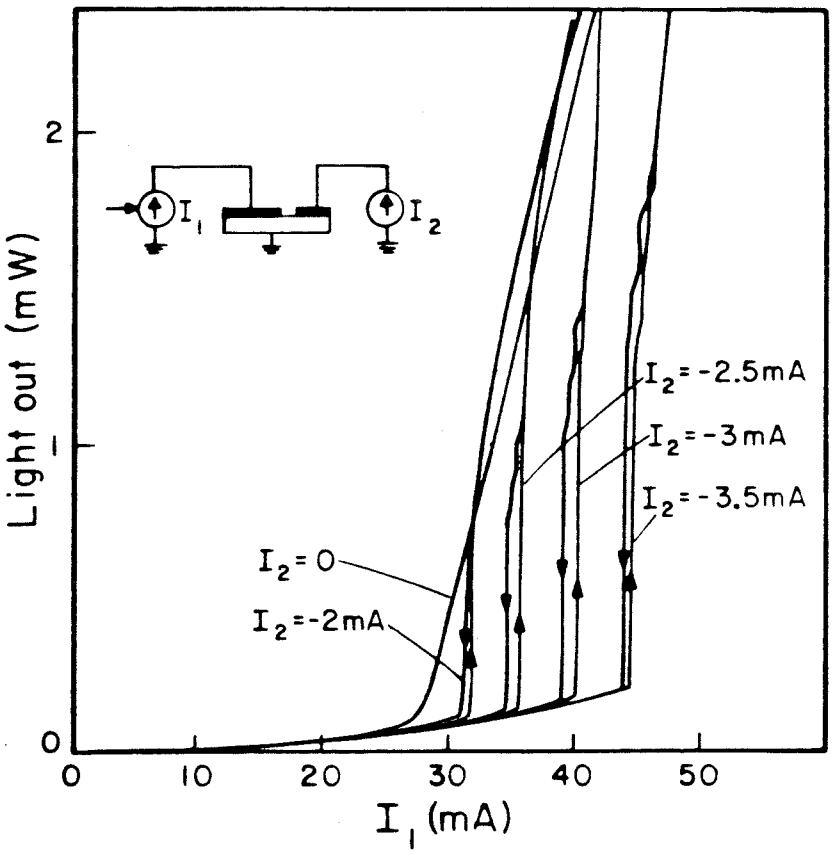

Figure 4.19. *Measured light-current characteristics of the segmented contact laser.*

of the unpumped section by spontaneous emission from the first section. With I_2 = -2 mA, however, non-linearities including a light-jump result. This kind of characteristic is expected from the presence of saturable absorbers. With further increase in the negative current ($-I_2$)through the second section, the jump becomes more spectacular and hysteresis is observed. These results are in agreement with the calculated light-current characteristics predicted in lasers including saturable absorbers, as shown in fig. 4.20. These results are the steady state solutions of the simple laser rate equations including an absorption which saturates as $\frac{1}{1+\frac{P}{P_s}}$, where P is the photon density and P_s is the saturation density. The rate equations are

$$\frac{dN}{dt} = J - N - NP \qquad 4.12(a)$$

$$\frac{dP}{dt} = NP - P(1 + \frac{L_0}{1+\frac{P}{P_s}}) + \beta N \qquad 4.12(b)$$

The quantity L_0 describes the amount of saturable absorption. It is directly proportional to the length of the absorbing section, and is related to the current passing through that section - L_0 increases as I_2 is decreased[43]. The steady state relationship between the pump current J (through the first section) and the photon density P is given by

$$J = (\frac{1+P}{2})(-\frac{P}{\beta} + [(\frac{P}{\beta})^2+\frac{4P}{\beta}(1+\frac{L_0}{1+\frac{P}{P_s}})]^{\frac{1}{2}}) \qquad 4.13$$

$$J = (1+P)(1 + \frac{L_0}{1+\frac{P}{P_s}} - \frac{\beta}{P}(1+\frac{L_0}{1+\frac{P}{P_s}})^2 + \cdots)$$

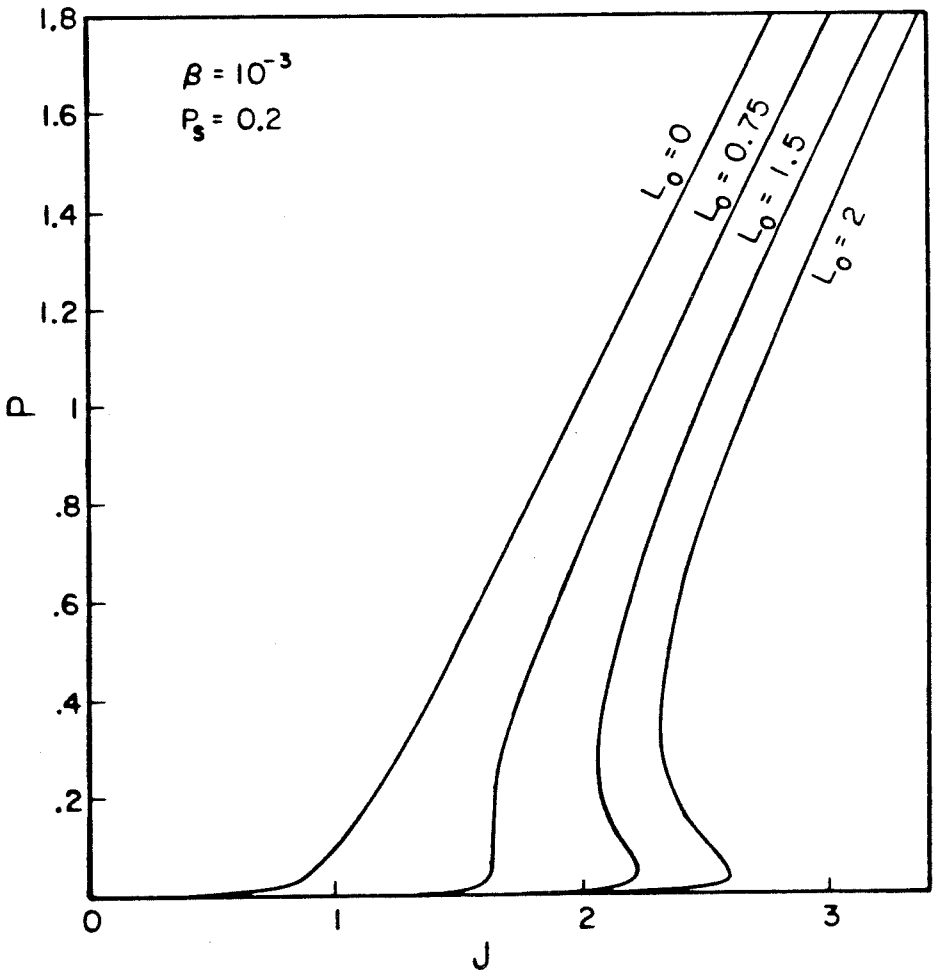

Figure 4.20. *Calculated light-current characteristics of a laser with satuarable absorption.*

4.14

The condition that light jump and hysteresis occur can be calculated in a straightforward manner:

$$\frac{1}{P_s} > 1 + \frac{1}{L_0} \qquad 4.15$$

This means that for bistability to occur, the saturation photon density P_s must be considerably smaller than one, which can be shown to be the case in real semiconductors. The results shown in fig. 4.20 are obtained with $P_s = 0.2$.

The microwave spectrum of the detected output was observed with a spectrum analyzer. It was found that self-pulsation occurs above the light jump. The pulsing frequency increases as the current through the first section I_1 is increased, in a manner similar to a typical self-pulsing laser, as shown in fig. 4.21. The lasing spectrum consisted of a single mode for $I_2 = 0$, but consisted of a large number of broadened lines when I_2 was decreased to a value where non-linearities in the light-current characteristics are observed. This is consistent with the occurence of self-pulsation in that regime of operation. Near the light jumps, the random fluctuations between the two possible light levels interacted with the external electricial circuitry to produce very narrow band oscillations, similar to that observed by Paoli [42]. Near and far field measurements indicate that despite self-pulsing, the transverse mode remains stable in the fundamental mode at all operating currents, showing the effectiveness of the waveguiding structure.

It was thus demonstrated that a controllable amount of saturable absorber can

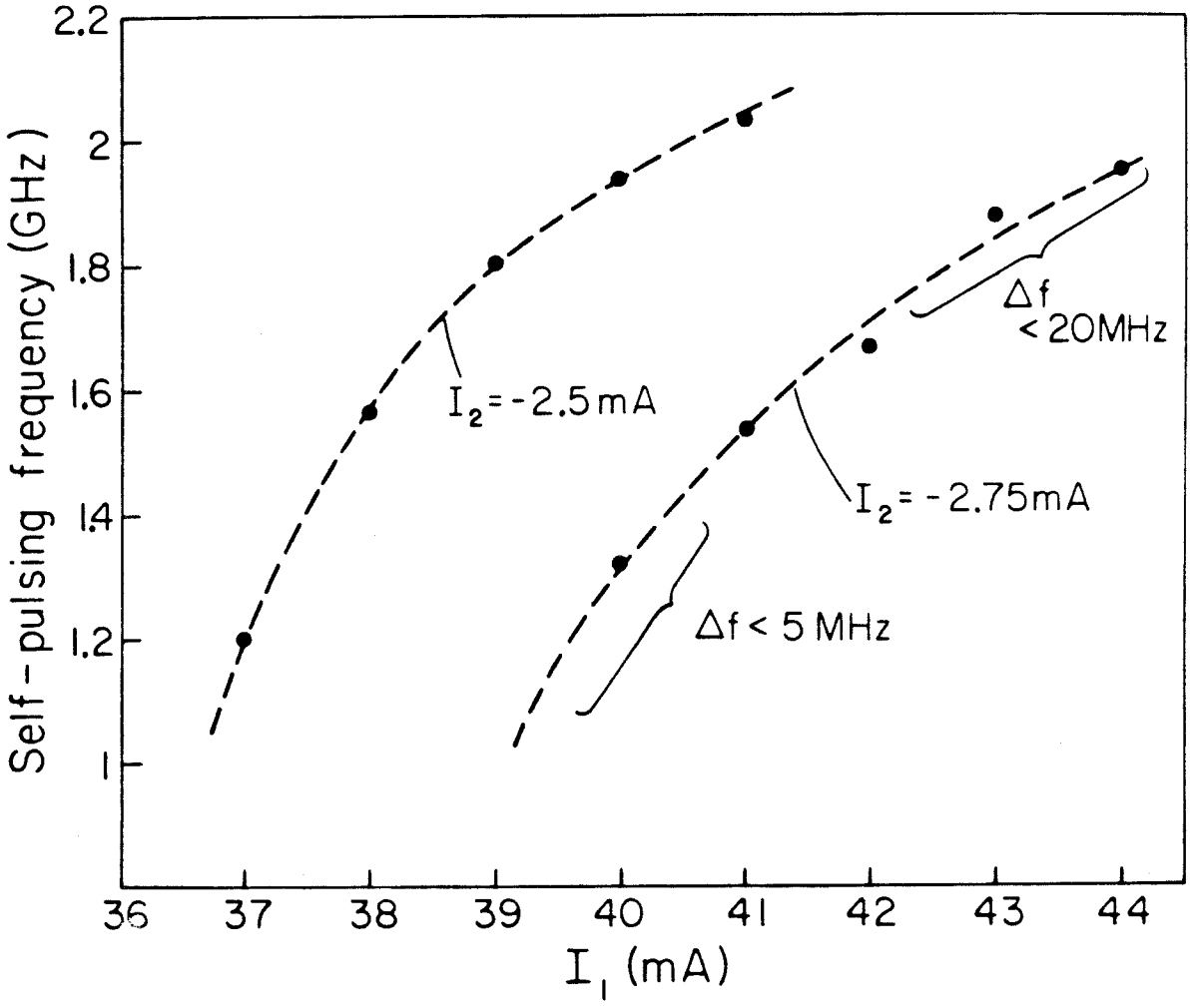

Figure 4.21. *Measured self-pulsation frequency of the segmented contact laser versus the pump current* I_1.

be introduced into an otherwise well-behaved laser to produce characteristics of a self-pulsing laser, which can be used for reliable picosecond pulse generation.

References - Chapter 4

1. N.G.Basov, IEEE J. Quant. Electron., **QE-4**, 855 (1968).
2. C.V.Shank and E.P.Ippen, Appl. Phys. Lett., **27**, 488 (1974).
3. E.P.Ippen and C.V.Shank, Appl. Phys. Lett., **27**, 488 (1975).
4. T.P.Lee and R.H.Roldan, IEEE J. Quant. Electron., **QE-6**, 339 (1970).
5. T.L.Paoli and J.E.Ripper., Phys. Rev. Lett., **22**, 1085 (1969).
6. M.Sargent III, M.O.Scully and W.E.Lamb,Jr., **Laser Physics** , pg127, Addison-Wesley 1974.
7. N.Chinone, K.Aiki and R.Ito, Appl. Phys. Lett., **33**, 990 (1978).
8. L.Figueroa, K.Y.Lau and A.Yariv, Appl. Phys. Lett., **36**, 248 (1980).
9. T.L.Paoli, IEEE J. Quant. Electron., **QE-13**, 351 (1977).
10. R.L.Hartman, R.A.Logan, L.A.Koszi and W.T.Tsang, J. Appl. Phys., **50**, 4616 (1979).
11. H.Imai, K.Isozumi and M.Takusagawa, Appl. Phys. Lett., **33**, 330 (1978).
12. J.A.Copeland., Electron. Lett., **14**, 809 (1979).
13. D.Kato, Appl. Phys. Lett., 588 (1977).
14. R.W.Dixon and W.B.Joyce, IEEE J. Quant. Electron, **QE-15**, 470 (1979).
15. J.P.Van der Ziel, J.L.Merz and T.L.Paoli, J. Appl. Phys., **50**, 4620 (1979).
16. J.C.Campbell, S.M.Abbott and A.G.Dentai, J. Appl. Phys., **51**, 4010 (1980).
17. T.L.Paoli and J.E.Ripper, IEEE J. Quant. Electron., **QE-6**, 335 (1970).
18. P.T.Ho, L.A.Glasser, E.P.Ippen and H.A.Haus, Appl. Phys. Lett., **33**, 241 (1978).
19. L.A.Glasser, Electron. Lett., **14**, 725 (1978).
20. P.T.Ho, Electron. Lett., **15**, 526 (1979).

21. L.Figueroa, K.Y.Lau, H.W.Yen and A.Yariv., J. Appl. Phys., **51**, 3062 (1980).

22. K.Y.Lau, L.Figueroa and A.Yariv., IEEE J. Quant. Electron., **QE-16**, 1329 (1980).

23. E.P.Ippen, D.J.Eilenberger and R.W.Dixon, Appl. Phys. Lett., **37**, 267 (1980).

24. R.F.Broom, E.Mohn, C.Risch and R.Salathe, IEEE J. Quant. Electron., **QE-6**, 335 (1970).

25. T.Kanada and K.Nawata, IEEE J. Quant. Electron., **QE-15**, 559 (1979).

26. R.Lang and K.Kobayashi, IEEE J. Quant. Electron., **QE-16**, 347 (1980).

27. D.Kato, J. Appl. Phys., **44**, 2756 (1973).

28. E.Mohn, Proceedings of the 1968 Symp. on GaAs, St. Louis, pg 101.

29. F.Stern, IEEE J. Quant. Electron., **QE-9**, 290 (1973).

30. R.P.Salathe, Appl. Phys., **20**, 1 (1979).

31. D.Botez, paper C3, IEEE International Semiconductor Laser Conference, San Francisco, 1978.

32. H.Kressel and J.K.Butler, **Semiconductor Laser and Heterojunction LEDs** , pg 472, Academic Press 1977.

33. F.P.Kapron, N.F.Borelli and D.B.Keck, IEEE J. Quant. Electron., **QE-8**, 222 (1972).

34. I.Ladany, H.J.Wakstein, R.S.Crandall and O.R.Patterson, RCA Research Report, PRRL-78-CR-43, pf 22, 1979.

35. T.Kobayashi, A.Yoshikawa, A.Morimoto, Y.Aoki and T.Sueta, 11th International Quantum Electronics Conf., paper W1, Boston 1980.

36. J.AuYeung, to be published.

37. L.Figueroa, K.Y.Lau and A.Yariv, Society of Photo-optical Inst. Engineers Tech. Symp., Los Angeles 1981.

38. O.Hirota and Y.Suematsu, IEEE J. Quant. Electron., **QE-15**, 142 (1979).

39. H.Kressel and J.K.Butler, **Semiconductor Lasers and Heterojunction LEDs** ,pg 214, Academic Press 1977.

40. H.Ito, N.Onodera, K.Gen-Ei and H.Inaba, Electron. Lett., **17**, 16 (1981).

41. J.K.Carney and C.G.Fonstad, Appl. Phys. Lett., **38**, 303 (1981).

42. T.L.Paoli, IEEE J. Quant. Electron., **QE-16**, 1248 (1980).

43. Ch. Harder, K.Y.Lau and A. Yariv, to be published.

CHAPTER 5

SMALL SIGNAL THEORY OF THE DYNAMICS OF LASER-EXTERNAL CAVITY INTERACTIONS

In the last chapter, the general pulsation behavior of injection lasers coupled to an external cavity was discussed, and a theory was presented to explain the experimental results. The theory made use of the fairly complicated electron trap model, which made analytic description of various important features of the results difficult. Among these features are the dependence of the pulsation characteristics on the external cavity length as shown in figs 4.5 and 4.14, and the minimum amount of coupling between the laser and the external resonator required for quenching or induced pulsation at various bias levels and trap densities. However, common to most models proposed for self-pulsation is the presence of a saturable loss or a superlinear gain inside the laser medium; the trap model is actually a combination of both : the traps are saturable absorbers, and when the traps are bleached, electrons are released into the conduction band which effects to increasing the optical gain. In order to gain additional understanding of the dynamics of the laser-external cavity system, we shall use a simple phenomenological saturable absorber in the following calculations. Through a small signal analysis, we shall derive analytical expressions for the ranges of external cavity length where quenching and induced pulsing occur. Intuitive understanding of the general cavity-length dependence can be gained by casting the model in the form of a microwave oscillator with a finite gain band, the width of which depends on the coupling cofficient between the laser diode and the external cavity.

5.1 Analysis of rate equations with a saturable loss or superlinear gain

As mentioned before, common to most proposed models for self-pulsations are two underlying effects : saturable loss and superlinear gain. It is thus reasonable to

believe that a general saturable loss description is applicable to most lasers. The rate equations with a simple saturable absorbing loss of the form $L = \frac{L_0}{(1+\frac{P}{P_s})}$ [1] are:

$$\dot{N} = J - N - NP \qquad 5.1(a)$$

$$\dot{P} = \gamma(N - 1 - L)P \qquad 5.1(b)$$

where N is the electron density, P is the photon density, P_s is the saturation photon density of the absorber, J is the pump current density γ is the ratio of the spontaneous to photon lifetimes as before,and the dot denotes derivative with respect to the normalized time. The absorber density L_0 here mimics the trap density T_0 of the last chapter. When L_0 exceeds a certain critical value, the system of equations(5.1) will become unstable and predict pulsation, as in the case of the trap model. Fig. 5.1 shows plots of the frequency of the pulsation versus pump current, for various absorber densities L_0. The plot looks surprisingly similar to fig 4.1(a), obtained using the trap model : the pulsation frequency decreases as the absorber density increases, and increases with the bias current.

Stability of the steady state of (5.1) is examined by the familiar small signal analysis, where we write $N = N_0+n$, $P = P_0+p$ where n and p are small perturbations and N_0 and P_0 are the steady state values. Assuming solutions of the form e^{st}, we have the following characteristic equation:

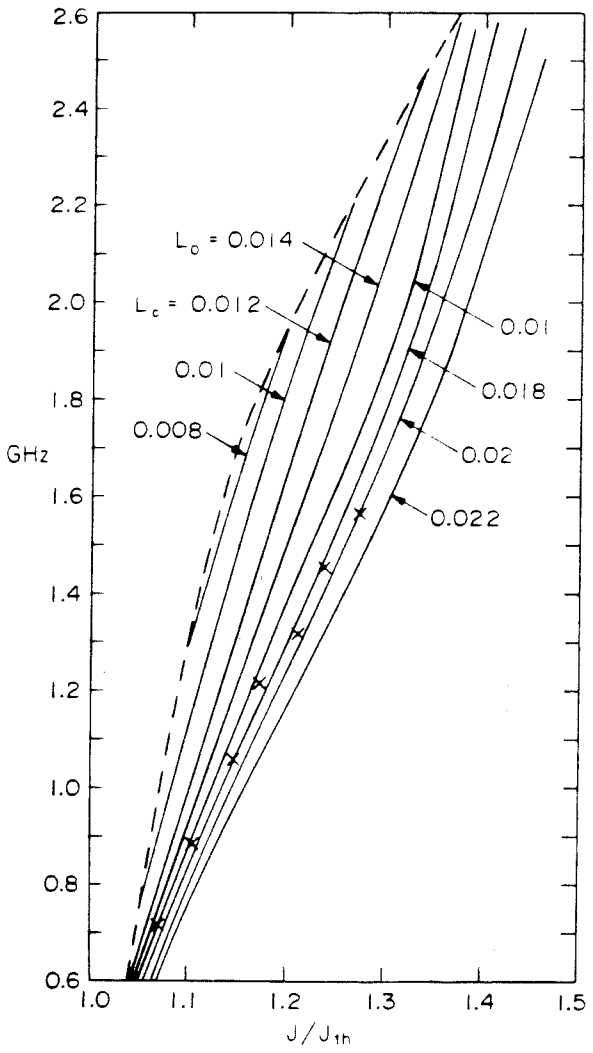

Figure 5.1. *Calculated self-pulsation frequency vs injection current using simple absorber model. No pulsing occurs above the dotted line.*

$$f(s) = s + \gamma P_0\left(\frac{N_0}{s+(1+P_0)} - \xi\right) = 0 \qquad 5.2$$

where

$$\xi = \frac{L_0}{[1+(P_0/P_s)]^2 P_s} \qquad 5.3$$

As is well known, instability results if any of the zeros of f(s) lies in the right half of the complex plane.

We shall perform a stability analysis using Nyquist diagrams [2,3]. Although (5.2) is simple enough for direct analytic solution, the Nyquist diagram approach proves to be very useful in the case when external cavity feedback is introduced. The Nyquist plot is generated by mapping the coutour C on the complex plane into a new contour Γ by an analytic function f(z), where C is the right half circle at infinity as shown in fig. 5.2. The number of times Γ encircles the origin in the clockwise direction is the number of zeros minus the number of poles of f(z) in the right half complex plane[2]. Fig. 5.3 shows a plot of Γ; the solid line is the locus $f(j\omega)$. It can be shown that Γ will encircle the origin twice if

$$\xi > \frac{1+P_0}{\gamma P_0} \qquad 5.4$$

Under this condition, the zeros have positive real parts and pulsations start to build up. Expressed in terms of the absorber density L_0, (5.4) can be written as

$$\frac{L_0}{P_s} \geq \frac{1+P_0}{\gamma P_0}\left(1+\frac{P_0}{P_s}\right)^2 \qquad 5.5$$

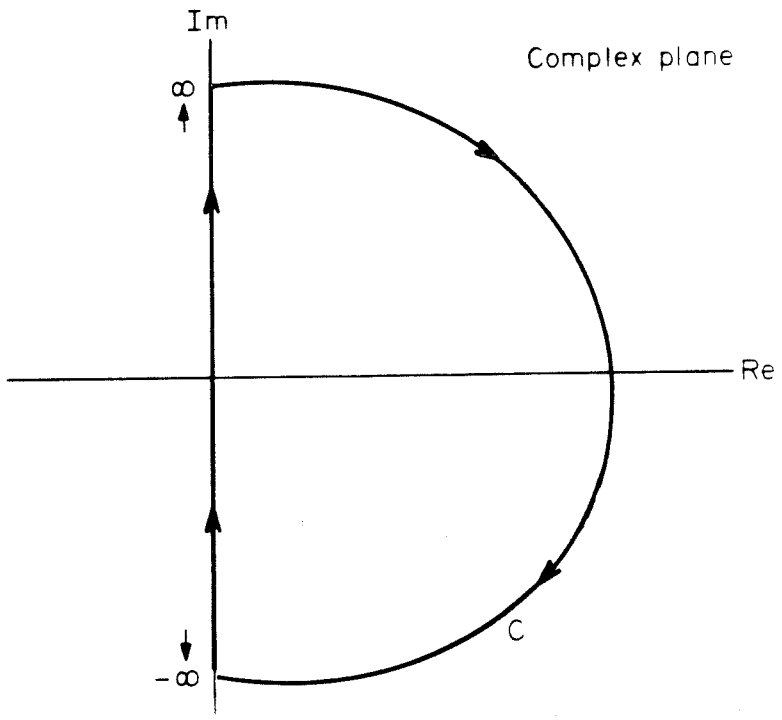

Figure 5.2. *The contour C on the complex plane.*

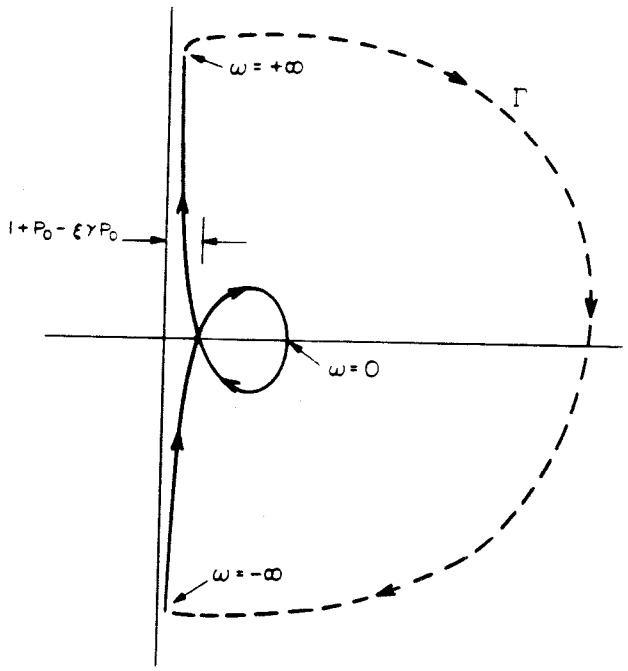

Figure 5.3. *Nyquist diagram for rate equations including saturable absorbers.*

This result is similar to that of Haus[1] in analyzing parameter ranges for passively mode-locked lasers.

It is hardly surprising to find that a superlinear gain - a stimulated gain that takes the form $g = NP(1+\xi P)$, where N and P are the electron and photon densities, respectively - would produce the same instability if ξ exceeds the amount given in (5.4).

5.2 Characteristic equation of the combined laser-external cavity system

The photon rate equation with a delayed feedback term is

$$\dot{P}(t) = \gamma(N(t)P(t) - P(t) - \frac{L_0 P(t)}{1+\frac{P(t)}{P_s}} + \varepsilon P(t-\tau)) \qquad 5.6$$

where τ is the roundtrip time of the external cavity, and ε is the coupling coefficient as defined in earlier chapters. This ε can be estimated experimentally by the shift in the lasing threshold as described in section 4.4. The steady state solution of the modified rate equation (5.6) is

$$N_0 = 1 + \frac{L_0}{1+\frac{P_0}{P_s}} - \varepsilon \qquad 5.7$$

The small signal photon equation is obtained in a straightforward manner:

$$\dot{p} = \gamma[P_0 n + \xi P_0 p + \varepsilon(-p + p(t-\tau))] \qquad 5.8$$

where ξ is defined as before ((5.4)). Note that as $\tau \to 0$, the feedback term disappears, showing that any quenching or induced pulsation effects are *retarded* effects and

not merely a change in the photon lifetime.

Equation (5.8) is a difference-differential equation which does not lend itself to easy solution. However, its stability can be analyzed through Laplace transformation [4] and the use of Nyquist diagrams, and simple expressions for the minimum ε required and the quenching bands can be deduced geometrically.

A Laplace transformation of equation (5.8) and (5.1(b)) gives the following transcendental characteristic equation:

$$f_{f.b.}(s) = s + \gamma[P_0\frac{N_0}{(1+P_0)+s} - \xi P_0 + \varepsilon(1-e^{-s\tau})] = 0 ; \qquad 5.9(a)$$

$$f_{f.b.}(s) = f(s) + \gamma\varepsilon(1-e^{-s\tau}) \qquad 5.9(b)$$

where $f(s)$ is the characteristic function of the laser without feedback.

5.3 Quenching range of self-pulsing lasers coupled to a short external cavity

We first consider the case of a self-pulsing laser. The Nyquist diagram of a self-pulsing laser is shown in fig. 5.4(a). The locus of $f(j\omega)$ as parametrized by ω passes very close to the imaginary axis. Since the locus is symmetric with respect to ω, we will just look at the positive branch of ω. The portion of the locus closest to the origin approximates a vertical straight line at a distance $K = 1+P_0-\xi\gamma P_0$ to the *left* of the origin (fig. 5.4(b). The value of ω at that part of the locus is approximately equal to ω_0, the imaginary part of the zero of $f(s)$, which corresponds roughly to the pulsing frequency of the laser. (The actual frequency is somewhat lower due to the large signal effect.) When feedback is included, the locus becomes $f_{f.b.}(j\omega) = f(j\omega)+\gamma\varepsilon(1-e^{-j\omega\tau})$. The effect of this additional term on the portion of the locus closest to the origin is shown in fig. 5.5. The locus is shifted to the right by an

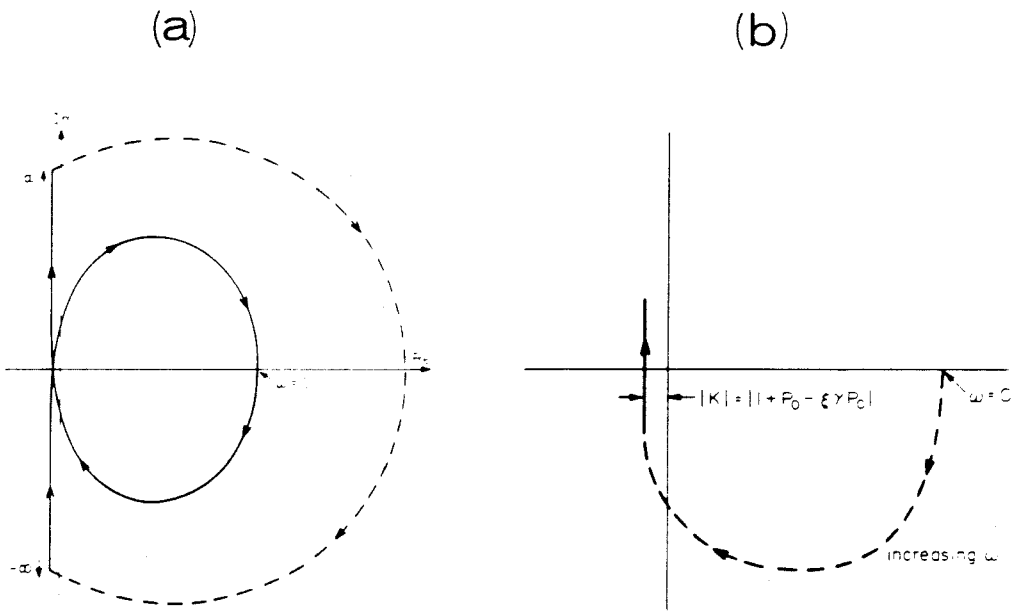

Figure 5.4. *(a) Nyquist diagram for a self-pulsing laser and (b) approximate locus near the origin. Only the +ve* ω branch is shown.

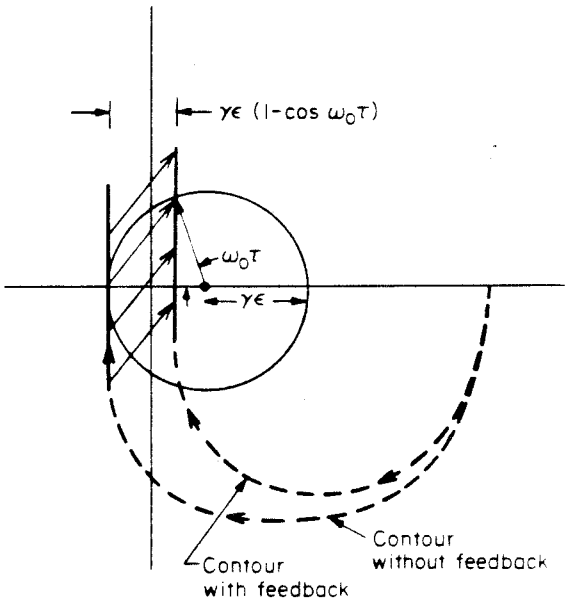

Figure 5.5. *Nyquist diagram illustrating the effect of external cavity on a self-pulsing laser.*

amount $\gamma\varepsilon(1-\cos\omega_0\tau)$. For sufficiently large ε and a suitable delay τ, we can see that the locus would no longer encircle the origin - the system becomes stable and pulsations are quenched. From fig. 5.5 we can see that the minimum amount of coupling ε required is

$$\varepsilon_{min} = -K/2\gamma \qquad 5.10$$

where $K = 1+P_0-\gamma P_0\xi < 0$ for a self-pulsing laser, $P_0 \approx J-1$, J is the pump current, and ξ is as defined previously (eqt. (5.3)). The range of external cavity round-trip time τ for which quenching occurs is

$$\frac{1}{\omega_0}(2\pi - \cos^{-1}\varphi) > \tau > \frac{1}{\omega_0}\cos^{-1}\varphi \qquad 5.11$$

where $\varphi = (1-K/\gamma\varepsilon)$ and ω_0 is approximately the self-pulsing frequency of the laser. We note that a very small ε is sufficient to harness the quenching effect. Taking a value of $L_0 = 0.02$ (which gives self-pulsation frequencies that fit typical experimental data, fig. 5.1), and assuming that the laser is operated at 1.1 threshold, $\gamma = 1000$, we have $\varepsilon_{min} \approx 0.002$. Of course, this amount of ε just barely pushes the zeros of the characteristic equation across the imaginary axis into the left half plane. To have a significant quenching effect, a larger ε is required so that the zeros lie deeper into the left half plane, which leads to a large damping.

To estimate the quenching band, we use the above numerical values, resulting in a self-pulsation frequency ω_0 of about 0.8 GHz. Then, $K = 1+P_0 - \gamma\xi P_0 \approx -0.49$, and if we let $\varepsilon = 0.01$, the quenching band is calculated using (5.11) to lie approximately between 3 and 15 cm. This is compared with the numerical results shown in fig. 4.5 calculated using the trap model. The trap density used in that case produced self-pulsations at roughly the same frequency as above (0.8 GHz) and the same coupling

coefficient $\varepsilon = 0.01$ was used. The approximate agreement shows that the above analysis of the quenching effect is quite general and model independent.

Thus, it appears that as the external cavity length is increased, we expect to find alternating bands of quenching and pulsations. However, the above analysis is suitable only for short cavity lengths (which is where the quenching bands occur). For long cavity lengths, the Nyquist plot takes the form of a spiral as shown in fig. 5.6. The origin could not escape the fate of being enclosed at long cavity lengths, as shown in the pulsation amplitude versus cavity length plot of fig. 4.5.

It is also obvious from eqn. (5.10) that it will become increasingly difficult to quench the pulsations at higher bias current - which is what we observe in our experiment.

5.4 The microwave gain lineshape and mode structure of the combined system

Non-pulsing lasers, when coupled to external cavities, can be made to self-pulse with a pulsewidth in the picosecond range. As mentioned in section 4.5, such induced pulsing occurs only over a certain range of the external cavity lengths. In some cases, induced self-pulsing occurs at twice the external cavity roundtrip frequency. It is also a common experience, when working with lasers coupled to long fiber pigtails, to observe on the microwave spectrum of the optical output a *cluster of spikes* around around 1 - 2 GHz, and the frequency separation between spikes corresponds to the inverse of the pigtail round-trip time. All of the above mentioned hitherto complex pulsation phenomena can be explained very intuitively by interpreting the combined laser-external cavity system as a microwave oscillator with a limited gain band and discrete mode structure. The small-signal microwave gain lineshape and the mode frequencies will be derived analytically.

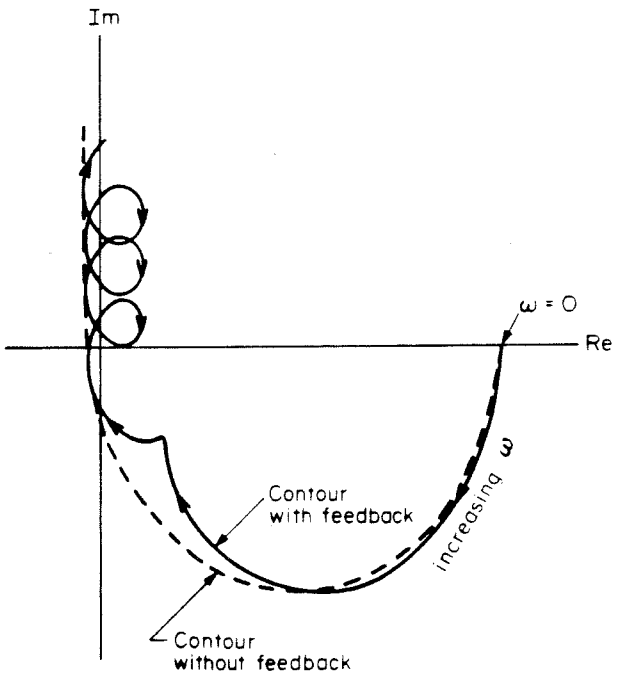

Figure 5.6. *Nyquist diagram for a self-pulsing laser coupled to a long cavity.*

As mentioned before, the dynamic behavior of the system is determined by the zeros of $f_{f.b.}(s)$ (eqn. (5.9)). Due to its transcendental nature, $f_{f.b.}(s)$ has an infinite number of complex zeros $g_k \pm i\omega_k$, $k = 1, 2, \cdots$. Alternatively, we can define a continuous function $g(\omega)$ such that $g(\omega_k)=g_k$. The imaginary part of the zeros ω_k indicates a resonant peak at the frequency $\frac{\omega_k}{2\pi}$ and these are the modes of the system. The system will spontaneously oscillate at the frequency ω_k if $g(\omega_k)> 0$.

The gain curve $g(\omega)$ can be derived with the help of the Nyquist diagram. This is done in the Appendix, resulting, for frequencies near the peak of the gain curve, in

$$g(\omega) = \frac{\omega^4 - 2\gamma P_0(N_0+\gamma\varepsilon\xi)\omega^2 + \gamma^2 P_0 N_0(P_0 N_0+2\varepsilon(1+P_0))}{2\gamma\varepsilon\omega^2} \qquad 5.12$$

and the mode frequencies

$$\omega_k = \frac{(2\pi k - \vartheta)}{\tau} \qquad 5.13$$

where τ is the external cavity roundtrip time, and ϑ is a small frequency pulling term given by

$$\vartheta \approx \frac{1}{\gamma\varepsilon} Im(f(2\pi k i)) \qquad 5.14$$

Fig. 5.7 shows a plot of $g(\omega)$ for various coupling coefficients ε, with $\gamma = 1000$, $P_0 = 0.3$, $N_0 = 1$, $\xi = 3.9\times10^{-3}$, and $\tau_s = 3$ns. As expected, the system is 'below threshold' unless ε is above a certain ε_{min}, and the linewidth widens with further increase in ε. For the modes near the line center (peak) of $g(\omega)$, the frequency pulling term ϑ is approximately given by $\vartheta = Im[f(\omega_0)]/\gamma\varepsilon$, where ω_0 is the line center frequency. For the above parameters, ϑ is approximately 0.05 rad so that the modes are virtually

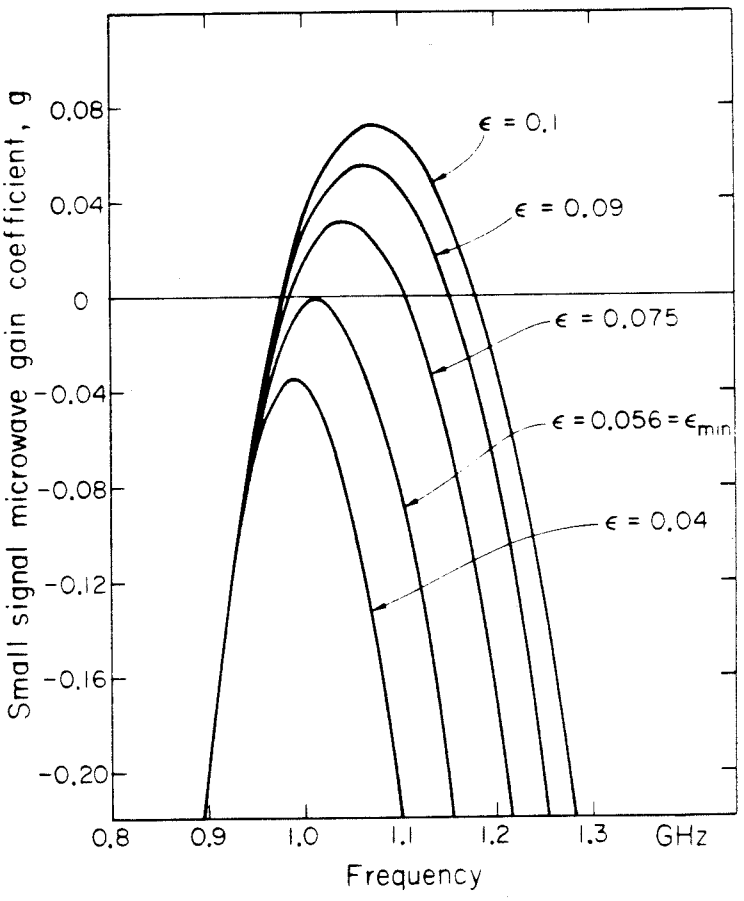

Figure 5.7. *The small signal microwave gain lineshape of the combined laser-external cavity system for various coupling coefficients ε.*

that of the passive external resonator.

We thus have the conditions for sustained microwave pulsation: first, the coupling between the laser and the external cavity must exceed a critical value so that there is a certain frequency range over which $g(\omega) > 0$. Then, at least one or more 'modes' given by (5.13) must lie within that frequency range. This range can be easily found by setting $g(\omega) = 0$, giving

$$\omega_{\pm}^2 = \gamma P_0(N_0+\gamma\varepsilon\xi) \pm \gamma^2 P_0 \xi \sqrt{\varepsilon(\varepsilon-\varepsilon_{min})} \qquad 5.15$$

where

$$\varepsilon_{min} = \frac{2N_0K}{\xi^2\gamma^2P_0} \qquad 5.16$$

is the minimum coupling for induced pulsing. The quantity K defined as $K=1+P_0-\gamma P_0\xi$ as before is an indication of how close the laser is to self-pulsing, or in the case when it is negative, it measures how deep the laser is into self-pulsing. The solid lines in fig. 5.8 are plots of ε_{min} versus the bias level as measured by the static photon density P_0 for two cases : 1) absorber density $L_0 = 0.005$ and saturation photon density $P_s = 0.5$; 2) $P_s = 1$ and $L_0 = 0.006$ (γ is taken to be 1000). (The calculated minimum absorber densities L_0 for self-pulsing are $L_0 \approx$ 0.006 and 0.007, respectively, for cases 1) and 2).) We can observe from fig. 5.8 that a very high coupling coefficient is required for inducing pulsations if the bias level is not optimized.

The hitherto complex behavior of the laser diode coupled to external cavities of various lengths can now be understood in very intuitive terms. When the external cavity length is very short, the microwave mode frequencies are very high and do not fall under the positive gain line. In fact, the value of $g(\omega)$ is large and negative at

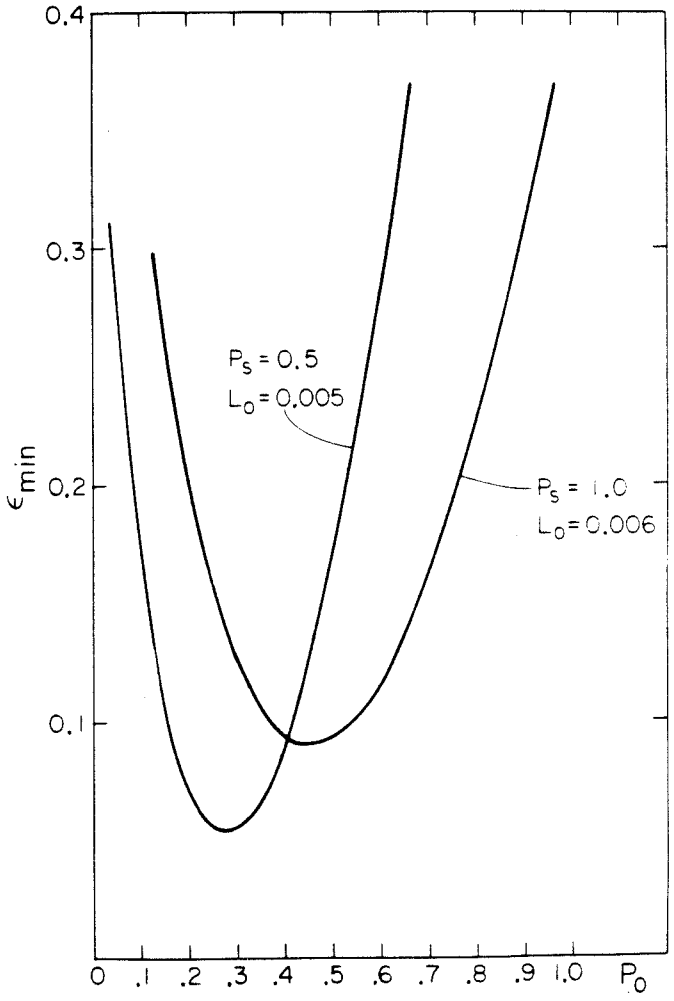

Figure 5.8. *Plot of ε_{min} required for induced pulsation in non-pulsing laser.*

high frequencies so that a short cavity actually serves to stablize the laser diode. As the external cavity length is increased, the first microwave mode ($\frac{kc}{2L}$,k=1) falls within the gain line and induced pulsation occurs at the fundamental roundtrip frequency. Further increase in the external cavity length brings the k=1 mode outside the gain line, and pulsation will cease until the k=2 mode moves in and induced pulsations occur at twice the roundtrip frequency, and so on. For very long cavities, several microwave modes lie within the gain line simultaneously, and 'multimode' microwave oscillation occurs, as often observed in lasers coupled to very long fiber pigtails. Badly degraded lasers, with a large absorbing defect density, are particularly vulnerable to such disturbance, as indicated by eqn. (5.16).

5.5 Effect of spontaneous emission on pulsation characteristics

In the analysis in previous sections, the spontaneous emission factor has been neglected for simplicity. However, if sufficiently large, it does influence the pulsation characteristics of the laser diode. It is known that a large spontaneous emission can suppress relaxation oscillation (section 3.2). Thus, suppression of self-pulsation should be expected for lasers with strong spontaneous emission[6]. This effect can be conveniently expressed in terms of an effective ξ, where ξ is a measure of the absorber strength as defined in equation (5.4). It will be shown that the effective value of ξ will be decreased, due to spontaneous emission. This, of course, is due to the physical fact the spontaneous emission saturates the absorber and effectively reduces its strength.

Inclusion of spontaneous emission modifies the photon rate equation (5.1(b)) into the following:

$$\dot{P} = \gamma[(N - 1 - \frac{L_0}{1+\frac{P}{P_s}})P + \beta N] \qquad 5.17$$

where β is the spontaneous emission factor as defined before (section 3.2). The steady state solution of (5.17) is

$$N_0 = \frac{(1 + \frac{L_0}{1+\frac{P_0}{P_s}})}{1+\frac{\beta}{P_0}} \qquad 5.18(a)$$

$$= 1 + \frac{L_0}{1+\frac{P_0}{P_s}} - \frac{\beta}{P_0} + \textit{higher order terms in } \beta \qquad 5.18(b)$$

The small signal photon equation is obtained as before:

$$\dot{p} = \gamma[(N_0 - \frac{L_0}{(1+\frac{P_0}{P_s})^2} - 1)p + (P_0+\beta)n] \qquad 5.20(a)$$

$$= \gamma[(\xi P_0 - \frac{\beta}{P_0})p + (P_0+\beta)n] \qquad 5.20(b)$$

Thus the effective ξ is given by

$$\xi_{eff} = \xi - \frac{\beta}{P_0^2} \qquad 5.21$$

Because ξ itself is of the order of 10^{-2} to 10^{-3}, the spontaneous emission will significantly reduce the absorber strength when $\beta \geq 10^{-3}$. The effect becomes more prominent when the laser is biased near threshold, for then most of the generated

photons are due to spontaneous emission. Thus, its inclusion does not affect the results we have obtained in previous sections, except for the reduction of the absorber strength. There is yet no direct experimental proof of this result. Wide stripe lasers, which have a smaller spontaneous emission factor, do tend to self-pulsate more often than lasers with good optical confinement, but this can be attributed to mode instability[7], which serves the opposite role of enhancing self-pulsation. Sophisticated structures such as the BH or the embedded laser eliminate this problem, but pulsations are still being observed in these lasers[8].

Appendix - Chapter 5

We shall derive $g(\omega)$ and the mode frequencies ω_k's with the help of the Nyquist diagram - a plot of $f_{f.b.}(s)$ in the complex plane. We assume that one or more zeros of $f_{f.b.}(s)$ lie very close to the imaginary axis. Then, the curve $f_{f.b.}(i\omega)$ makes its closest approach to the origin when ω equals the imaginary part ω_k of a zero, and the distance of closest approach is the real part g_k of that zero. The quantity g_k is by convention positive (negative) if the locus does(does not) encircle the origin.

To see what $f_{f.b.}(j\omega)$ looks like, we first plot $f(j\omega)$ (the case without feedback) as shown by the dashed line in fig. A5.1*. This curve will itself encircle the origin if K> 0, as defined in (5.10), ie., the laser self-pulses. Now we divide this curve into tiny segments with end points parametrized by $\omega = 2\pi k/\tau$ and $\omega = 2\pi(k+1)/\tau$, k=0,1,2,... Then, it is obvious that addition of the feedback term $\gamma\varepsilon(1-exp(-i\omega\tau))$ transforms each segment into (roughly) a circle of radius $\gamma\varepsilon$, as shown in fig. A5.1.

From simple trigonometry, the closest approach distance of this circle to the origin is $g = \gamma\varepsilon - \sqrt{(\gamma\varepsilon+x)^2+y^2}$ where x and y are, respectively, the real and imaginary part of $f(j\omega)$:

---

* Since $f(-j\omega) = f^*(j\omega)$, the locus is symmetric about the real axis so that only the +ve ω branch is considered.

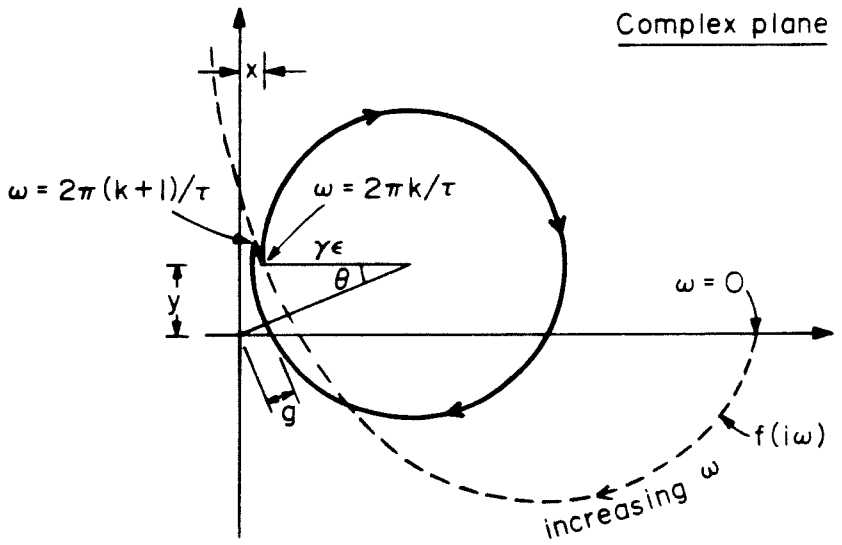

Figure A5.1. *Nyquist diagram for the derivation of $g(\omega)$ and the mode spectrum.*

$$x(\omega) = \frac{\gamma(1+P_0)P_0N_0}{(1+P_0)^2+\omega^2} - \gamma P_0\xi \qquad \text{A5.1(a)}$$

$$y(\omega) = \omega[1 - \frac{\gamma P_0N_0}{\omega^2+(1+P_0)^2}] \qquad \text{A5.1(b)}$$

The value of g is then the real part of a zero of $f_{f.b.}(s)$; the imaginary part ω_k of this zero is the value of ω at which the closest approach occurs. From fig. A5.1, we have

$$\omega_k = 2\pi k - \vartheta \qquad \text{A5.2}$$

where ϑ is the angle as shown,

$$\vartheta \approx \tan^{-1}[\frac{y(2\pi ki)}{\gamma\varepsilon+x(2\pi ki)}] \qquad \text{A5.3}$$

In the frequency range of interest (where the locus is closest to the origin), $\omega >> 1+P_0$ and for induced pulsation to occur ε has to be sufficiently large such that $\gamma\varepsilon >> x,y$. Making approximations and substituting (A5.1) into the expression for g, we obtain the gain spectrum (5.12) and the mode frequencies (5.13) and (5.14).

Reference - Chapter 5

1. H.A.Haus, IEEE J. Quant. Electron., **QE-12**, 169 (1976).

2. H.W.Bode, **Network Analysis and Feedback Amplifier Design** ,Van Nostrand 1959.

3. L.A.Glasser, IEEE J. Quant. Electron., **QE-16**, 525 (1980).

4. N.Minosky, **Nonlinear Oscillations** , Krieger 1974.

5. E.P.Ippen, D.J.Eilenberger and R.W.Dixon, Appl. Phys., Lett., **37**, 267 (1980).

6. H. Kuwahara, Appl. Phys., **20**, 67 (1979).

7. R.Lang, Jap. J. Appl. Phys., **19**, L-93 (1980).

8. L.Figueroa, K.Y.Lau and A.Yariv, Appl. Phys. Lett., **36**, 248 (1980).

CHAPTER 6

NON-LINEAR DISTORTIONS IN THE MODULATION OF NON-SELF-PULSING AND WEAKLY SELF-PULSING INJECTION LASERS

In analog transmissions systems, the linearity of a component is weighed heavily in determining its quality. In fiber optic systems, the general modulation responses of laser diodes are well known[1] and have been discussed in some detail in chapter 3, and their harmonic distortion characteristics have been considered theoretically[2 - 4]. In this chapter, we present a perturbation analysis of the non-linear distortion characteristics and results of experimental studies of the non-linear distortions in the current modulation of various types of lasers. These results show that harmonic distortions become extremely high at frequencies far lower than the relaxation oscillation(RO) resonance frequency. The Q of this resonance significantly affects the distortion characteristics both quantatively and qualitatively, in good agreement with theoretical predictions. Moreover, it is known that many lasers exhibit self-pulsation(SP) of some kind after a period of operation much shorter than the time to failure. As described in the last two chapters, when the pulsations first develop they are in the form of weak sinusoidal undulations at relatively high frequencies (> 1.5 GHz). The small signal modulation response of a weakly pulsing laser remains relatively flat up to the self-pulsing frequency. One might then ask whether such lasers can still be used in a system with a bandwidth lower than the pulsation frequency. Unfortunately, intermodulation in such lasers generates undesirable distortions at relatively low frequencies. Thus, extreme care must be taken in designing wideband (> 1 GHz) analog fiber systems, for even minor degradation of the laser can be devastating. It is known that by aligning the laser with an external cavity of appropriate length, RO can be suppressed[6], and SP can be quenched[7,8]. This has been analyzed in some detail in the last two chapters. We found that various nonlinear distortions in analog modulation can be significan'

reduced by the same arrangement. In the event the laser suffers minor degradation and exhibits weak pulsations, this measure becomes a necessity rather than a luxury.

6.1 Perturbation analysis of non-linear distortions in non-self-pulsing injection lasers

We start with the dimensionless rate equations introduced in chapter 3:

$$\dot{N} = J - N - NP \tag{6.1(a)}$$

$$\dot{P} = \gamma(NP - P + \beta N) \tag{6.1(b)}$$

where the variables are the same as defined in chapter 3. The fact that these rate equations are nonlinear leads to harmonic distortions in the pure sinusoidal responses calculated from the small signal analysis of chapter 2, especially when the oscillation amplitude becomes large. To determine the amount of distortion, we shall assume a sinusoidal modulation current, and expand the electron and photon responses in harmonics of the modulation frequency. It is convenient to employ the complex notation:

$$J = J_0 + \tfrac{1}{2}j_1 e^{i\omega t} + \tfrac{1}{2}j_1^* e^{-i\omega t} \tag{6.2}$$

$$N = N_0 + \sum_k [\tfrac{1}{2}n_k e^{ik\omega t} + \tfrac{1}{2}s_k^* e^{-ik\omega t}] \tag{6.3}$$

$$P = P_0 + \sum_k [\tfrac{1}{2}p_k e^{ik\omega t} + \tfrac{1}{2}p_k^* e^{-ik\omega t}] \tag{6.4}$$

where * represents complex conjugate. The steady state values N_0 and P_0 have been evaluated in section 3.1.

Substituting (6.2) into the rate equations (6.1) and applying harmonic balance (ie., equating terms with the same ω dependence) we obtain

$$i\omega n_i = j_1 - (N_0 p_1 + P_0 n_1 + n_1) - \tfrac{1}{2} n_2 p_1^* - \tfrac{1}{2} n_1^* p_2 + \cdots \qquad 6.5$$

$$2i\omega n_2 = -(N_0 p_2 + P_0 n_2 + n_2 + \tfrac{1}{2} n_1 p_1) + \cdots \qquad 6.6$$

$$i\omega p_1 = \gamma(N_0 p_1 + P_0 n_1 - p_1 + \beta n_1) + \tfrac{1}{2}\gamma n_2 p_1^* + \tfrac{1}{2}\gamma n_1^* p_2 + \cdots \qquad 6.7$$

$$2i\omega p_2 = \gamma(N_0 p_2 + P_0 n_2 + \tfrac{1}{2} n_1 p_1 - p_2 + \beta n_2) + \cdots \qquad 6.8$$

Equations (6.5) and (6.7), except for the higher order product terms $n_2 p_1^*$ etc. are just the small signal equations. The non-linear product term $n_1 p_1$ in equations (6.6) and (6.8) serves as a drive for the second harmonic. Since to first approximation, both n_1 and p_1 oscillate at ω, the product oscillates at 2ω and thus drives the second harmonic. Based on the same reasoning, the third harmonic is being driven by $\frac{1}{2}(n_1 p_2 + n_2 p_1)$, the fourth harmonic by $\frac{1}{2}(n_1 p_3 + 2n_2 p_2 + n_3 p_1)$, $\cdots$.

We employ the conventional perturbation approach. First we solve for the first harmonic, assuming absence of higher harmonics (which are weak compared with the first), then for the second harmonic using products of the first harmonics as the drive, assuming absense of third and higher harmonics, and so on.

1) First harmonic: Eqns. (6.5) and (6.7) are just the small signal solutions given in section 3.5, when the higher order terms are ignored:

$$n_1 = j_1 \frac{g(\omega)}{f(\omega)} \qquad 6.9(a)$$

$$p_1 = \frac{\gamma j_1 (P_0 + \beta)}{f(\omega)}$$

6.9(b)

where

$$g(\omega) = i\omega + \gamma(1-N_0) \tag{6.10}$$

$$h(\omega) = i\omega + 1 + P_0 \tag{6.11}$$

$$f(\omega) = h(\omega)g(\omega) + \gamma N_0(P_0+\beta) \tag{6.12}$$

2) Second harmonic: using eqns. (6.6) and (6.8), we have:

$$n_2 = \tfrac{1}{2}n_1p_1[\frac{-g(2\omega)-\gamma N_0}{f(2\omega)}] \tag{6.13}$$

$$p_2 = \tfrac{1}{2}n_1p_1[\frac{-\gamma(P_0+\beta)+\gamma h(2\omega)}{f(2\omega)}] \tag{6.14}$$

3) Third and higher harmonics: based on the same reasoning, the N^{th} harmonic is given by

$$n_N = \tfrac{1}{2}[\sum_{i=1}^{N-1} n_i p_{N-i}][\frac{-g(N\omega)-\gamma N_0}{f(N\omega)}] \tag{6.15}$$

$$p_N = \tfrac{1}{2}[\sum_{i=1}^{N-1} n_i p_{N-i}][\frac{-\gamma(P_0+\beta)+\gamma h(N\omega)}{f(N\omega)}] \tag{6.16}$$

The factor $f(\omega)$ in (6.12) gives rise to the RO resonance characteristic. The Q of this resonance is determined primarily by β which, apart from its definition as the spontaneous emission factor, can be adjusted to account for other physical mechanisms such as lateral carrier diffusion[9] described in section 3.4. The factors $f(N\omega)$ in the

expressions for higher harmonics indicate that the N^{th} harmonic has N resonance peaks at modulation frequencies $\frac{\omega_r}{N}$, where $\omega_r \approx \sqrt{\gamma(J_0-1)}$ is the RO frequency. The modulated output is thus especially rich in harmonics at modulation frequencies equal to submultiples of ω_r.

Fig. 6.1 shows a plot of the harmonic distortion characteristics when prefiltering is applied to the modulation current to compensate for the RO resonance, ie., let $j_1 = j_m f(\omega)$ in eqn. (6.1), where j_m is a constant, so that the first harmonic response is flat. The parameters used are $\beta = 10^{-3}$, $J_0 = 1.6$, $\gamma = 2000$, spontaneous lifetime = 3 ns, and the optical modulation depth (of the first harmonic) = 80%. It shows that the harmonic distortion is actually worst *not* at the RO frequency but at submultiples of it.

6.2 Harmonic distortions in various types of lasers

Since the same factor $f(\omega)$ giving rise to the RO resonance is also responsible for the resonance peaks of higher harmonics, it follows that lasers having a high RO resonance Q would have larger harmonic distortions. Indeed, this is what is observed experimentally. Fig. 6.2(a) shows experimentally measured harmonic distortions for a proton stripe laser which has an RO resonance at about 1.7 GHz in the small signal response; the peak is about 10 dB (in amplitude) above the 'midband' (low frequency) value. The data were obtained with the laser biased at 1.2 threshold, and driven with a sweep oscillator to an optical modulation depth of about 70%. The drive amplitude is adjusted at different frequencies so that the first harmonic response is constant (ie., prefilter the modulation signal). The detected output from the APD is fed into a microwave spectrum analyzer. Fig 6.2(b) shows a similar plot for a TJS [10] laser, which has no discernable resonance peak in the small signal response up to the fall-off frequency at 1.8 GHz (section 3.3). The distortion

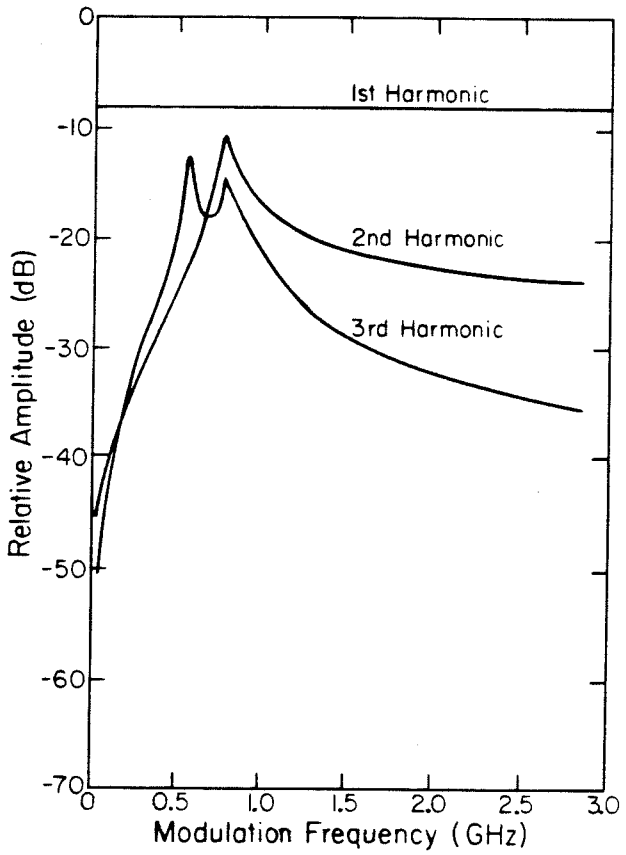

Figure 6.1. *Calculated harmonic amplitudes with prefiltering of modulation current.*

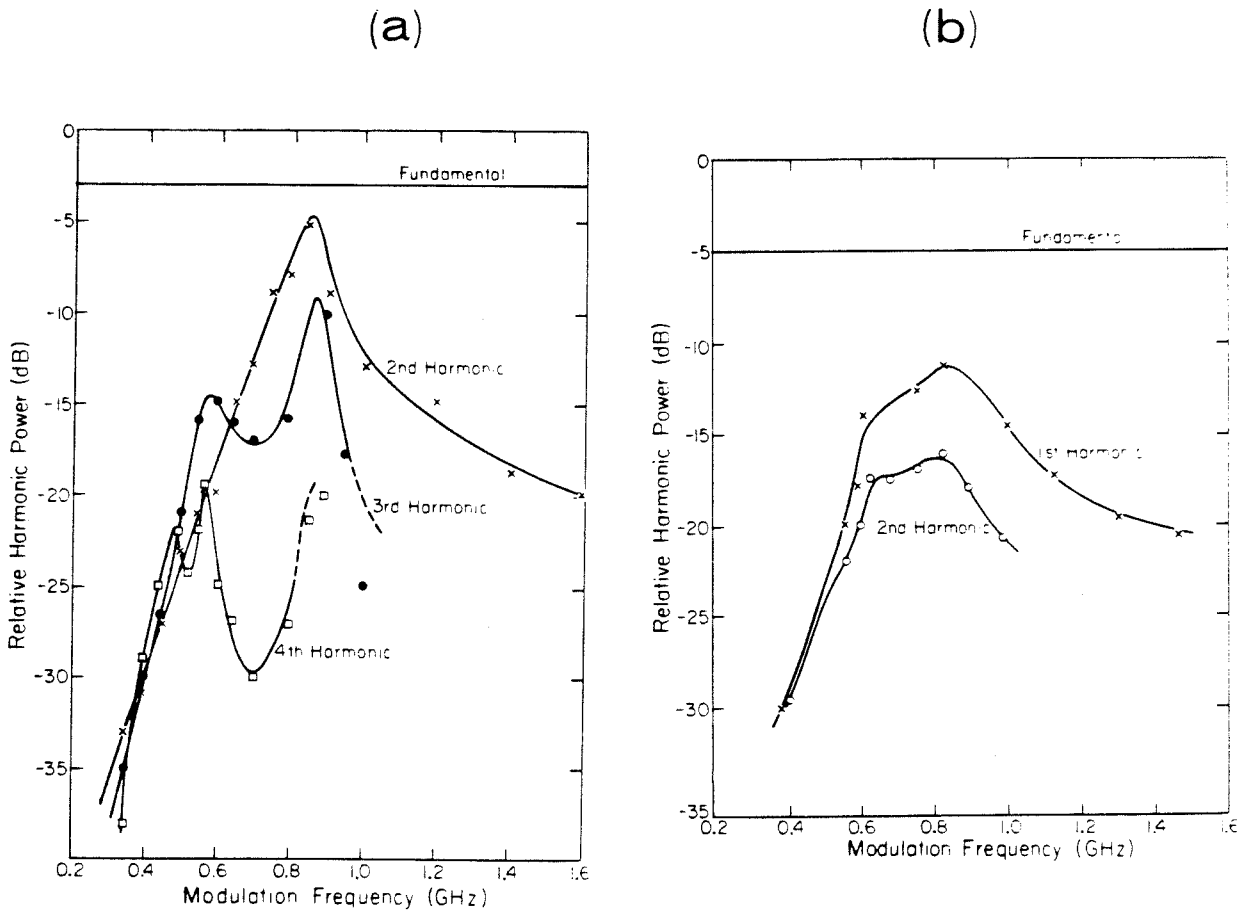

Figure 6.2. *Measured harmonic distortions of lasers (a) with and (b) without R.O. resonance. Prefiltering is applied to the modulation current to keep the first harmonic constant at all frequencies.*

characteristic contrasts sharply to that of fig. 6.2(a).

While the above results show that harmonic distortions are extremely high when modulated at frequencies above approximately 1/3 of the RO frequency, they nevertheless would not affect system performance in a significant way if we limit the baseband to frequencies below the RO frequency (ie. low-pass filter the *recieved* optical signal). This measure, however, would not be effective for a self pulsing laser. In addition to harmonic distortions, such lasers exhibit additional distortions within the baseband due to the beating of the modulation signal with the self-pulsation.

Experiments were performed with a weakly self-pulsing proton stripe laser: when operated at 1.15 threshold, this laser self-pulses at 2.15 GHz, the output waveform showing sinusoidal undulation of < 10% modulation depth. The result of applying a sinusoidal modulation at 0.95 GHz to the laser is shown in fig. 6.3. In addition to the signal at 0.95 GHz, one observes its second harmonic at 1.9 GHz and the self-pulsation at 2.15 GHz (both of which can be low-pass-filtered) and in addition the sidebands at 2.15 ± 0.95 GHz. The modulation current in this case produces an optical modulation depth of only 30%, stronger modulation would further increase the intermodulation sideband amplitudes and even the second lower sideband at 2.15 - 2 × (0.95) GHz = 250 MHz would become significant. Such performance is unacceptable in a wideband analog transmission system. Thus, even minor degradation of the laser diode can be detrimental.

6.3 Reduction of non-linear distortions by negative feedback

Based on the results presented in the previous sections, some measures should be taken to reduce the various distortions in laser diodes. It is well known that negative feedback can in general reduce distortions in systems. We found that this is also the case with injection lasers. One has the choice of applying the feedback

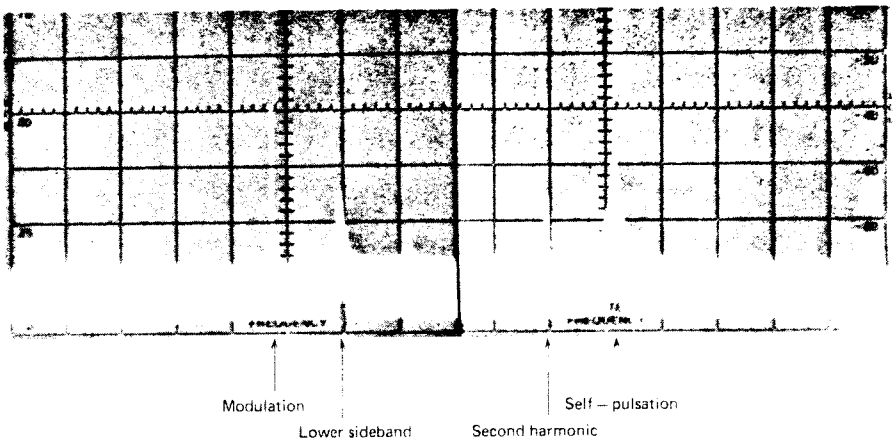

Figure 6.3. *Microwave spectrum of a weakly self-pulsing laser modulated at 0.95 GHz. Vert.:10dB/div, Hori.: 180MHz/div.*

electrically or optically. At the range of frequencies involved (> 1.5GHz) electrical feedback (or more precisely, *optoelectronic* feedback) is extremely difficult because of the short feedback loop length required. It is, however, not impossible if one carefully designs a compact module for the feedback circuitry, and developments in integrated optoelectronic circuits[12] could make important contribution in this respect. This problem does not arise in optical feedback[7,8], for the external cavity length can be easily adjusted to make the feedback negative at the self-pulsing frequency range. Mechanical instablilty of the optical elements can be avoided, as has been demonstrated in chapter 4, by using an optical fiber as the external cavity [8,11]. Fig. 6.4 shows the modulation response of a self-pulsing proton-stripe laser with and without optical feedback. When a 5 cm multimode optical fiber (with a lens formed at the end, cleaved and gold coated on the other end , as described in section 4.4) is aligned with the laser, the highly undesirable lower sideband vanishes along with the self-pulsation. The coupling reduces the threshold by only about 2% in this case. The fundamental response becomes flat up to 1.7 GHz, and the harmonic distortions have the general characteristics of a TJS laser as in fig 6.2(b). In other words, the output is indistinguishable from a laser with no RO resonance.

In conclusion, we have examined and compared the nonlinear distortion characteristics of several types of lasers. Modulating non self-pulsing lasers at frequencies higher than approximately 1/3 of the RO frequency results in very high distortions, but they can nevertheless be filtered out at the output. Self-pulsation, even though weak and occuring at high frequencies, would lead to distortions at low frequencies via intermodulation. In wideband analog transmission systems, suitable feedback should be applied to the laser to prolong its *useful* life as a signal transmitter.

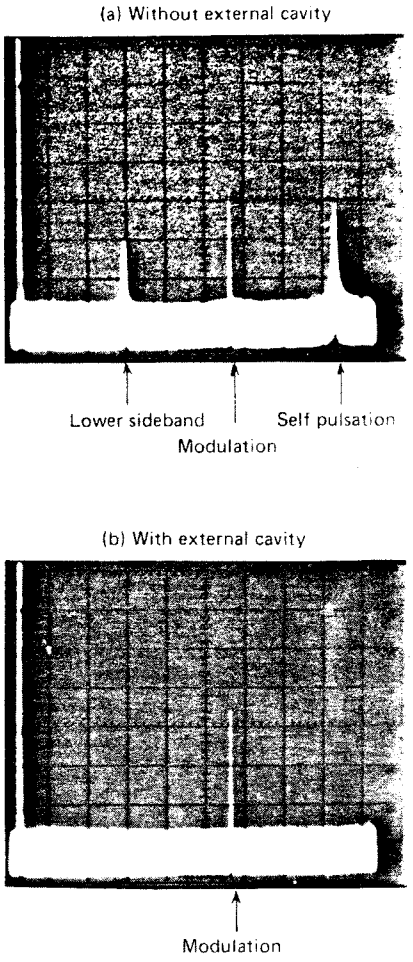

Figure 6.4. *Microwave spectrum of a weakly self-pulsing laser (a) without and (b) with negative optical feedback. Vert.:10dB/div. Hori.: 180MHz/div.*

References - Chapter 6

1. G.Arnold and P.Russer, Appl. Phys., **14**, 255 (1977).

2. T.Ikegami and Y.Suematsu, Electron. and Communic., Japan, **53B**, 69 (1970).

3. T.H.Hong and Y.Suematsu, Trans. IECE Japan, **E62**, 142 (1979).

4. K.E.Stubkjr, Electron. Lett., **15**, 61 (1979).

5. G.Arnold and K.Petermann, Optic. and Quant. Electron., **10**, 311 (1978).

6. K. Kobayashi, Trans. IECE, Japan, **E59**, 8 (1976).

7. N.Chinone, K.Aiki and R.Ito, Appl. Phys. Lett., **33**, 990 (1978).

8. L.Figueroa,K.Y.Lau and A.Yariv., Appl. Phys. Lett., **36**, 248 (1980).

9. K. Otsuka, IEEE J. Quant. Electron., **QE-13**, 520 (1977).

10. M.Nagano and K.Kasahara, IEEE J. Quant. Electron., **QE-13**, 632 (1977).

11. L.Figueroa, K.Y.Lau, H.W.Yen and A.Yariv., J. Appl.Phys., **51**, 3062 (1980).

12. N.Bar-Chaim, S.Margalit, I.Ury, D.Wilt, A Yariv and M.Yust., 11th International Quantum Electronic Conference, paper W6, Boston 1980.

CHAPTER 7

PULSE CODE MODULATION AND Gbit/sec RATE BIPOLAR PULSE MODULATION OF SEMICONDUCTOR LASERS

7.1 Intersymbol interference in high rate digital modulation of injection lasers

For digital transmission, laser diodes are modulated by pseudorandom current pulses at high rates. Based on the results of chapter 3, the most obvious problem encountered in the digital modulation of injection lasers is transient relaxation oscillations. The problem, can, nevertheless, be solved by using lasers of suitable structures which exhibit little or no relaxation oscillation (section 3.3). However, the damping mechanism in these lasers, in addition to suppressing the relaxation oscillation, at the same time slows down the response. The strength of the relaxation oscillation is an indication of how stable the system is. An unstable system can respond swiftly, but requires careful control - the price one has to pay for a ultra-high bit rate fiber optic transmission system.

Both the numerical simulation and the experimental evidence of sections 3.2 and 3.3 indicate that the first spike of the relaxation oscillation is extremely short. Common experimental observations indicate detector limited pulse widths of approximately 100 ps. Ultrafast streak camera measurements show pulse widths on the order of 15 - 30 ps generated in some lasers under very high current pulse excitation[1]. Thus it appears that by employing the first spike of the relaxation oscillation, modulation pulses can be spaced approximately 30 - 40 ps apart, corresponding to bit rates of 25 - 30 Gbit/sec! Two factors render the above proposition improbable. First, there is a finite time delay between the onset of the current pulse and the turn on of the laser - the time required for the electrons to fill up to above the threshold level, as illustrated in fig. 3.2. This turn-on delay can be minimized by prebiasing the laser at or slighly above the lasing threshold, although this will

introduce a small optical background. A more serious problem is the intersymbol interference, or the pattern effect. This arises from the relatively long spontaneous carrier lifetime of 1 - 3 ns. After emission of an optical pulse, the electron population inside the laser is usually not the same as the pre-pulse level - the system will take a length of time, on the order of a spontaneous lifetime, to relax back to the equilibrium pre-pulse level. When a second modulation pulse is applied during this period, the resulting optical pulse will not be identical to the previous one due to a different starting condition. Fig. 7.1 shows a simulation of the response of a laser to a long series of pseudorandom digital modulation pulses, at 1.5 Gbit/sec - the pattern effect is apparent. The effect can be even more severe when a different modulation pulse width is used, or at higher data rates. Danielsen[2] suggested that by carefully adjusting the area of the modulating current pulse, it should be possible to make the electron density at the end of the current pulse return to the pre-pulse level. In this way, a second modulation pulse immediately following the first one will see the same starting conditions as the first pulse and hence would produce an identical optical pulse. The modulation pulses in fig. 7.1 are in fact somewhat too long, and it can be observed that the electron density after the current pulse is higher than the pre-pulse level. Fig. 7.2 shows a numerical simulation of the case when the pulse area is optimized, resulting in pattern effect-free modulation. This was subsequently verified experimentally[3], resulting in a 1.1 Gbit/sec pattern-effect-free modulation capability with clean, background-free optical pulses. As predicted theoretically, the bias current and the drive current pulse area had to be carefully controlled, to within 1% and 10% respectively, to attain the pattern-effect free condition. Lee and Derosier[4] had suggested that pattern effect can be reduced by adding a backward swing to the drive current pulse (bipolar pulsing) which removes the excess carriers left in the active region after the optical pulse. This also requires a carefully controlled current pulse to assure the " identical before

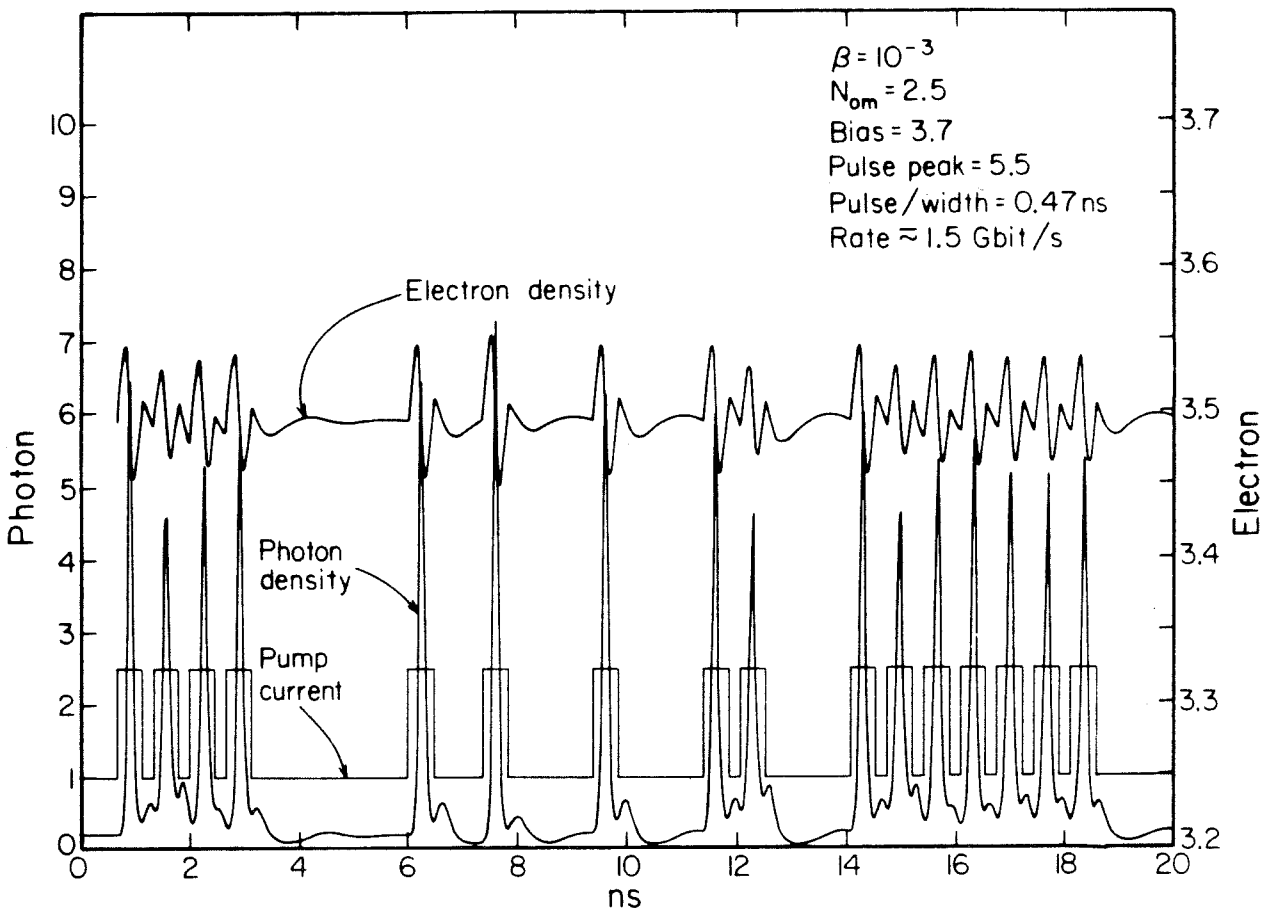

Figure 7.1. *Simulation of pseudorandom pulse code modulation of semiconductor lasers at ~1.5 Gbit/sec.*

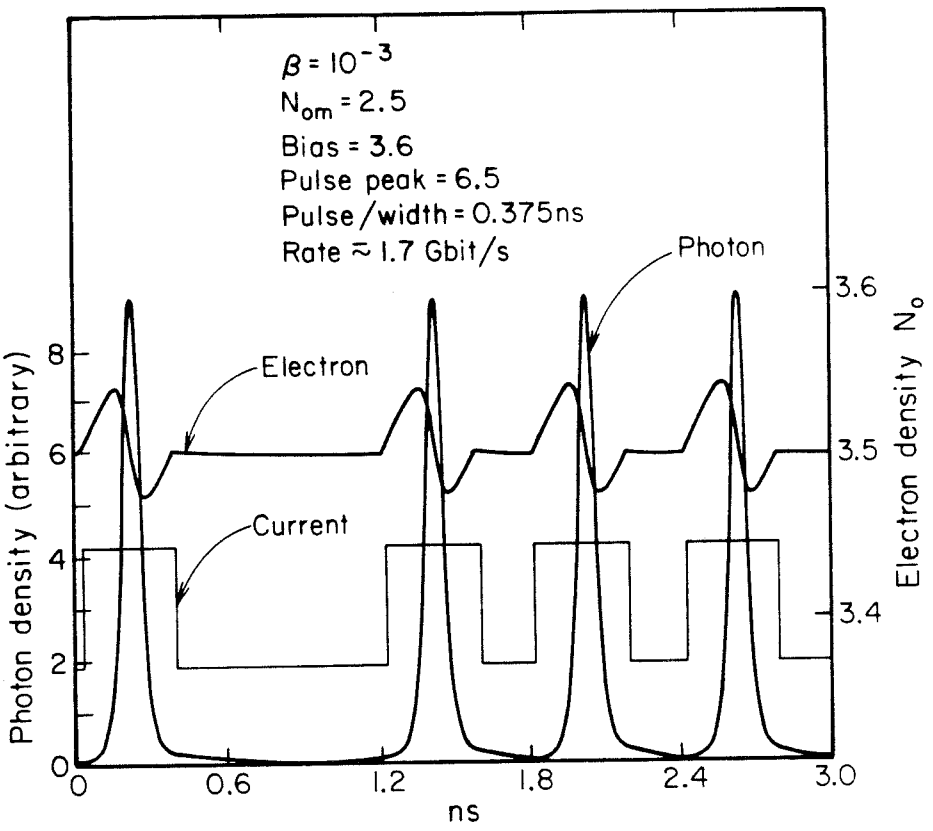

Figure 7.2. *Pulse code modulation with optimum current pulse area.*

and after" condition, and has only been demonstrated at 500 Mbit/sec. The pattern effect can also be reduced when the laser diode is biased very high above threshold and driven with relatively small current pulses. This just pushes the resonance frequency of the laser to a very high frequency by increasing the bias, and modulates in the small signal regime. In addition to shortening the life of the laser, this also introduces a constant optical background and reduces the modulation depth of the optical pulses. Russer and Schulz[5] achieved 2.3 Gbit/sec optical transmission with return-to-zero* received pulses, but the modulation depth was less than 20%. If non-return-to-zero pulse output from the detector is acceptable, the pulse-bits can be packed considerably closer and can result in a two- to three-fold increase in the transmission bit rate. Recently, Tell and Eng[6] applied this scheme to a TJS laser and achieved 8 Gbit/sec non-return-to-zero optical transmission; the modulation depth was not shown though.

In the following section, a scheme will be described in which a bipolar drive current pulse shape and very low threshold (9mA) lasers are used to generate return-to-zero pulses at a rate of up to 4 Gbit/sec without a pattern effect.

7.2 Gbit/sec rate bipolar pulse modulation of injection lasers

It appears that if one desires high bit rate optical modulation devoid of pattern effects and with a zero background, one has to resort to Lee and Derosier's or Danielsen's scheme. The requirement for careful control of bias and drive current parameters is a setback for Danielsen's scheme. This is also the case with the bipolar pulsing scheme, unless a dc bias current is not required. If a dc bias current is applied to the laser, the amount of backward swing in the drive current pulse has to be carefully controlled in order to have identical carrier density immediately before

* Of course, here the optical pulses do not actually return to "zero" because there is a constant optical background –it is better termed return –to –background.

and after the current pulse. However, if no dc bias is applied to the laser, the carrier density before the current pulse would be zero, and the carrier density after the current pulse would also be zero if the backward swing is sufficiently large that all the excess carriers are withdrawn. No parameter needs to be carefully controlled - not the bias (there is no bias), nor the amplitude of the forward swing of the current pulse (provided that it is sufficiently large to cause lasing), nor the precise amplitude of the backward swing (so long as it depletes the inversion).

The highest modulation bit rate that can be achieved with the above scheme is apparantly *not* limited by the response of the laser diode itself. Provided the drive current amplitude is sufficient to drive the carrier density above the threshold level, the laser responds immediately with a single optical pulse that has been shown to be as short as 30 - 40 ps [7]. Fig. 7.3 shows a computer simulation using the rate equations (normalized):

$$\dot{N} = J - N - (N - N_{om})P \qquad 7.1(a)$$

$$\dot{P} = \gamma[(N - N_{om})P - P + \beta N] \qquad 7.1(b)$$

where N and P are the normalized electron and photon density respectively, with $\gamma = \frac{\tau_s}{\tau_p}$, $\tau_s = 2ns$, $\tau_p = 2ps$, $N_{om} = 5$ and $\beta = 10^{-3}$. The cw threshold current is given by $J = 1 + N_{om} = 6$. The response to a single injected current pulse of 70 ps wide (FWHM) (a raised cosine functional form is assumed) and of amplitude = 180, is shown in fig. 7.3. No dc bias current is applied. No backward swing is added to the current pulse in this case, and we notice the large residual charge left after the optical pulse, as contrasted to the result of applying a bipolar drive as shown in fig. 7.4. The response of the laser can made arbitrarily fast provided the drive current pulse can be made

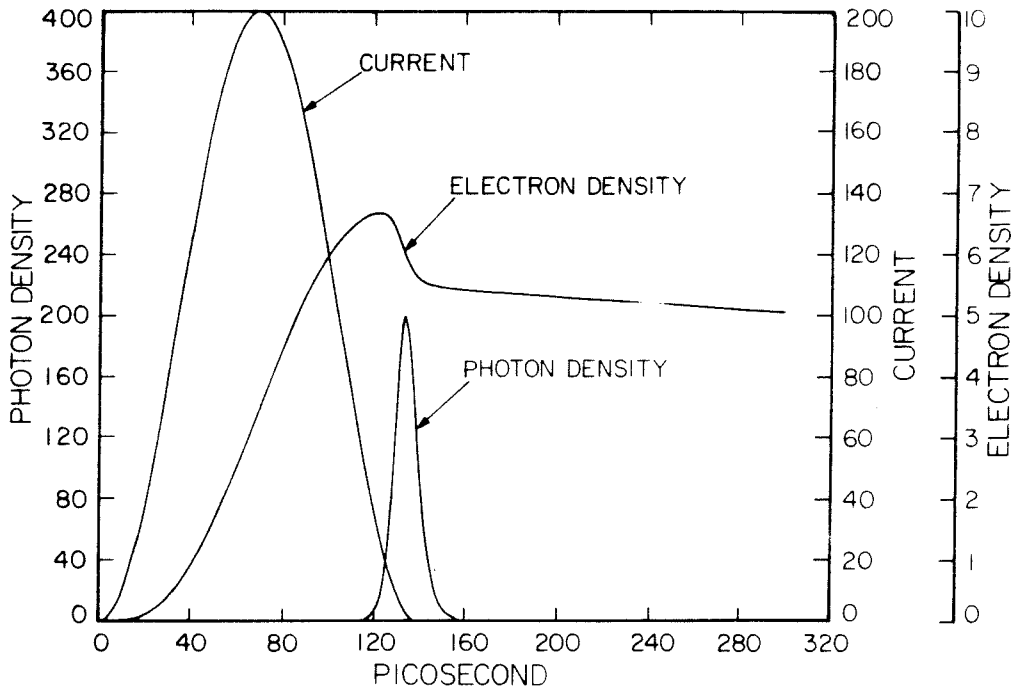

Figure 7.3. *Calculated responses of the electron and photon densities to a short intense current pulse. No dc bias current is applied.*

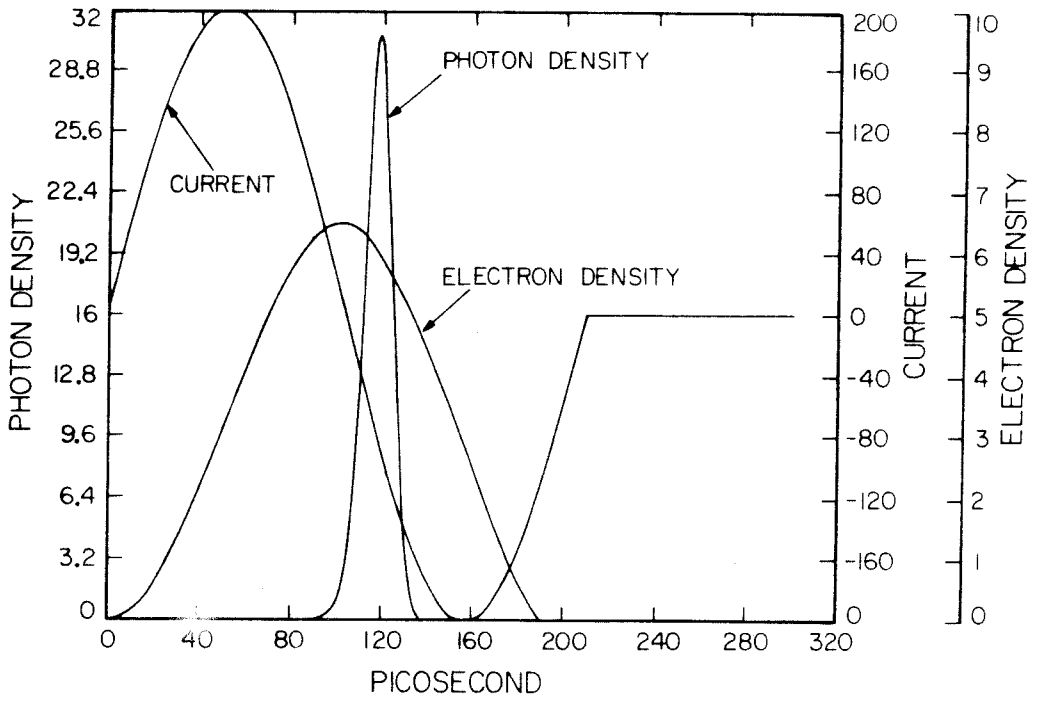

Figure 7.4. *Calculated responses of the electron and photon densities to a short current pulse with a backward swing.*

arbitrarily short and its amplitude arbitrarily large, *simultaneously*. For a very short drive current pulse of width τ, its minimum amplitide I_{min} required for lasing to occur (without any dc bias) is given approximately by

$$I_{min} = I_{threshold}(\frac{\tau_s}{\tau}) \qquad 7.2$$

where $I_{threshold}$ is the cw threshold current of the laser. With the above parameters, the minimum pulse amplitude is about 30 times that of the cw threshold current. The highest bit rate that can be attained is thus limited by the ability to generate short current pulses of sufficient amplitude.

7.3 Experimental demonstration of a 3.3 Gbit/sec modulation of a semiconductor laser

An experimental simulation of pseudorandom bit modulation at 3.3 Gbit/sec was performed with the scheme described in section 7.2. The experimental setup is shown in fig. 7.5. The current pulses were generated with a step recovery diode (SRD)(Hp33002A) which produces pulses with amplitude up to 20V (into 50Ω) and of 70ps duration at 100MHz repetition rate. These pulses were passed through a high pass filter (HPF) which differentiated the input pulse and produced an output pulse consisting of a forward and backward swing, about 70 ps wide with 12V amplitude in each swing. The SRD-HPF combination thus forms our pulse generator. Two of these generators are mounted on the ends of two 50Ω microstrip lines converging on the laser diode. This arrangement allows the laser to be driven by two consecutive current pulses with maximum available amplitude; the separation between the drive pulses can be varied by varying the relative phases of the RF drives to the SRDs. Fig. 7.6 shows two such consecutive current pulses separated by 300ps; the amplitudes of the pulses were 12V (into 50Ω). The laser used was a BH laser with 9mA threshold. Its forward bias impedance of about 5Ω was quite small compared to the sys-

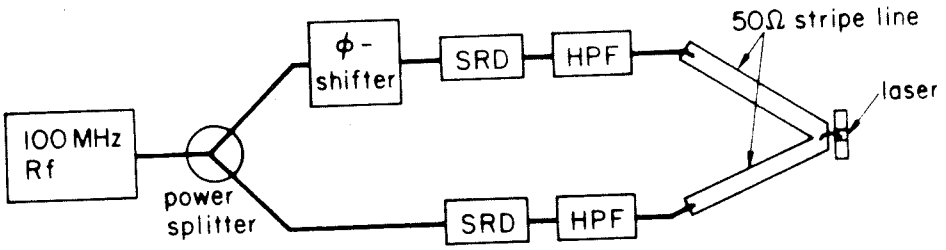

Figure 7.5. *Schematic diagram of the experimental setup.*

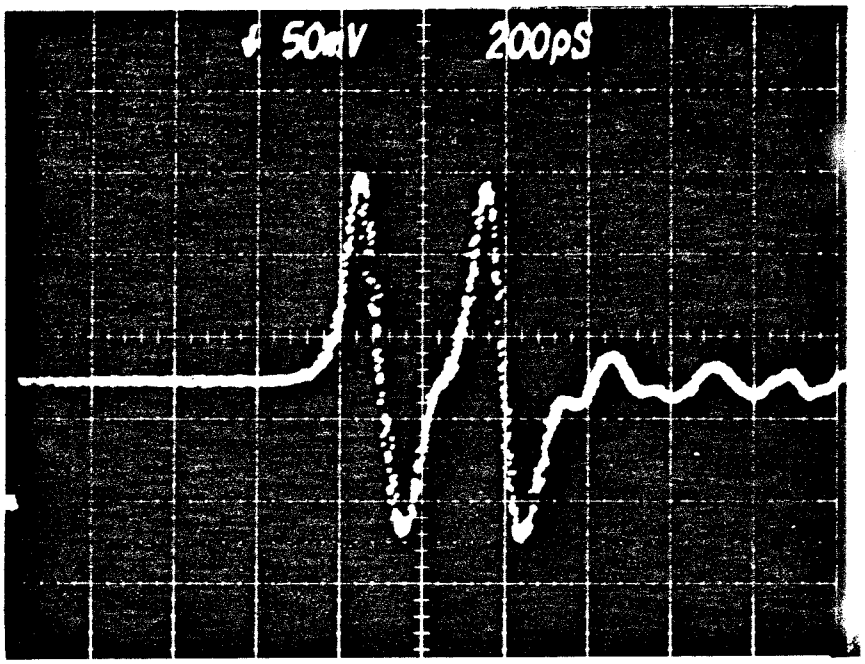

Figure 7.6. *Electrical pulses generated with a step recovery diode followed by a high pass filter. The pulse height was 12V (into 50Ω).* Hori. : 200ps/div.

tem impedance of 50Ω, and the peak pulse current delivered into the diode was $[1 - \frac{50\Omega - 5\Omega}{50\Omega + 5\Omega}] \times (12V/50\Omega) \approx 430mA$. Of course, this is only an optimistic estimate of the actual current passing through the active region - the parallel parasitic capacitance would reduce the actual current; its magnitude is hard to estimate. No dc bias was applied to the laser. The minimum amplitude for a 70 ps current pulse to cause lasing is, as estimated above, about 30 times the cw threshold current, which in this case amounts to 270 mA.

The response of the laser to the drive pulse pattern of fig. 7.6 is shown in fig. 7.7(a). The output was detected with a fast APD (Telefunken BPW28) with about 100 ps risetime. No significant pattern effect was seen for a pulse separation as small as 250 ps. This was not the case when there was no backward swing in the drive current pulse, or when a dc bias current was applied, which would have been required had the lasing threshold not been very low (< 10 mA). The pulses are not completely return-to-zero, which is mostly due to the detector limited response. At a lower modulation rate of 1.9 Gbit/sec, the pulses are completely return-to-zero, as shown in fig. 7.7(b).

It was thus demonstrated that by using a bipolar drive current pulse shape and very low threshold lasers, zero background pseudorandom optical pulses can be generated and detected at a rate of 3 - 4 Gbit/sec without a pattern effect. This bit rate was limited, in our experiment, by both the width and amplitude of the SRD drive current pulse and by the response of the APD detector. This bit rate can be made higher if it is acceptable for the pulse output to be non-return-to-zero. The laser itself should not be a limiting factor - its response to a strong current pulse drive is expected to be almost instantaneous and the actual pulse width has been reported to be less than 40 ps[7]. By employing shorter and more intense current pulse

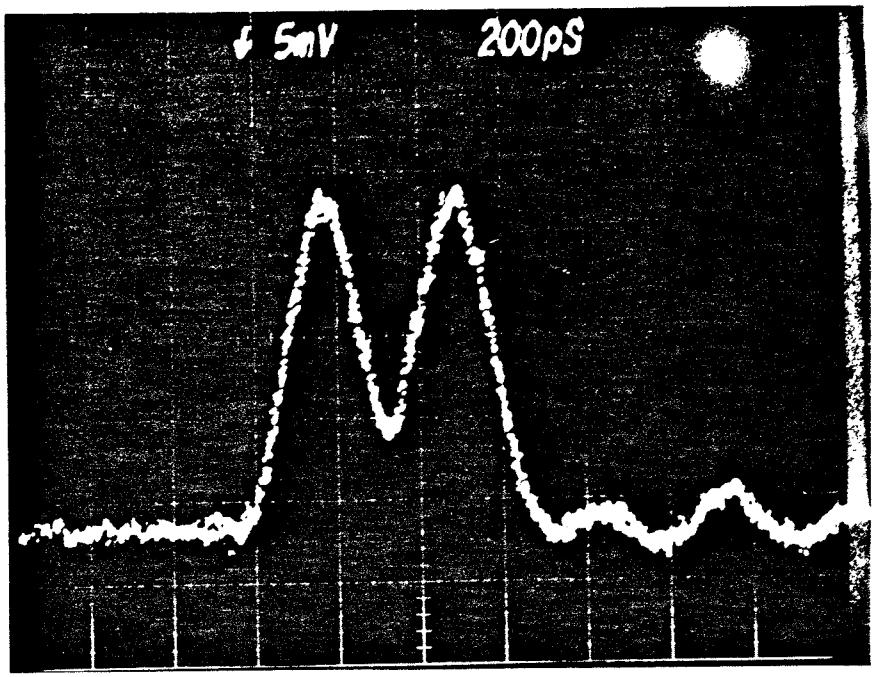

(a)

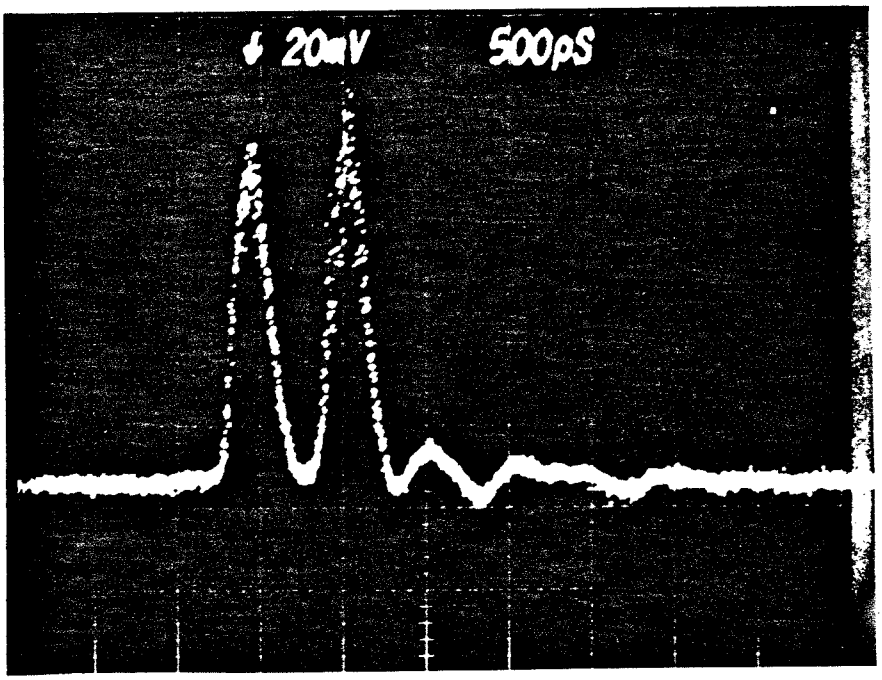

(b)

Figure 7.7. *(a) Response of the laser to the drive pulse in fig. 7.6, corresponding to a 3.3Gbit/sec modulation rate. The cw threshold of the laser was 9mA. Hori. : 200ps/div. (b) Bipolar pulse modulation at 1.9 Gbit/sec. Hori. : 500ps/div.*

generators, it should prove possible to modulate the laser to well above 10Gbit/sec without a pattern effect, using the drive scheme described above. The real limitation to the transmission bit rate, then, is on the detector side of the link.

Reference - Chapter 7

1. T.Kobayashi, A.Yoshihawa, A.Morimoto, Y.Aoki and T.Sueta, 11th Internatinal Quantum Electronics Conference, paper W1, Boston 1980.

2. M.Danielsen, IEEE J. Quant. Electron., **QE-12**, 657 (1976).

3. P.Torphammar, R.Tell, H.Eklund and A.Johnston, IEEE J. Quant. Electron., **QE-15**, 1271 (1979).

4. T.P.Lee and R.M.Derosier, Proc. IEEE , **62**, 1176 (1974).

5. P.Russer and S.Schulz, A.E.U., **27**, 193 (1973).

6. R.Tell and S.T.Eng, Electron. Lett., **16**, 497 (1980).

7. P.L.Liu, C.Lin, T.C.Daman and D.J.Eilenberger, Topical Meeting on Picosecond Phenomena, N.Falmouth, Cape Cod.,1980.

CHAPTER 8

TRANSVERSE MODAL BAHAVIOR OF A TRANSVERSE JUNCTION LASER EXCITED BY SHORT ELECTRICAL PULSES

8.1 Introduction

Among the many laser structures developed for optical communication, the transverse junction stripe (TJS) laser[1-4] has established itself as an outstanding candidate - low threshold, high reliability [5], and as we have seen in chapters 3 and 6, a flat frequency response - all these are favorable factors for a signal transmitter. Since its inception[1], significant improvement in performance was made possible by fabricating the laser on semi-insulting substrate[2], with MBE grown layers[3] and with multiple active regions having multiwavelength output[4]. The transient response of this laser shows little relaxation oscillation and has been explained with an effective pump rate model[6] which accounts for both the junction capacitance and the lasing wavelength shift due to heating. The TJS laser has also proven itself capable of generating ultra-short optical pulses (13ps) by direct current pulse modulation[7]. In the preceding chapters, the transverse modal behavior of lasers has not been considered. In this chapter, we present results on the transverse modal behavior of TJS lasers under short (70ps) intense electrical pulse excitation. It was experimentally found that the transverse mode profile depends on the excitation pulse amplitude and , to a lesser extent, on the bias level. Conventional stripe geometry lasers do not show this kind of mode shift. The results are successfully explained by theoretical calculations that include injected carrier diffusion [8] which significantly affects the gain-guided mode profile. These results are important in high data rate communication links using single mode fibers, for the transverse mode pattern of the laser significantly affects the coupling between the laser and the fiber.

A schematic diagram of a TJS laser is shown in fig. 8.1. Confined by the heterostructure in the vertical direction, the carriers are injected across the p^+n homojunction in the active layer, thus creating an inverted population near the junction. It has been suggested that[1] the p^+n homojunction actually consists of a p^+pn junction in the parallel direction which provides a built-in index guide, due to a lower refractive index in the highly doped p^+ and n region. The carrier concentrations in the p^+, p and n regions are typically 10^{19}, 10^{18} and $2\times10^{18} cm^{-3}$, respectively. Recent theoretical and experimental results by Ueno and Yonezu[14] show that with these carrier concentrations, index guiding should not be a dominant mechanism. It seems more likely that guiding is provided mainly by the injected holes in the n region. Our experimental observation that the optical mode actually shifts with injected current density tends to confirm this asumption.

8.2 Transient mode-gain calculations

The carrier density distribution $p(x)$ in the steady state takes the form of an exponential extending into the n region :

$$p_0(x) = \sqrt{\frac{\tau}{D}} J_0 e^{\frac{-x}{\sqrt{D\tau}}} \qquad 8.1$$

where x is the distance measured from the junction into the n side, τ is the recombination lifetime of the carriers, D is the diffusion coefficient, and J_0 is the injected current density. The optical mode guided by a gain distribution given by (8.1) was found to be a Bessel function of complex order and argument[9]. The boundary conditions were that the optical field vanishes at $x=0$ and $x=\infty$. We will use this same boundary condition in solving the transient problem under an injected current pulse.

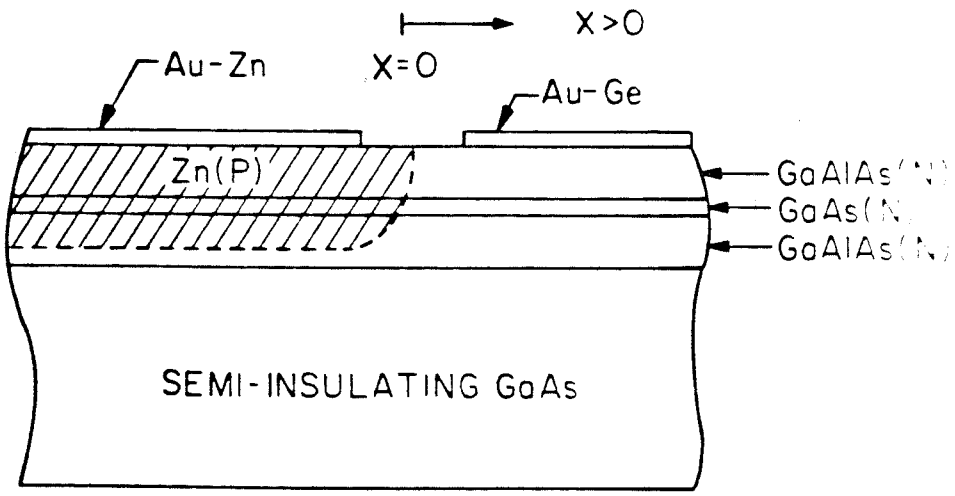

Figure 8.1. *Schematic diagram of the cross section of a TJS laser.*

We shall calculate the time evolution of the optical mode gain after the injection of an intense narrow current pulse. We assume that the laser is biased far below threshold so that very few photons exist in the cavity. When the current pulse is injected across the junction, the carriers initially accumulate at the junction and do not support a mode with positive gain. Only after the carriers diffuse to a certain width will the mode experience net gain, and an optical pulse follows. The transverse mode structure of this optical pulse clearly depends on the amplitude and width of the carrier profile at the moment that the mode gain crosses (from below) the threshold. Up to this moment, we can neglect the optical field and treat the conventional carrier diffusion problem in a straight-forward manner.

The transient carrier density distribution satisfies the following field-free diffusion equation:

$$\frac{\partial p}{\partial t} = D\frac{\partial^2 p}{\partial x^2} - \frac{p}{\tau} \qquad 8.2$$

where the variables are defined as before. Suppose that the laser is biased by a dc current and we asume at t=0, a δ-function current pulse of total charge Q is injected across the junction:

$$D\frac{\partial p}{\partial x}(x=0) = J_0 + \sigma\delta(t) \qquad 8.3$$

where $\sigma = Q/wl$, w is the thickness of the active layer, and l is the length of the laser. We assume that before t = 0, the system is in equilibrium, ie., $p(x, t=0)=p_0(x)$ as given by that in (8.1). The carrier distribution after t=0 is obtained by solving (8.2) subject to condition (8.3), resulting in

$$p(x,t>0) = \frac{\sigma}{\sqrt{\pi}d(t)} e^{-\frac{t}{\tau}} e^{-\frac{x^2}{d^2}} + p_0(x) \qquad 8.4$$

where the time dependent width of the gaussian $d(t) = 2\sqrt{Dt}$. In using (8.3) as an initial condition, we have assumed that the source impedance of the drive circuit is infinite, ie. a current source drive. The exact solution in the case of a finite source impedance is highly non-linear[11] and complex. However, it is evident from an equivalent circuit of the laser diode [6,12] that the above assumption holds for cases where the source impedance is large compared with the diode shunt resistance. This condition, to a fair extent, applies to the actual situation, in which the source impedence is 50Ω and the diode shunt resistance is less than 5Ω .

We will next apply the solution $p(x,t)$ of (8.4) to obtain the transient solution of the electromagnetic laser mode. Since $\sqrt{d\tau} \approx 2\mu m$ for $D = 20cm^2/sec$ and $\tau = 2ns$, we can approximate $p_0(x) = p_0(0) = J_0\sqrt{\frac{\tau}{D}}$ for the region within one or two μm of the junction. Futhermore, we assume that this carrier profile in (8.4) produces a gain proportional to the carrier concentration p. The relative permittivity of the medium can thus be written as

$$\varepsilon(x) = \varepsilon_r + iG(p(x,t) - P_0) \qquad 8.5$$

where P_0 is the carrier density for transparency, G is the coefficient as defined in (8.5), which is directly related to the gain coefficient of the laser mode in a straight forward manner, and ε_r is the square of the refractive index. With the gaussian profile in (8.4) we have

$$\varepsilon(x) = \varepsilon_r + i(Ae^{-\frac{x^2}{d^2}} - B + C) \qquad 8.6$$

where $A = C\frac{\sigma}{\sqrt{\pi}d(t)}e^{-\frac{t}{\tau}}$, $B = GP_0$, $C = GJ_0\sqrt{\frac{\tau}{D}}$. Expanding the gaussian in power series and keeping the first two terms only, the one dimensional scalar wave equation with the above permittivity profile reads

$$\frac{d^2E}{dx^2} + [\frac{\omega^2}{c^2}(\varepsilon_r + iA - iB + C) - \beta^2 - \frac{iAx^2\omega^2}{d^2c^2}]E = 0 \qquad 8.7$$

where β is the propagation constant of the mode. This is analogous to the harmonic oscillator, but with an imaginary quadratic potential instead of a real one[10]. The mode profile, with the boundary conditions $|E| = 0$ at $x = 0$ and $x = \infty$, is therefore the odd parity Hermite-Gaussians:

$$E_m(x) = H_m(\alpha x)e^{-\alpha^2\frac{x^2}{2}} \qquad 8.8$$

where $\alpha = [i\omega^2 A/(c^2d^2)]^{\frac{1}{4}}$, and with the 'energy levels'

$$\frac{\omega^2}{c^2}[\varepsilon_r + iA - iB + iC] - \beta_m^2 = (2m+1)\frac{\sqrt{A}\,\omega}{dc}e^{i\frac{\pi}{4}} \qquad 8.9$$

We are only interested in the lowest order mode m = 1 which is closest to the junction where the quadratic approximation is valid. The maximum of this mode occurs at

$$x_m = \sqrt{2\frac{\lambda}{\pi}}d^{3/4}(\frac{2}{Ad})^{1/4} \qquad 8.10$$

β_i gives the mode gain:

$$\beta_i \approx \frac{1}{2\sqrt{\varepsilon_r}}\left[\frac{2\pi}{\lambda}(A-B+C) - \frac{3}{d}\sqrt{\frac{A}{2}}\right] \qquad 8.11$$

The product of the width d and the amplitude A of the gaussian gain profile is, from equation (8.4)

$$Ad = \frac{G\sigma}{\sqrt{\pi}} e^{-\frac{t}{\tau}} \qquad 8.12$$

so that the mode gain, as a function of time, is

$$\beta_i = \frac{1}{2\sqrt{\varepsilon_r}}\left[\frac{2\pi(G\sigma/\sqrt{\pi})e^{-\frac{t}{\tau}}}{2\lambda\sqrt{Dt}} - \frac{3(G\sigma/\sqrt{\pi})^{1/2}e^{-\frac{t}{2\tau}}}{4(Dt)^{3/4}} - \frac{2\pi}{\lambda}(B-C)\right] \qquad 8.13$$

The first two terms are due to the δ-function current pulse, B is due to intrinsic loss and C is the contribution from the bias current. The threshold value of β_i for lasing is $(1/l)ln\ R + \alpha$, where l is the length of the laser, R is the intensity reflectivity and α is the internal loss.

We have assumed for convenience, in the above calculations, that the current pulse is a δ-function. In actual experiments, the current pulse is of both finite width and amplitude. In the following numerical calculations, we shall therefore describe the strength of the δ-function by an equivalent current amplitude such that a current pulse of this amplitude and of 70 ps duration (the actual value in our experiments) contains the same amount of charges as in the δ-function pulse. The other parameters used are τ = 2 ns, G = $6.9\times10^{-8}\mu m^3$ as calculated from Stern's result[13] and that the thickness of the active layer is 0.2 μm and the cavity length is 250 μm. The carrier density for transparency is taken to be $2.6\times10^{18}cm^{-3}$. Fig.

8.2(a) shows a plot of $\beta_i' = \beta_i - \frac{\pi}{\sqrt{\varepsilon_r}\lambda}(B-C)$, ie., the contribution to mode gain due to the current pulse, for various injection pulse strengths. We notice that β_i' diverges to ∞ as $t \to 0$ according to eqn. (8.13). This is non-physical and results from the quadratic approximation: at t = 0, the carrier distribution is a δ-function at the junction, so that in the quadratic approximation it becomes $-\infty$ everywhere except at x = 0. An exact numerical solution of the wave equation with the gaussian profile shows that β_i' actually converges to zero at $t \to 0$ as shown in fig. 8.2(a). This, as mentioned before, results from the fact that a δ-function gain profile does not support a mode with gain. The minimum value of β_i' for lasing to occur is

$$\beta_i' = \frac{\pi}{\sqrt{\varepsilon_r}\lambda}(B-C) + \frac{1}{l}\ln R$$

$$= \frac{\pi}{\sqrt{\varepsilon_r}\lambda} G P_0 + \frac{1}{l}\ln R - \frac{G J_0 \pi}{\sqrt{\varepsilon_r}\lambda}\sqrt{\frac{\tau}{D}} \qquad 8.14$$

where J_0 is the dc current. The cw threshold current calculated with the above parameters is about 30 mA. From fig. 8.2(a) we see that the time delay for the mode gain to go above threshold is less for a pump pulse of higher amplitude. Since the carrier diffusion distance d and time t are related by $d = 2\sqrt{Dt}$, we can plot β_i' as a function of d, as shown in fig. 8.2(b). This plot shows that for a given bias level, at the time lasing occurs, d would be smaller for higher pulse current. The peak of the actual optical mode when lasing first occurs is at a position x_m related to d as in (8.10). Fig. 8.3 shows a plot of x_m for different bias levels and various pulse current amplitudes.

8.3 Experimental observation of the transverse mode

The dependence of the transverse mode position on the pulse current amplitude predicted above has been observed experimentally. The laser used was a TJS laser on

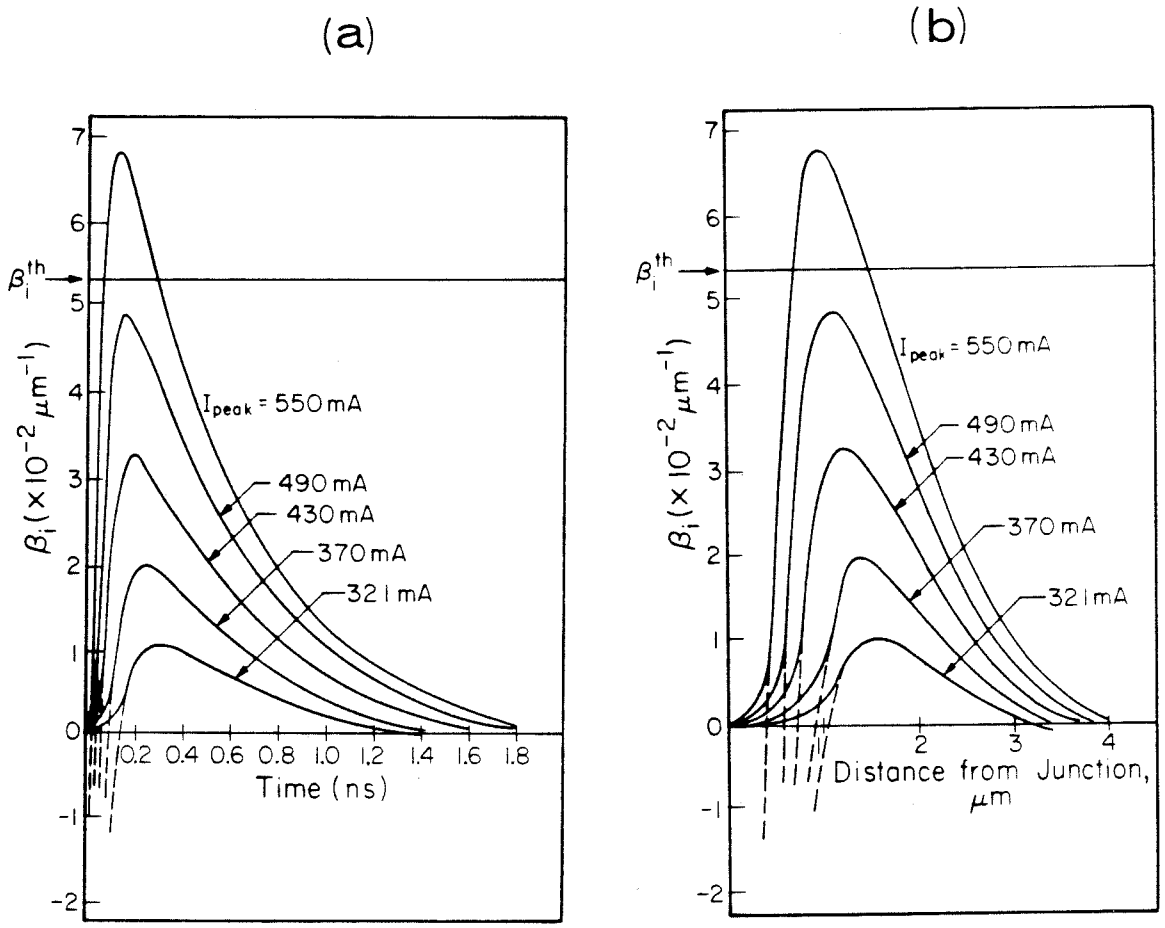

Figure 8.2. *Plots of mode gain vs (a) time after a current pulse is injected and (b) width of the diffused hole profile in the N side of the junction, for various pump current amplitudes.* β_i^{th} is the minimum mode gain for lasing when no dc is applied.

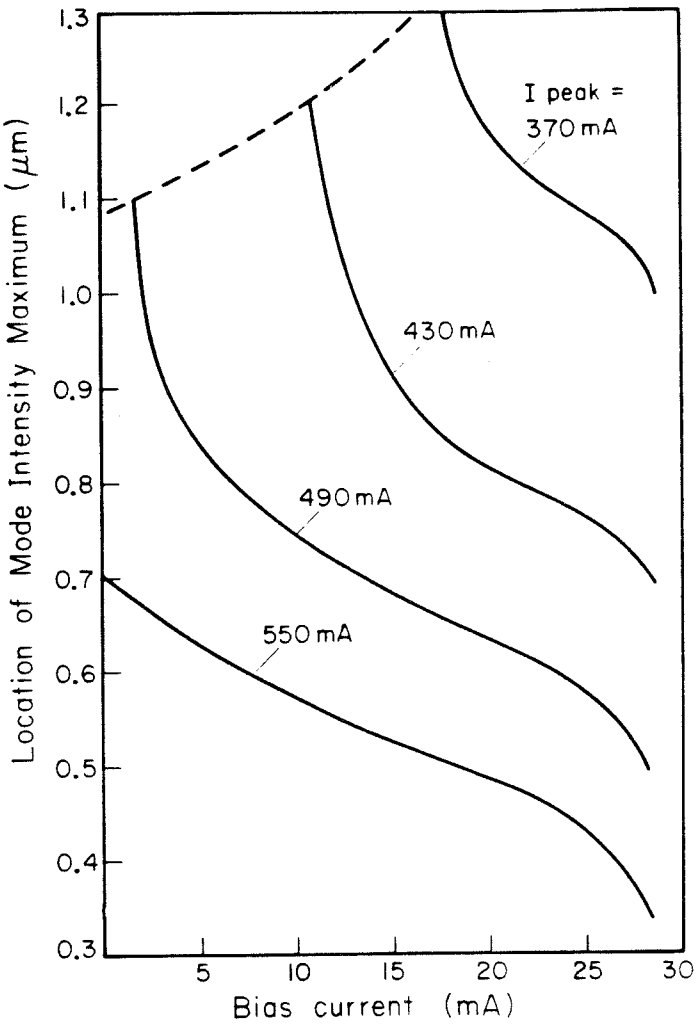

Figure 8.3. *Plots of positions of the optical mode intensity maxima at lasing vs dc bias current, for various pump current pulse amplitudes.*

semi-insulating substrate with a cw threshold of about 30mA. The laser was biased with a dc current below threshold, ranging from 5 - 15 mA. It was driven with a step recovery diode(SRD) similar to the one described in section 7.3. The near field was imaged with a 40x, 0.85 NA microscope objective and the time resolved nearfield pattern was measured with a 12 μm slit at the image plane, at a distance of 12 cm from the lens (fig. 8.4); the output was detected with a fast APD followed by a wideband amplifier, and displayed on a sampling scope. The peak voltage of the pulse output from the SRD was variable between approximately 6 - 15V (into 50Ω), which roughly corresponds to peak currents between 200 to 450 mA through the laser. The laser responds to the current pulse with a single sharp optical pulse, the width of which is very possibly below 100 ps - the risetime of the APD used. The transverse mode structure of this optical pulse is measured by scanning the 12 μm slit along the image plane. It is possible that the transverse mode structure changes within an optical pulse, but cannot possibly be resolved with the APD.

Fig. 8.5 shows the transverse mode structure of the optical pulses under different excitation conditions. As the peak current of the exciting pulse is increased, the mode shifts closer to the junction. Compared with the mode structure when the laser is operated cw above threshold, the pulsed mode shows a second 'bump', which is possibly the second order transverse mode. The measurements at different pulse amplitudes are made at different bias levels, for the laser diode cannot be pulsed too high above threshold without risking destruction. The amount of mode shifts measured are in good agreement with theoretical predictions in fig. 8.3.

The mode structure of the cw operated laser, contrary to what is expected from a gain guided mode, does not shift significantly with bias current. This can be due to spatial bole burning. At higher bias levels, the mode in principle should narrow down and shift toward the junction. Spatial hole burning would, however, counter the

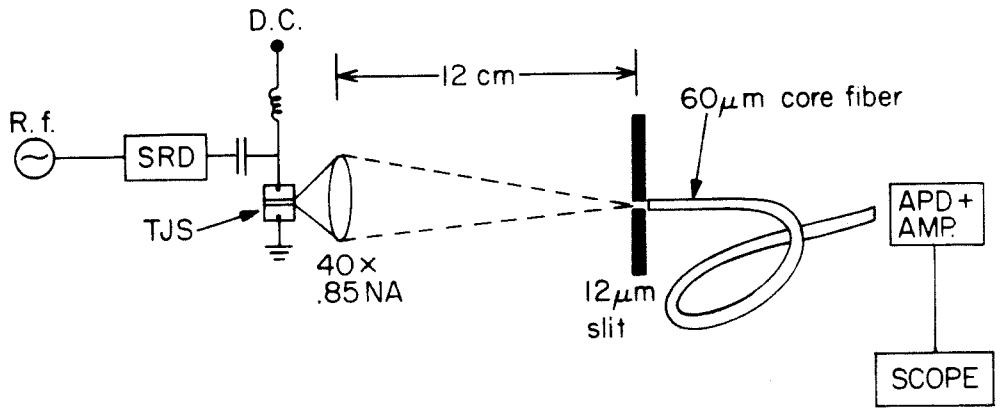

Figure 8.4. *Schematic diagram of the experimental arrangement for measuring the transient transverse mode pattern.*

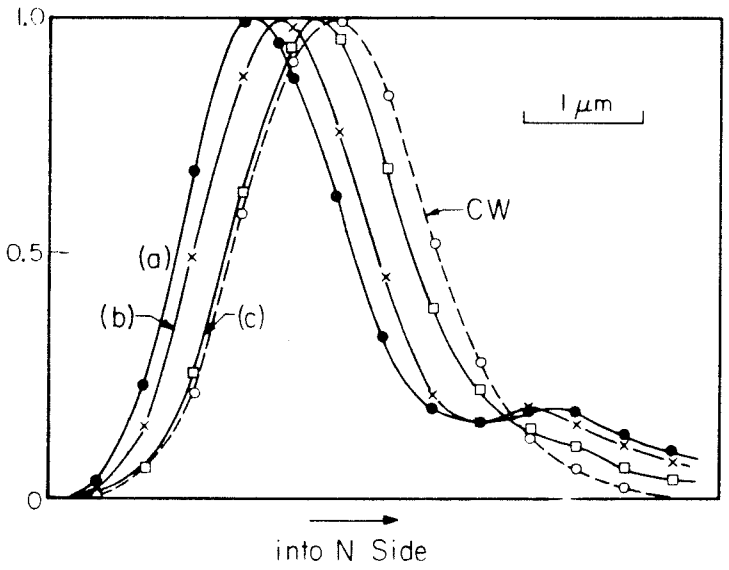

Figure 8.5. *Measured transverse mode profile with bias and peak pulse currents respectively equal to (a) 12mA, 430mA, (b) 15.5mA, 350mA, (c)20mA, 205mA. For comparison, the mode profile under cw operation is also shown.*

above effect and result in a broader mode width than expected. This does not occur in the case of short pulse excitation, because when the photons deplete the gain, the optical pulse is already over. The observed mode shift under pulse excitation, as shown in fig. 8.5 just reflects this mechanism.

At a certain fixed bias level, the pump current pulse has to exceed a certain amplitude before an optical pulse is produced. At this threshold, the optical pulse has a significant delay, approximately 150 - 200 ps. When the current pulse amplitude is increased, the delay rapidly shortens and becomes undiscernible. This is also in rough accord with the calculations of fig. 8.2(a). Delays of less than 100 ps, as shown in the figure, cannot possibly be detected by the 100 ps risetime APD. Moreover, since the current pulse itself is of a finite width of 70 ps, the difference in the delay at various pump pulse amplitudes might be even smaller than that shown in fig. 8.2(a). The transverse mode position, on the other hand, shows much larger variations than the time delay.

This pump-dependence of the transverse mode structure is strongly manifested when the TJS laser is pulsed by two closely spaced electrical pulses of different amplitudes. In our experiment, the second pump pulse is actually due to electrical reflection. The impedance of the laser constitutes a large mismatch to the 50Ω line and consequently there is a reflected electrical pulse, of about ½ the amplitude of the original pulse and of opposite polarity, propagating from the TJS back to the SRD. The SRD, looking from the output, is a perfect short which then reflects the reflected pulse and inverts its polarity. The separation between these two pump pulses in our experiments is about 1.3 ns, which is comparable to the spontaneous lifetime of the carriers. Even though the second electrical pulse is weaker than the first, the second optical pulse can be equal or even larger than the first one because of charge left-over - the pattern effect, as shown in fig. 8.6. The transverse mode

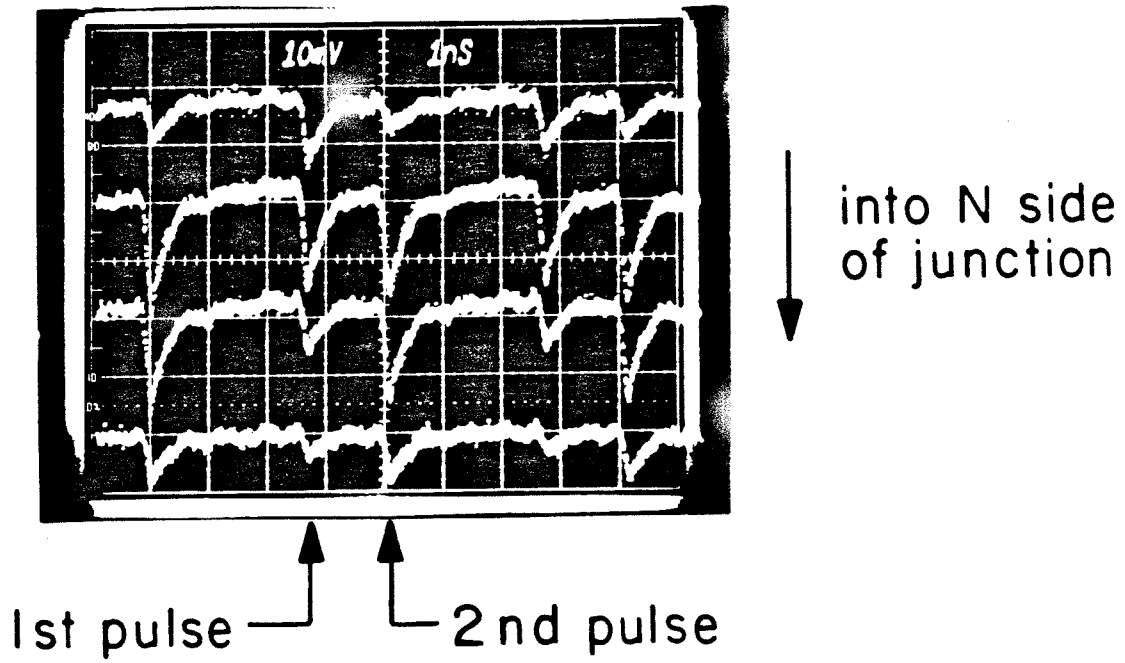

Figure 8.6. *Output pulses (- ve going) from a TJS laser taken at four different positions of the transverse mode, successively going into the N side. The laser is excited with two consecutive current pulses, 1.4ns apart and repetitive at 250MHz.*

structure of the two successive optical pulses are distinctively different. As seen from the picture, the *relative* amplitudes of the two optical pulses are different when scanned across the transverse mode profile, which is a clear indication that the mode structures of the two successive pulses are non-identical. Fig. 8.7 shows the transverse mode pattern of the two pulses. We have performed similar experiments with several other kinds of lasers including proton stripe and CSP lasers, but did not observe the effects described above. Thus, it can be concluded that the results are specific to lasers with such a time dependent gain-induced guiding as the TJS.

Finally, we speculate that the guiding mechanism of the TJS laser is responsible for its ability to generate ultra-short pulses under current modulation[7]. Since the mode is primarily gain guided, the mode loss (or gain) depends crucially on whether the gain profile exists. Because of the short stimulated lifetime, the optical pulses can evolve extremely rapidly (within 10 - 20 ps) once the gain breaks above threshold. However, as soon as the optical pulse emerges, the gain is immediately depleted and the guiding no longer exists, resulting in extra-high mode loss and the optical pulse self- terminates after a few cavity transits. Experimental verification of the above proposition, however, would be very dificult since it calls for measuring the transverse mode pattern on a picosecond timescale.

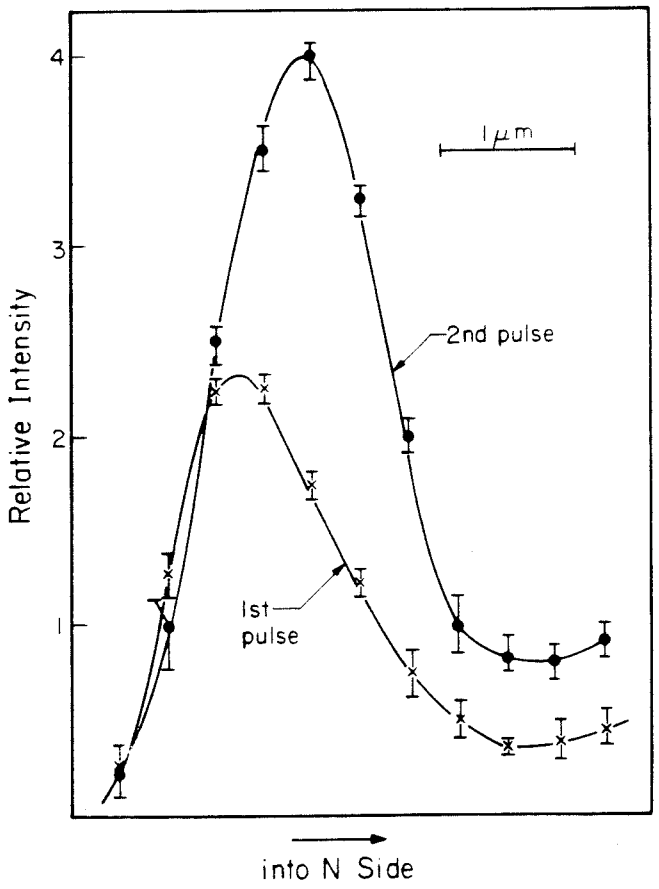

Figure 8.7. *Transverse mode profile of the first and second pulse of fig. 8.6.*

References - chapter 8

1. H. Namizaki, IEEE J. Quant. Electron., **QE-11**, 427 (1975).

2. C.P.Lee, S.Margalit, I.Ury and A.Yariv, Appl. Phys. Lett., **32**, 410 (1978).

3. T.P.Lee, C.A.Burrus and A.Y.Cho, Integrated and Guided-wave Optics Meeting, Incline Village, Nevada, 1980.

4. W.T.Tsang, Appl. Phys. Lett., **36**, 441 (1980).

5. S.Nita, H.Namizaki, S.Takamiya and W.Susaki, IEEE J. Quant. Electron., **QE 15**, 1208 (1979).

6. M.Nagano and K.Kasahara, IEEE J. Quant. Electron., **QE-13**, 632 (1977).

7. T.Kobayashi, A.Yoshihawa, A.Morimoto, Y.Aoki and T.Sueta, 11th International Quantum Electronics Conference, Boston 1980.

8. N.Cinone, K.Aiki, M.Nakamura and R.Ito, IEEE J. Quant. Electron., **QE-14**, 625 (1978).

9. C.P.Lee, S.Margalit and A.Yariv, Optics Commun. , **25**, 1978.

10. T.L.Paoli, IEEE J. Quant. Electron., **QE-13**, 662 (1977).

11. B.Lax and S.F.Neustadter, J. Appl. Phys., **25**, 1148 (1954).

12. M.Maeda, K.Nagano, M.Tanaka and K.Chiba, IEEE Trans. Commun, **COM-26**, 1076 (1978).

13. H.C.Casey and M.B.Panish, **Heterostructure Laser** ,Part A, pg 167, Academic Press, 1978.

14. M.Ueno and H.Yonezu, J. Appl.Phys., **51**, 2361 (1980).

CHAPTER 9

MODULATION RESPONSE OF SUPERLUMINESCENT LASERS

9.1 Introduction

The superluminescent diode is one alternative to the well established GaAs injection lasers and LEDs as light sources for fiber-optic communications. A superluminescent diode is a laser diode without mirrors. The first investigation of the superluminescent diode was carried out by Kurbatov et al.[1], its static properties were evaluated in detail by Lee el.al.[2] and Amann et al.[3,4]. Superluminescent diodes have also been integrated monolithically with detectors for optical memory readout, their fabrication being simpler than that involved in laser-detector integration since a mirror facet is not required within the integrated device [13]. It has also been observed that [5,6] the optical modulation bandwidth increases substantially as light emitting diodes enter the superluminescent regime. This regime is characterized by a rapid increase in the optical power output and a narrowing of the emission spectrum. An increase in the modulation capability also occurred in some edge emitting LEDs, though they were not purposely operated in the superluminescent regime[7]. This increase in modulation speed was attributed to the shortening of the carrier lifetime due to the stimulated emission of photons.

Due to the non-uniformity in the longitudinal distribution of the photon and carrier densities in the active region, the modulation response of superluminescent lasers cannot be described by the usual spatially uniform rate equations, so successfully applied to describing laser dynamics. This is evident from the discussions in chapter 2. Rather, the 'local' rate equations of chapter 2 should be used in their original form. Results on numerical calculations of the small signal modulation frequency response are presented in this chapter. The results show that in most cases, the responses are of single-pole type, unlike the pole-pair response of a laser. The

cut-off frequency increases with the pump current, as has previously been observed, in a rather non-linear fashion. Under some conditions, the frequency response can be much higher than a laser diode of similar construction, under the same pump current density. These conditions require that the reflectivity of the mirrors be less than 10^{-4}, and the spontaneous emission factor be less than 10^{-3}. The second of these conditions can be achieved with special designs, but the first condition is difficult to attain under the present state of the art of laser fabrication.

9.2 The small signal superluminescent equations and numerical results

The superluminescent diode is assumed to be constructed as a double heterostructure laser with guiding in both transverse directions, but with no mirrors. The local rate equations for the photon and electron densities were first introduced in chapter 2, eqns. (2.1(a)) - (2.1(c)). In the pure superluminescent case (no mirror), the steady state is given by the solutions (2.3) - (2.7) with R = 0. Fig. 9.1(a) shows a plot of the steady state relative output optical power, $X_0^+(L/2) = X_0^-(-L/2)$, as a function of pumping level indicated by the unsaturated gain g, for various values of the spontaneous emission factor β. The linear part of the curves at the higher values of the pump level is the saturated regime, where most of the optical power is extracted from the inverted population by stimulated emission. Fig. 9.1(b) shows the static gain and photon distributions inside a superluminescent laser, illustrating the effect of spontaneous emission on the distributions.

To investigate the modulation frequency response of the superluminescent diode we employ the usual perturbation expansion

$$X^{\pm}(z,t) = X_0^{\pm}(z) + x^{\pm}(z)e^{i\omega t} \qquad 9.1(a)$$

$$N(z,t) = N_0(z) + n(z)e^{i\omega t}$$

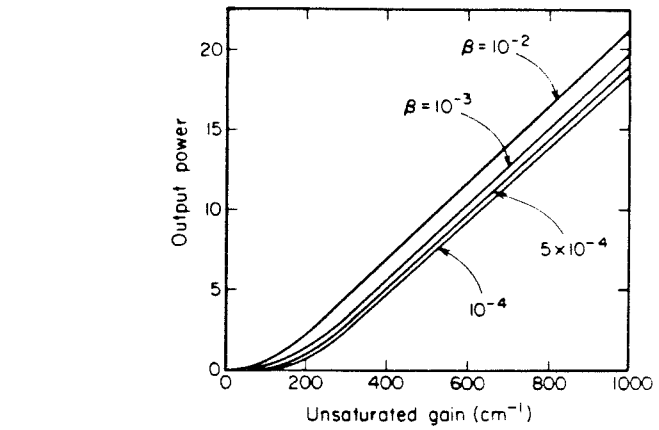

(a)

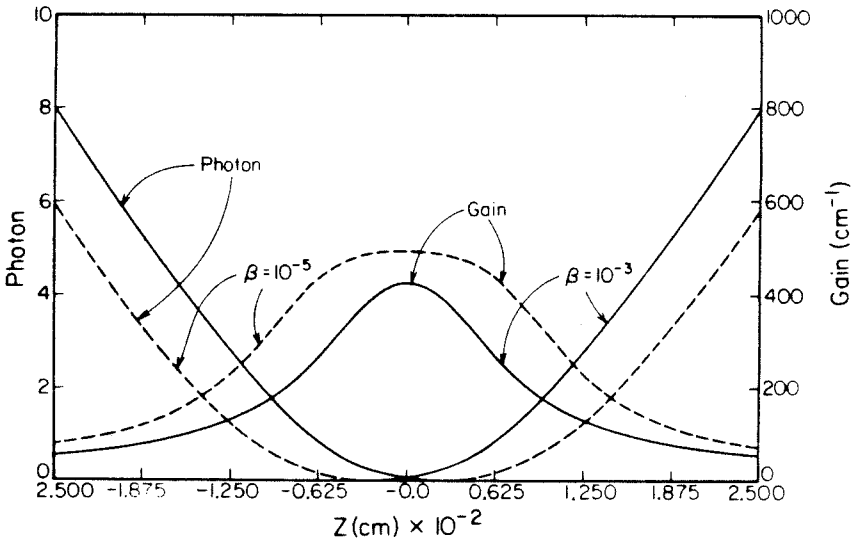

(b)

Figure 9.1. *(a) Static photon output of, and (b) gain and photon distibutions in a superluminescent diode. The unsaturated gain in (b) is 500cm^{-1}.*

9.1(b)

where $x^{\pm}$ and n are "small" variations about the steady states. This assumes that the electron and photon densities throughout the length of the diode vary in unison. This is true when propagation effects are not important, ie, when modulation frequencies are small compared with the inverse of the photon transit time. This would amount to over 15 GHz even for very long diodes(0.25 cm) considered in later sections.

Adopting the usual technique of substituting (9.1) into the superluminescent equations (9.1), and neglecting the nonlinear product terms, we obtain the following small signal equations:

$$\frac{dx^+}{dz} = Ax^+ + Bx^- + C \qquad 9.2(a)$$

$$\frac{dx^-}{dz} = Dx^+ + Ex^- + F \qquad 9.2(b)$$

where A,B,C,D,E,F are given by the following :

$$A = g_0 - \frac{i\omega}{c\tau_s} - \frac{(X_0^+ + \beta)g_0}{1+i\omega+(X_0^+ + X_0^-)} \qquad 9.3(a)$$

$$B = \frac{-(X_0^+ + \beta)g_0}{1+i\omega+(X_0^+ + X_0^-)} \qquad 9.3(b)$$

$$C = \frac{g_m(X_0^+ + \beta)}{1+i\omega+(X_0^+ + X_0^-)} \qquad 9.3(c)$$

$$D = \frac{(X_0^- + \beta)g_0}{1+i\omega+(X_0^+ + X_0^-)}$$

9.3(d)

$$E = -[g_0 - \frac{i\omega}{c\tau_s} - \frac{(X_0^- + \beta)g_0}{1+i\omega+(X_0^+ + X_0^-)}] \qquad 9.3(e)$$

$$F = \frac{-g_m(X_0^- + \beta)}{1+i\omega+(X_0^+ + X_0^-)} \qquad 9.3(f)$$

where $g_0(z) = \alpha N_0(z)$= small signal gain distribution, $g_m = \alpha j \tau_s / (ed)$ = small signal gain due to RF pump current, and ω has been normalized by the inverse of spontaneous lifetime.

The boundary conditions for solving (9.2) are the same as that in solving the steady state case, eqn.(2.2):

$$x^+(0) = x^-(0) \qquad 9.4(a)$$

$$x^-(L/2) = 0 = x^+(-L/2) \qquad 9.4(b)$$

Equation (9.2) is solved by assuming an arbitrary value for $x^+(0) = x^-(0) = \kappa$ and integrating (9.2) to give $x^+(L/2) = P$, $x^-(L/2) = Q$, these quantities are complex in general. The system (9.2) is integrated again assuming $x^+(0) = x^-(0) = \rho \neq \kappa$, to give $x^+(L/2) = T$, $x^-(L/2) = S$. The solution is given by a suitable linear combination of the above two solutions such that $x^-(L/2) = 0$. The small signal output of the superluminescent diode is

$$x^+(\frac{L}{2}) = x^-(-\frac{L}{2}) = \frac{QT - SP}{Q - S} \qquad 9.5$$

The frequency response curve is obtained by solving (9.2) for each ω. One set of

results is shown in fig. 9.2, where we show the frequency response of a 500 μm diode pumped to various levels of unsaturated gain. The spontaneous emission factor β is taken to be 10^{-4}, and the spontaneous lifetime 3ns. The dashed curves are the phase responses. One noticeable feature is that the response is flat up to the fall-off frequency, and the fall-off is at approximately 10dB/decade. The cut-off frequency (defined to be the abcissa of the intersection point between the high frequency asymptote and the 0 dB level of the amplitude response) easily exceeds 10GHz at pump levels corresponding to unsaturated gain values of 1000 cm^{-1}. This kind of gain may be unrealistic in real devices, but we shall show that equally high frequency responses can be attained with longer devices at much lower pump levels.

In conventional (ie. two-mirror) lasers, the spontaneous emission factor is found to play an important part in damping the resonance in the modulation response, while its effect on the corner frequency is not significant (see chp. 3). In the case of superluminescent diodes, the spontaneous emission has a strong effect on both the damping as well as the magnitude of the resonance. This is shown in fig. 9.3, where we plot the frequency response of a 500 μm diode pumped to an unsaturated gain of 500 cm^{-1}, at different values of β. The modulation capability increases extremely fast as β is decreased, and at values below 5×10^{-6} a resonance peak appears and the fall-off approaches 20 dB/decade. Fig. 9.4(a) shows plots of the corner frequency versus pumping, with different spontaneous emission factors β. The corner frequency increases rapidly as β falls below 10^{-3}. For comparison, the frequency response of a conventional laser with the same length of 500 μm, with an end mirror reflectivity of 0.3, is also shown in the figure. This curve is calculated using the well known formula described in chapter 3:

$$f_r = \frac{1}{2\pi}\sqrt{\frac{1}{\tau_s \tau_p}\left(\frac{g}{g_{th}}-1\right)}$$

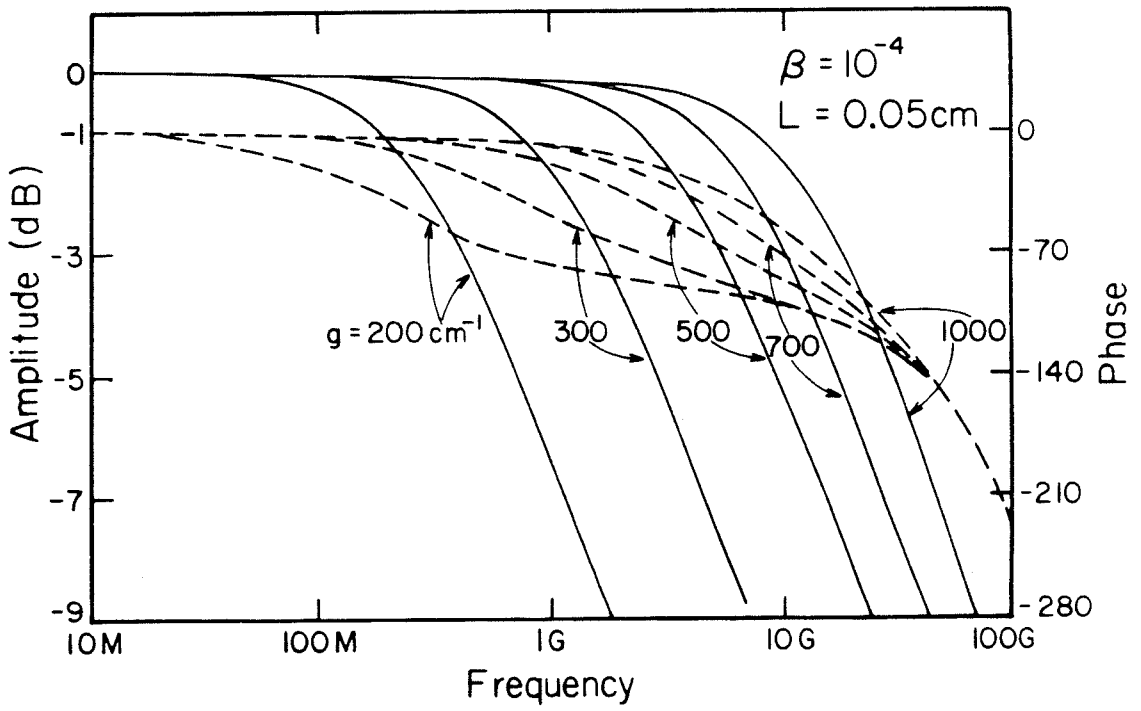

Figure 9.2. *Amplitude and phase responses of a 500 μm superluminescent diode at various pumping levels.* $\beta=10^{-4}$.

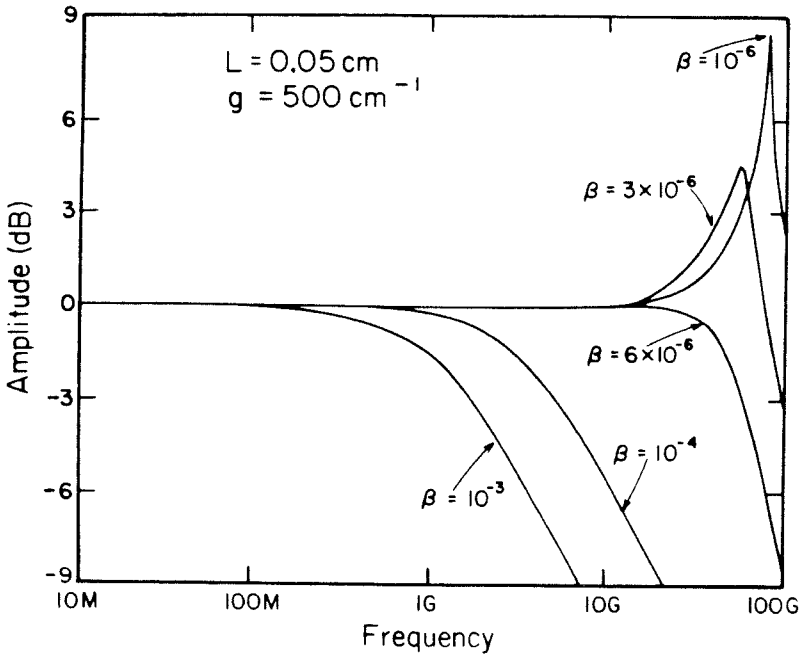

Figure 9.3. *Amplitude and phase responses of a 500 μm diode with various β.* Unsaturated gain = 500 cm^{-1}.

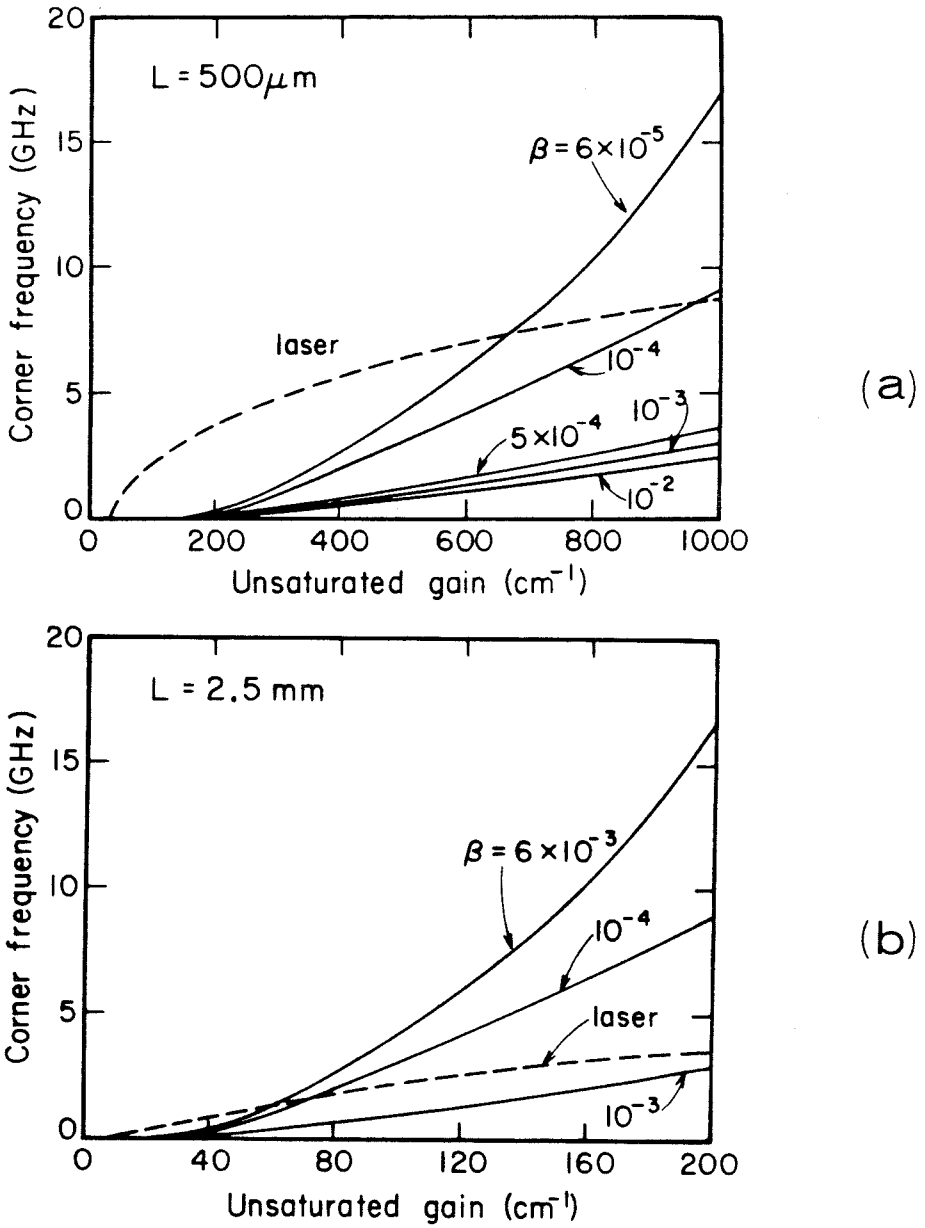

Figure 9.4. *Corner frequencies of a superluminescent diode vs pump, with various β, (a) for a 500μm diode and (b) a 2.5mm diode. The responses of conventional (0.3 mirror reflectivity) laser diodes of similar lengths are shown in dotted lines.*

9.6(a)

assuming a linear dependence of gain on pump current density, and where τ_p= photon lifetime, g = unsaturated gain, g_{th} = threshold gain. Since $1/\tau_p = cg_{th}$, eqn. (9.6(a)) can be rewritten as

$$f_r = \frac{1}{2\pi}\sqrt{\frac{c}{\tau_s}(g - g_{th})} \qquad 9.6(b)$$

It is apparent from fig. 9.4(a) that superluminescent diodes are not competitive with lasers of similar construction except at extremely high pump levels and for very small spontaneous emission factors. The spontaneous emission factor, depending on the waveguiding geometry, varies from about 10^{-5} in simple stripe geometry to 10^{-4} in lasers with real lateral guiding[12]. Since the superluminescent spectrum is at least an order of magnitude wider than the laser spectrum, the actual spontaneous emission factor must lie around 10^{-3} to 10^{-4}. To obtain values of β as low as 10^{-5} would require some special effort. However, one interesting feature of the frequency response of superluminescent diodes is that the corner frequency is invariant to gL, total unsaturated gain of the device. This is true for diode lengths as long as 0.3 cm. thus, the frequency response of a 0.2 cm diode pumped to an unsaturated gain of 200 cm^{-1} is identical to that of a 500 μm diode pumped to 800 cm^{-1} - an unrealistic value. Conventional lasers do not have this property since longer diodes have a longer photon lifetime, and would have a lower corner frequency when pumped at the same level of g/g_{th}. In other words, very high frequency responses can be attained at very modest pump current densities by using very long diodes, as illustrated in fig. 9.4(b), which is a similar plot to fig. 9.4(a) but for a 0.25cm diode.

9.3 Effect of a small but finite mirror reflectivity

In practice, the reflection from mirror facets cannot be reduced to zero. By using Lee's structure[2] or by placing the waveguide at an angle to the facets, the only feedback into the waveguide mode is due to scattering, which can be made quite small. However, even with a reflectivity of 10^{-6}, the conventional threshold gain (neglecting internal absorption loss) of a 500 μm laser is $\frac{1}{L}\ln\frac{1}{R} \approx 276cm^{-1}$; for longer diodes the threshold decreases inversely to L. Thus at pumping levels where we are interested in (gL > 20) the diode can well be above the conventional lasing threshold. The question arises as to whether the frequency response of such a device behaves like that of a conventional laser diode, with a square root dependence as in (9.6), or like that of a superluminescent diode. There is actually no reason to believe that a laser with mirror reflectivities as low as 10^{-6} should behave as predicted by the spatially uniform rate equations. The optical spectrum, though wider than common laser diodes because of the extremely low finesse cavity, would be considerably narrower than the free superluminescent spectrum. The following calculations are carried out to illustrate the effects of a small but finite mirror reflectivity on the frequency response of the superluminescent diode. It also serves to illustrate the actual range of validity of the conventional rate equations.

In the case of a finite reflectivity the pertinent boundary conditions are

$$x^{-}(L/2) = Rx^{+}(L/2) \qquad 9.7(a)$$

$$x^{+}(-L/2) = Rx^{-}(-L/2) \qquad 9.7(b)$$

where R is the mirror reflectivity. The above boundary conditions modify (9.5) into

$$x^{+}(L/2) = x^{-}(-L/2) = \frac{QT - SP}{(Q-P) + R(T-P)} \qquad 9.8$$

A set of results is shown in fig. 9.5(a) and 9.5(b), where we show the frequency response of a long (0.25cm) diode with $\beta = 10^{-3}$ and 10^{-4}, and assuming a mirror reflectivity of 10^{-6}. Features of both the laser diode and the superluminescent diode can be observed in the frequency response. The corner frequency is sensitive to the spontaneous emission factor, increases much faster than a square root dependence on pumping, but at a sufficiently high pump level a resonance peak ocurs similar to a conventional laser. Fig. 9.6 shows plots of the corner frequency versus pump level, for spontaneous emission factors of 10^{-3} and 10^{-4}. Also shown is the response of a laser of similar length (0.25cm) with a reflectivity of 0.3. As the mirror reflectivity increases from 10^{-6}, the superluminescent response curve merges continuously onto the laser curve and becomes essentially the laser curve at reflectivities around 10^{-3}.

Using a plausibility argument one can formulate a rough criterion as to how small the end mirror reflectivity should be for the frequency response to be superluminescent-like. In the pure superluminescent case the photons are generated at one end through spontaneous emission , and are amplified as they traverse the active medium. Thus, if the product of the reflectivity and the outward travelling photon density at a mirror facet is larger than β, then the device resembles more closely a conventional laser than an amplified spontaneous emission device. With $\beta = 10^{-4}$ and a typical normalized photon density of 10 near the output end, the mirror reflectivity must be smaller than 10^{-5} for the response to be superluminescent-like. This plausibility argument is supported by results of numerical calculations.

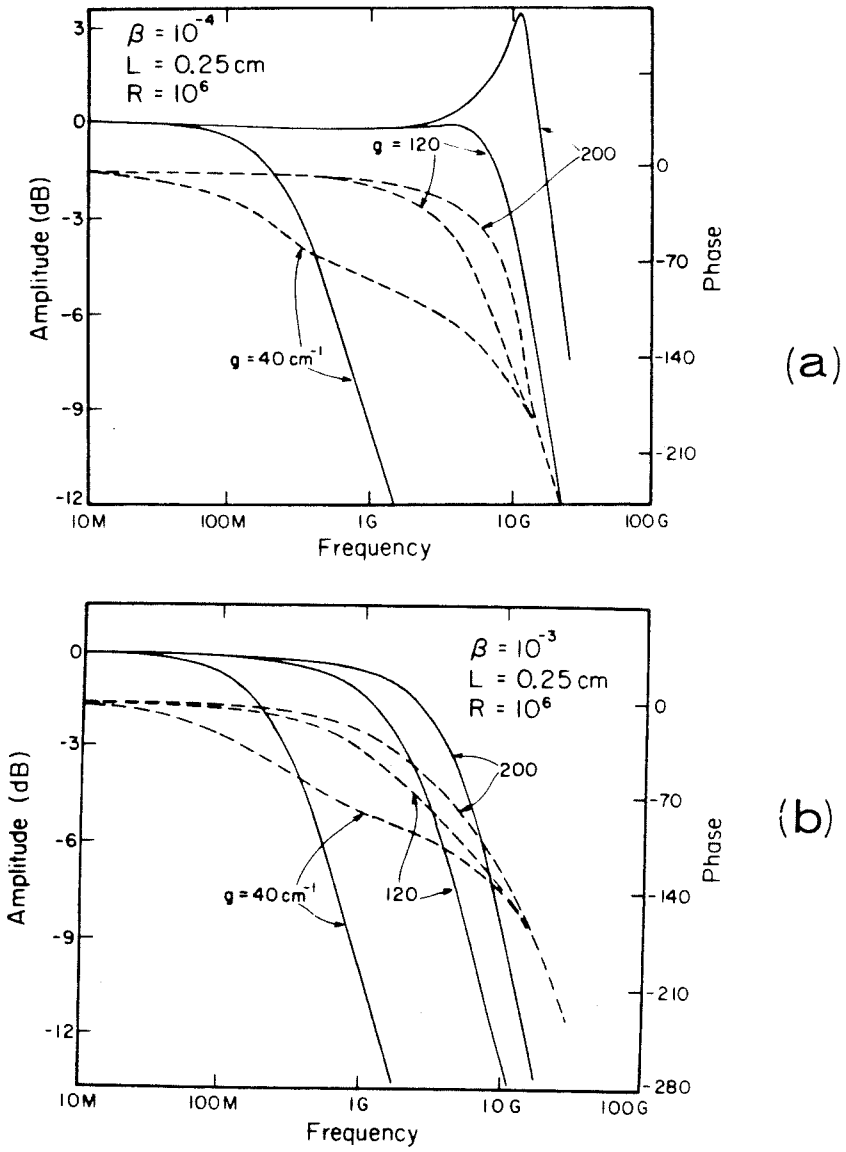

Figure 9.5. *Frequency response of a 0.25cm diode with mirror reflectivity of* 10^{-6}, *and* $\beta = 10^{-4}$ *in (a) and* 10^{-3} *in (b). g is the unsaturated gain in* cm^{-1}.

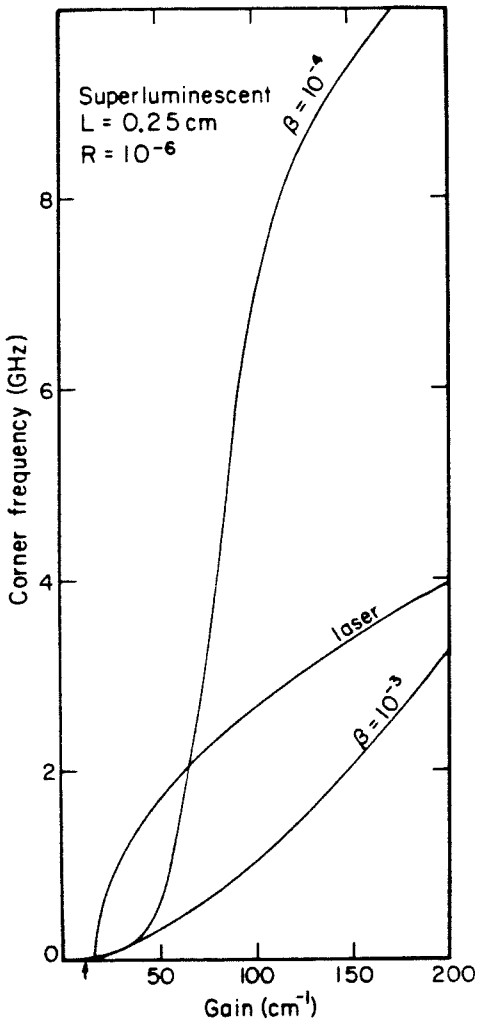

Figure 9.6. *Corner frequency of a 0.25cm diode with mirror reflectivity of* 10^{-6}, *at spontaneous emission factors of* 10^{-4} *and* 10^{-3}. *The response of a conventional 0.25cm laser is shown in dotted line.*

Finally, in going to longer devices one cannot neglect the internal optical loss, which amounts to about 10 - 20 cm^{-1} [11] in common GaAs laser materials. The optical output power will not increase linearly as shown in fig. 9.1(a), but will saturate at a value X_s given by

$$\frac{g}{1+X_s} = f \qquad 9.9$$

where f is the internal loss in cm^{-1}, g is the unsaturated gain. For devices as long as 0.25 cm, the internal loss is considerably lower than the saturated gain anywhere inside the active medium except for a small region near the ends, where the photon density is highest. The effect on the frequency response proves to be insignificant.

Reference - Chapter 9

1. L.N.Kurbatov, S.S.Shakhidzhanov, L.V.Bystrova, V.V.Krapukhin and S.J.Kolonenkov, Soviet Phys. Semiconduct., **4**, 1739 (1971).
2. T.P.Lee, C.A.Burrus and B.I.Miller, IEEE J. Quant. Electron., **QE-9**, 829 (1973).
3. M.C.Amann and J.Boeck, Electron. Lett., **15**, 41 (1979).
4. M.C.Amann, J.Boeck and W.Harth, Int. Jour. Electron., **45**, 635 (1978).
5. W.Harth and M.C.Amann, Electron. Lett., **13**, 291 (1977).
6. M.C.Amann and J.Boeck, AEU, **33**, 64 (1979).
7. G.H.Olsen, F.Z.Hawrylo, D.J.Channin, D.Botez and M.Ettenberg, IEDM, paper 20.2, Washington D.C. 1980.
8. J.B.Moreno, J.Appl.Phys., **48**, 4152 (1977).
9. Y.Reuven and M.Baer, IEEE J. Quant. Electron., **QE-16**, 1117 (1980).
10. L.W.Casperson, J. Appl. Phys., **48**, 256 (1977).
11. H.Kressel and J.K.Butler, **Semiconductor Lasers and Heterojunction LEDs** , Academic Press 1977.
12. K.Petermann, IEEE J. Quant. Elecron., **QE-15**, 566 (1979).
13 M.C.Amann, A.Kuschmider and J.Boeck, Electron. Lett., **16**, 58 (1980).